THE UNIVERSITY OF CALGARY

TORSION IN CURVED PRESTRESSED BRIDGES

BY

Patrick G. Maher

A THESIS

SUBMITTED TO THE FACULTY OF GRADUATE STUDIES

IN PARTIAL FULFILMENT OF THE REQUIREMENTS FOR THE

DEGREE OF MASTER OF SCIENCE IN ENGINEERING

DEPARTMENT OF CIVIL ENGINEERING

CALGARY, ALBERTA

NOVEMBER, 1985

© Patrick G. Maher 1985

Permission has been granted to the National Library of Canada to microfilm this thesis and to lend or sell copies of the film.

The author (copyright owner) has reserved other publication rights, and neither the thesis nor extensive extracts from it may be printed or otherwise reproduced without his/her written permission.

L'autorisation a été accordée à la Bibliothèque nationale du Canada de microfilmer cette thèse et de prêter ou de vendre des exemplaires du film.

L'auteur (titulaire du droit d'auteur) se réserve les autres droits de publication; ni la thèse ni de longs extraits de celle-ci ne doivent être imprimés ou autrement reproduits sans son autorisation écrite.

ISBN 0-315-29970-3

THE UNIVERSITY OF CALGARY

FACULTY OF GRADUATE STUDIES

The undersigned certify that they have read, and recommend to the Faculty of Graduate Studies for acceptance, a thesis entitled "TORSION IN CURVED PRESTRESSED BRIDGES", submitted by Patrick G. Maher in partial fulfilment of the requirements for the degree of Master of Science in Engineering.

A. Ghali

Dr. A. Ghali (Supervisor)
Department of Civil Engineering

Dr. W. H. Dilger
Department of Civil Engineering

Dr. A. E. McMullen
Department of Civil Engineering

Dr. R. I. Gilbert
Department of Civil Engineering
University of New South Wales

Dr. W. K. D. Davies
Department of Geography

Date November 22, 1985

ABSTRACT

A space frame computer program, SFRAME, has been developed for the analysis of post-tensioned, curved, continuous box girder bridges. The multi node curved beam element of Jirousek is incorporated into the program to model curved bridge geometries. The element is suitable for the analysis of bridges in which warping of the cross section is not significant. The automatic computation of prestressing forces, due to cables of arbitrary geometry in space, is included in the element formulation. The program also computes prestress losses due to anchorage slip and due to friction. In this regard, no approximations are required in calculating the change in angle in space along the cable.

The behaviour of the element is investigated under a number of simple loading cases. It is shown that while the element gives exact results under distributed loads, or under concentrated loads at the end nodes, inexact results are produced by concentrated loads applied to internal degrees of freedom. An investigation of the element flexibility matrix identifies the reasons for these inaccuracies.

The computer program is used to analyse torsional effects in horizontally curved continuous bridges. It is shown that while prestressing may balance out the bending

moments due to dead loads, the induced torsional moments add to, rather than negate, the dead load torsional moments. A technique is presented for computing cable profiles and appropriate amounts of prestressing in box girder sections, which simultaneously balance both bending and torsional moments along the bridge. In this technique higher order cable profiles, factored by computed coefficients, are superimposed on the basic cable profile to produce a resultant cable layout, that gives a least squares approximation to an exactly balanced configuration of both bending and torsional moments. The closeness of the fit is shown to depend upon the number of higher order terms added to the basic profile. The method is applied to two design examples: a two span symmetric, circularly curved bridge and a three span bridge with reverse curvatures.

ACKNOWLEDGEMENTS

To my supervisor, Dr. A. Ghali, I would like to express my sincere gratitude for his guidance and encouragement during the preparation of this thesis. In particular, his availability at all times, no matter how busy, to discuss problems as they arose in the course of the work, is most appreciated.

I wish to thank my fellow graduate students, Eugene O' Brien and Fred Griffiths, for their assistance in the final preparation and submission of the thesis. Thanks are also due to Ms. Carolyn Macarthur for her excellent typing.

The financial assistance provided by the Civil Engineering Department at The University of Calgary and by the National Research Council of Canada is gratefully acknowledged.

Finally, a most sincere thank you to my fiancee, Denise, for her love and encouragement from across the miles.

To Denise

TABLE OF CONTENTS

		PAGE
ABSTRACT		iii
ACKNOWLEDGEMENTS		v
DEDICATION		vi
TABLE OF CONTENTS		vii
LIST OF FIGURES		xi
LIST OF TABLES		xiv
NOTATION		xvi
CHAPTER		
ONE	INTRODUCTION	1
	1.1 General Overview	1
	1.2 Scope of Thesis	4
	1.3 Thesis Outline	5
TWO	LITRATURE REVIEW	8
	2.1 Curved Girders	8
	2.1.1 Introduction	8
	2.1.2 Simplified Methods of Analysis	9
	2.2 Applicability of Simplified Analysis to Box Girder Bridges	10
	2.3 Available Beam Finite Elements	12
	2.3.1 Introduction	12
	2.3.2 Curved Beam Elements	14
	2.4 Computation of Prestressing Forces	17
	2.5 Torsion Due to Prestressing in Curved Bridges	18

THREE CURVED ELEMENT DEVELOPMENT 23

3.1 Introduction 23

3.1.2 Timoshenko Beam Theory 23

3.1.3 Isoparametric Element Formulation .. 27

3.2 Theoretical Formulation 28

3.2.1 Element Geometry 28

3.2.2 Displacement Functions 29

3.3.3 Coordinate Transformation 31

3.2.4 Cross Section Properties 36

3.2.5 Strain / Displacement Relation 37

3.2.6 Element Stiffness Matrix 43

3.2.7 Consistent Nodal Load Vector 44

3.3 Prestressing Effects 45

3.3.1 Introduction 45

3.3.2 Geometric Description 48

3.3.3 Cable Anchorage Loads 51

3.3.4 Distributed Loads Due to Prestressing 55

3.4 Short Term Prestress Losses 60

3.4.1 Friction Loss 60

3.4.2 Anchorage Slip Loss 65

3.5 Concluding Remarks 69

FOUR VERIFICATION OF ELEMENT BEHAVIOUR 70

4.1 Introduction 70

4.2 Results of Single Element Examples 72

4.2.1 Variable Section Cantilever 81

4.3 Analysis of Element Stiffness Matrices ... 83

4.3.1 4 Node Cantilever 84

4.3.2 5 Node Cantilever 90

4.3.3 5 Node Simple Beam 95

4.3.4 Uniform Load on a 5 Node Cantilever 97

4.4 Conclusions 98

FIVE TORSION CONTROL IN CURVED CONTINUOUS BRIDGES 99

5.1 Introduction 99

5.2 Demonstration Example 102

5.2.1 Parameters Affecting Behaviour 109

5.3 A Method for Control of Bending and Torsion 115

5.4 Superposition of Eccentricities 116

5.5 Formulation of the Method 121

5.6 Residual Moments 128

5.7 Geometrical Constraint of the Cable Profile 129

5.8 Method of Torsional Moment Control, Applied to a Two Span Bridge 132

5.8.1 Profile Adjustment 133

5.8.2 Constraint of the Cable Profile 144

5.9 Optimum Prestressing Forces 152

5.10 Opimum Prestressing Forces for the Bridge in Figure 5.11 153

5.11 Three Span Example 160

5.11.1 Analysis of Results 168

5.12 Concluding Remarks 175

SIX CONCLUSIONS AND RECOMMENDATIONS 176

6.1 Summary and General Conclusions 176

6.2 Recommendations for Future Research 179

REFERENCES 181

APPENDIX A LOCATION OF SHEAR CENTRE IN BOX SECTIONS 186

APPENDIX B OPTIMIMIZED RESULTS FOR THE TWO SPAN BRIDGE, FIGURE 5.11 191

LIST OF FIGURES

FIGURE	TITLE	PAGE
1.1	Typical Bridge Cross Sections	1
2.1	Available Beam Elements in the Computer Program SFRAME	12
2.2	Unbalanced Forces due to Cables of Different Sag	20
2.3	A Prestressing Cable with Both Horizontal and Vertical Eccentricities	21
3.1	A Simple Beam Subject to Pure Bending and Pure Shear	25
3.2	Assumed Constant Shear Strain Through a Cross Section	26
3.3	Description of Local Axes for the Jirousek Element.....	26
3.4	Definition of ϕ Value When a Cross Section Lies in the Global xy Plane	33
3.5	Relative Translation of the Shear Centre and Centroid due to Twisting of the Cross Section	33
3.6	Assumed and Actual Force Distribution due to Curvature of a Prestressing Cable	47
3.7	A Cable Profile to be Used with the Jirousek Curved Beam Element	49
3.8	Forces at Cable Anchorage Points	54
3.9	Principal Normal and Tangent Vectors to A Cable in Space	57
3.10	Definition of Terms α_{ij} and s_{ij}.....	61
3.11	Typical Force Variation along a Prestressing Cable	61
3.12	A Prestressing Cable with Both Vertical and Horizontal Components of Angular Change	64
3.13	Prestress Loss due to Anchor Slip	67

4.1 Examples Used to Check Behaviour of Jirousek Element 71

4.2 Cantilever Beam with Linearly Varying Cross Section Properties 82

4.3 Bar and Jirousek Element Models of the Four Node Cantilever, Figure 4.1 85

4.4 Exact and computed Deflections and Rotations Using a Four Node Jirousek Element 91

4.5 Degrees of Freedom of the Five Node Cantilever, Figure 4.1 92

4.6 Degrees of Freedom of the Five Node Simple Beam, Figure 4.1 92

5.1 Two Span Circular Curved Beam 100

5.2 Torsional Support 101

5.3 Two Span Circular Bridge 103

5.4 Bending and Torsion Diagrams for the Two Span Bridge in Figure 5.3 108

5.5 Bending and Torsional Moments when Torsional Rotation is Free to Occur at the Central Support of the Beam in Figure 5.3 110

5.6 Variation, with Radius of Curvature, of Torsional Moment due to Dead Load and Prestressing 112

5.7 Variation in Torsional Moments with I/J Ratio, for the Bridge in Figure 5.3, for R = 130 m ... 113

5.8 Variation in Torsional Moments with I/J Ratio, for R = 65 m 114

5.9 Unit Cable Profiles 117

5.10 Superposition of Cable Profiles 118

5.11 Two Span Circular Bridge 122

5.12 Location of Bending and Torsional Moments at Element Nodes 124

5.13 Torsional Moment Diagram due to Dead Load and Basic Prestressing, for Two Span Example, Figure 5.11 134

5.14 Unit Cable Profiles, Quadratic, Cubic and Quartic 136

5.15 Decreasing the Cable Eccentricity to Fit within Beam 142

5.16 Torsional Moments, for Constrained Profile, Quadratic Terms Added 150

5.17 Variation of Sum of Squared Residual Moments, I, with Outer Web Prestressing Force 151

5.18 Variation of I and M_z, with P_{inner} 157

5.19 Residual Torsional Moments Obtained for the Bridge in Figure 5.11, when P_{min} is set to 9.35 MN 159

5.20 Comparison of Adjusted Profiles for Two Span Example, with P_{min} = 9.35 MN 161

5.21 Three Span Bridge with Reverse Curvatures 162

5.22 Basic Cable Profile for the Bridge in Figure 5.21 164

5.23 Torsion Diagram due to Dead Load and Basic Prestressing in Three Span Bridge, Figure 5.21 165

5.24 Unit Cable Profiles Used in Three Span Bridge, Figure 5.21 167

5.25 Adjusted Cable Profiles for Solutions 6 and 7, Table 5.10 172

5.26 Residual Torsional Moments for Solutions 2,3,5 and 7, Table 5.10 173

A.1 Unsymmetric Box Section 187

A.2 Definition of Term A_s in Equation A.1 187

A.3 Shear Flow Diagrams 190

LIST OF TABLES

TABLE	TITLE	PAGE
4.1	4 Node Cantilever, Example 1, Figure 4.1	73
4.2	5 Node Cantilever, Example 2, Figure 4.1	74
4.3	5 Node Cantilever, Example 3, Figure 4.1	75
4.4	5 Node Simple Beam, Example 4, Figure 4.1	76
4.5	5 Node Cantilever, Example 5, Figure 4.1	77
4.6	5 Node Simple Beam, Example 6, Figure 4.1	78
5.1	Comparison of Closed Form and Computer Results For the Beam in Figure 5.3	106
5.2	Uconstrained Cable Profile, Quadratic Terms Added	139
5.3	Unconstrained Cable Profile, Quadratic and Cubic Terms Added	140
5.4	Unconstrained Cable Profile, Quadratic, Cubic and Quartic Terms Added	141
5.5	Effect of Bringing Outer Cable Profile Within Bridge Depth	144
5.6	Constrained Cable Profile, Quadratic Terms Added	146
5.7	Constrained Cable Profile, Quadratic and Cubic Terms Added	147
5.8	Constrained Cable Profile, Quadratic, Cubic and Quartic Terms Added	148
5.9	Condensed Results for Two Span Bridge, Figure 5.11	155
5.10	Results for Three Span Bridge, Figure 5.11	169
B.1	Quadratic Terms Added to Basic Profile, P_{min} = 4.70 MN	191
B.2	Quadratic Terms Added to Basic Profile, P_{min} = 7.00 MN	192

B.3 Quadratic Terms Added to Basic Profile, P_{min} = 9.35 MN 193

B.4 Quadratic Terms Added to Basic Profile, P_{min} = 11.70 MN 194

B.5 Quadratic and Cubic Terms Added to Basic Profile, P_{min} = 4.70 MN 195

B.6 Quadratic and Cubic Terms Added to Basic Profile, P_{min} = 7.00 MN 196

B.7 Quadratic and Cubic Terms Added to Basic Profile, P_{min} = 9.35 MN 197

B.8 Quadratic and Cubic Terms Added to Basic Profile, P_{min} = 11.70 MN 198

B.9 Quadratic, Cubic and Quartic Terms Added to Basic Profile, P_{min} = 4.70 MN 199

B.10 Quadratic, Cubic and Quartic Terms Added to Basic Profile, P_{min} = 7.00 MN 200

B.11 Quadratic, Cubic and Quartic Terms Added to Basic Profile, P_{min} = 9.35 MN 201

B.12 Quadratic, Cubic and Quartic Terms Added to Basic Profile, P_{min} = 11.70 MN 202

NOTATION

a	Parameter used in the calculation of $\{\hat{n}\}$, the principal normal vector to a point on a prestressing cable
A	Cross Sectional Area
A	Action due to a prestressing cable
A_{ps}	Area of prestressing cable
A_r	Reduced shear area of cross section
A_s	Area enclosed by a box section
$A_{y'}$, $A_{z'}$	Reduced shear areas in the local y'and z' directions respectively
b	Distance between outer webs of box girder bridge
[B]	Strain/Displacement matrix
c	Length of prestressing cable affected by anchorage slip
[C]	Rectangular matrix of constraint coefficients
[D]	Elasticity matrix
{D}	Vector formed when $\{\Delta M\}$ is premultiplied by the matrix $[\Delta A_u]$
e	Eccentricity of prestressing cable
e'_y , e'_z	Eccentricity of prestressing cable at node i with respect to the local y' and z' axes respectively
E	Young's modulus
E_{ps}	Young's modulus of prestressing steel
f'_c	Concrete design strength
f_r	Concrete modulus of rupture
[f]	Flexibility matrix

$\{F\}$, $\{F'\}$	Vectors of global and local components, respectively, of prestressing anchorage forces
$\{F\}$	Consistent nodal load vector
G	Shear modulus
[H]	Transformation matrix from global to local coordinates
I	Objective function in optimization of prestressing forces, equal to the sum of the squared residual moments
$I_{y'}$, $I_{z'}$	Moments of Inertia about local y' and z' axes respectively
$J_{x'}$	Torsional constant with respect to local x' axis
k	Wobble friction coefficient
[K]	Rectangular transformation matrix used to generate global coordinates of prestressing cable
ℓ	Length of cable
ℓ	Developed length of curved beam span
l_o	Length of curved bridge span between points of zero dead load moment
[L]	Transformation matrix from local to global coordinates
$M_{x'}$, $M_{y'}$, $M_{z'}$	Moments about element local axes
n	Magnitude of principal normal vector (curvature) at a point on a prestressing cable
$\{\hat{n}\}$	Principal normal vector to a point on a prestressing cable
$N(\xi)$	Interpolation Function
$N_{x'}$	Element axial force
$P(\xi)$	Prestressing force at any point along a Prestressing cable

P'	Rate of change of prestressing force due to anchor slip
P_i	Prestressing force at node i
P_n	Normal component of prestressing load
P_t	Tangential component of prestressing load
P_o	Prestressing jacking force
q	Shear flow distribution in a cross section
q_o	Assumed shear flow in closed box section
q_r	Constant shear flow term to be added to the assumed shear flow to give the correct distribution of shear flow
Q	First moment of area
$\{Q\}$	Vector of constraint constants
R	Radius of curvature of a bridge segment, or of a prestressing cable in space
$\{R\}$	Vector of residual bending and torsional moments from optimization of prestressing forces
s	Curvilinear length measured along prestressing cable
s_{ij}	Distance along a given cable between nodes i and j
$[S]$	Stiffness matrix
t	Magnitude of vector $\{\hat{t}\}$
t_x, t_y, t_z	Components of vector $\{\hat{t}\}$
$\{t\}$	Tangent vector to curved beam or prestressing cable
$[T]$	Transformation matrix from global to local coordinates
u_c, v_c, z_c	Displacement components of any point on a Jirousek beam element: the subscript c refers to the centroidal axis of the beam

$\{u\}$	Vector of element displacements in global coordinates
$\{u'\}$	Vector of local element displacement components
$[U]$	Rectangular matrix formed by the product $[\Delta A_u]T[\Delta A_u]$
v'_s, w'_s	Local components of translation of cross section shear centre
V	Shear force
$V_{y'}, V_{z'}$	Shear force components in the local y' and z' directions respectively
x_c, y_c, z_c	Global coordinates of any point on the centroidal axis of a Jirousek element
x_{ci}, y_{ci}, z_{ci}	Global coordinates of beam node i
x_p, y_p, z_p	Global coordinates of any point on a prestressing cable
x_{pi}, y_{pi}, z_{pi}	Global coordinates of cable node i
$\{X_p\}$	Vector of global cable coordinates
y'_s, z'_s	Local coordinates, with respect to section centroid, of section shear centre
α	Angle subtended by a segment of prestressing cable
α_H	Horizontal component of α
α_V	Vertical component of α
α_{ij}	Angle subtended by cable between nodes i and j
γ	Shear strain
$\Delta\ell$	Anchorage slip at jacking end of prestressing cable
ΔP	Prestress loss due to anchor slip
$[\Delta A_u]$	Matrix of nodal moments due to unit cable profiles

$\{\Delta M\}$	Vector of nodal moments equated to the product $[\Delta A]\{\eta\}$
$\{\Delta M\}_{adjusted}$	Vector of nodal moments after superposition of unit cable profiles
$\{\Delta M\}_{basic}$	Vector of nodal moments due to dead load and basic prestressing
$\{\varepsilon\}$	Vector of nodal strains
$\{\eta\}$	Vector of scaling factors applied to unit cable profiles
$\theta_x, \theta_y, \theta_z$	Global components of rotation of beam cross section
$\theta'_x, \theta'_y, \theta'_z$	Local components of rotation of beam cross section
κ	Curvature
$\{\lambda_x\},\{\lambda_y\},\{\lambda_z\}$	Direction cosine vectors
$\{\lambda_{cn}\}$	Principal normal vector to a point on a prestressing cable
$\{\lambda_{ct}\}$	Tangent vector
$\{\lambda\}$	Vector of Lagrange multipliers
μ	Coefficient of friction
ν	Poisson's ratio
ξ	Natural coordinate along curved beam and prestressing cable
$\{\sigma\}$	Vector of generalised stress components
ΣR_i^2	Sum of squared residual moments after cable profile adjustment
ϕ	Angle between local y' axis of beam cross section and global xy plane
χ	Natural coordinate along prestressing cable
ω	Angle of twist

CHAPTER ONE

INTRODUCTION

1.1 General Overview

During the past two decades concrete box girder bridges have become an obvious feature of modern highway systems. Cross sections may be either single or multicell, depending on span and width requirements. Prestressing is generally used in box girder bridges enabling longer spans, with shallower and more slender sections to be used, thus yielding benefits with regard to space restrictions. Moreover, from an aesthetic standpoint, prestressed box girder sections are more satisfactory than many alternative sections.

With the development of complex highway interchange facilities in most major cities, curved highway bridges have become an obvious part of the urban infrastructure. It is likely that with continued highway construction in modern cities, the use of curved bridges will become an increasing necessity in fitting new developments within the pre-existing infrastructure. The recent Bow River bridge at Edmonton Trail and Memorial Drive in Calgary (43), is an example of such a structure. As in the case of straight bridges, post-tensioned, curved box girder bridges are an

economically and aesthetically satisfactory cross section. Box sections are particularly suitable for curved bridges because of their high torsional rigidity. For this same reason solid or voided sections, Figure 1.1, may also be used in curved bridges.

Curved prestressed box girder bridges are complex three dimensional structures and are most accurately analysed using curved plate and membrane finite elements. However, the longitudinal distribution of bending and torsional moments along a curved bridge may be obtained with satisfactory accuracy using a less rigourous space frame analysis; in which the structure is modelled as an assemblage of one dimensional beam elements.

Several authors (11,14,37,49), have identified the problem of induced torsional moments due to prestressing in curved beams. In the case of straight beams the load balancing concept of Lin (29), enables the designer to balance out a predetermined portion of the beam's dead load by appropriate prestressing. For curved beams, however; while the longitudinal bending moments may still be largely balanced out by prestressing the beam, the horizontal radial forces due to prestressing produce torsion in the beam which tends to add to, rather than negate, the torsion due to external loads.

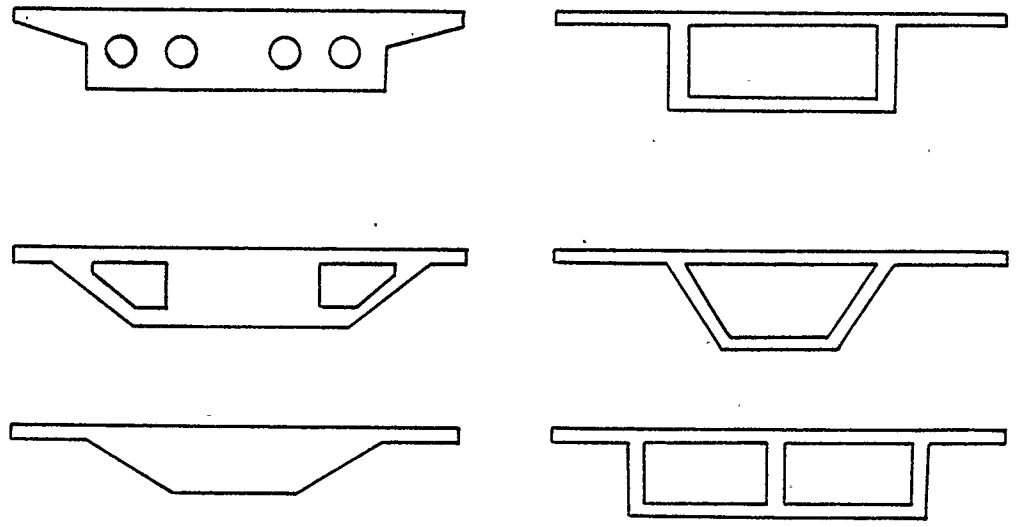

Figure 1.1 Typical Bridge Cross Sections

1.2 Scope of Thesis

The major aim of this thesis is to develop a technique for designing prestressing cable profiles in curved, box girder bridges such that both longitudional bending and torsional moments , due to the applied dead load, are simultaneously balanced at all points along the bridge. To perform the analysis a computer program, SFRAME (19), incorporating straight and curved beam finite elements was developed. The analysis of curved, prestressed bridges required the inclusion in the program of a general curved element, of arbitrary geometry in space, with the automatic computation of prestressing forces included in the element formulation. In the present analysis no account is taken of concrete cracking or of material non-linearities. Similarly time dependent effects due to creep and shrinkage in the concrete are not considered. Thus only the behaviour of curved prestressed bridges in the linear elastic range is investigated. However, it is generally accepted that for design purposes, a knowledge of the distribution of forces within a structure based on linear elastic analysis is adequate.

1.3 Thesis Outline

In Chapter Two of this thesis the appropriate literature, dealing with curved bridges and suitable methods of analysis, is identified. Specifically, traditional methods of analysing curved beams are outlined and the applicability of certain simplifying assumptions is discussed. In particular, the use of three dimensional beam analysis to model the behaviour of curved box girder bridges is presented.

The availability of different curved, beam finite elements is discussed and the reasons for the choice of the multi node element of Jirousek (25), are justified. In addition, the need for automatic computation of equivalent nodal loads due to prestressing is advocated, and the advantages of being able to cater for cables of arbitrary geometry in space is outlined. Material dealing with prestressing of curved beams is presented, and a review of available techniques for controlling torsional effects in prestressed curved beams is given.

In Chapter Three the formulation of a discrete isoparametric beam element, based on Timoshenko beam theory, is presented. The incorporation of prestressing loads due to cables of arbitrary geometry in space, and with varying prestressing force is also outlined. The

method of computing short term prestressing losses due to friction and anchor slip is discussed, and it is shown that losses due to vertical and horizontal components of angular change are computed exactly.

Chapter Four deals with the behaviour of the curved beam element under some simple loading conditions. An investigation of the element stiffness and flexibility matrices is carried out to help in understanding the inexact behaviour of the element in certain instances. Based on the results obtained, recommendations are made as to the appropriate use of the element and its suitability under particular conditions of loading.

In Chapter Five torsional effects in curved, post-tensioned box girder bridges are investigated using SFRAME (19), and situations in which torsional moments may be a problem are identified. A method is developed for computing prestressing cable profiles that minimize the torsional moments along the bridge. To demonstrate the method, two examples are considered; a circularly curved, two span continuous bridge and a three span continuous bridge with reverse curvatures.

Conclusions are drawn in Chapter Six as to the applicability and practicality of the technique developed in the previous chapter. In addition, the benefits of using the computer program, SFRAME, are outlined. In

particular, the availability of a curved beam element of arbitrary geometry in space and the facility for automatic computation of prestressing forces are shown to have been of most importance.

CHAPTER TWO

LITERATURE REVIEW

2.1 Curved Girders

2.1.1 Introduction - In designing any curved structural element the engineer is faced with a complex force distribution, involving the interaction of bending and torsional moments along the member length. The amount of material dealing with the analysis of horizontally curved beams is substantial and the reader is referred to the list of references in the state of the art review by McManus et al. (30), for a comprehensive listing of available literature up to 1968. While closed form solutions to the static response of curved girders have been obtained, these are in most cases not suitable for the design engineer because of their complexity.

The governing differential equations for horizontally curved girders were formulated by Vlasov (48). The resulting sixth order equations include the effects of warping and are thus suitable for the analysis of sections in which warping torsion is significant. However, their inherent complexity preclude their use in practical design situations. A closed form solution to the equations was obtained by Heins and Spates (23). This method of

solution, however, is limited to situations with simple combinations of loads and boundary conditions. Numerical solutions have been obtained by Bell and Heins (7), and Heins (22), in the form of a finite difference and a Fourier series solution. These techniques are more generally applicable than the closed form solution and are suitable for the analysis of bridges in which warping effects may be substantial, such as multi girder curved bridges.

2.1.2 Simplified Methods of Analysis - All simplified methods of analysis of curved girders are based on the assumption that warping torsion is not significant and that it can therefore be neglected. Thus, curved girders are analysed as beams in space with just six degrees of freedom, three displacements and three rotations, at each cross section. The traditional methods of structural analysis, such as virtual work (16), stiffness (47), and flexibility methods (35), have been applied to determine the longitudional distribution of bending moments and torques in curved members.

Vreden (49), analysed continuous curved beams using the flexibility method. Influence lines were computed by the author and a number of curved beams were analysed under different loading conditions. Witecki (50) developed an approximate method for the analysis of curved bridges.

Bassi et al. (4), have shown that this method is accurate for small curvatures and/or short spans but becomes increasingly less so for longer spans or for sharply curved geometries.

2.2 Applicability of Simplified Analysis to Box Girder Bridges

Two assumptions govern the applicability of elastic space frame analysis to the analysis of box girder bridges (18):

(1) Plane sections remain plane on bending i.e. no warping of the cross section occurs.

(2) There is no transverse distortion of the cross section.

In all thin walled beams subject to torsion, out of plane deformation or warping will occur (32). If the warping is restrained, warping torsion will be induced in the member. In general, however, it may be assumed that for closed box beams warping effects are not significant. This is particularly true in situations where the span to width ratio of a box girder bridge is sufficiently large. As a general rule the ratio l_o/b should be greater than 4, where l_o is the distance between points of zero dead load moment and b is the distance between outer webs (18). This

limitation is satisfied by the majority of modern curved box girder bridges, particularly single box sections.

Box sections are very suited for curved bridges because of their high torsional stiffness. However, a box section will tend to distort transversely under the applied loading (22). The provision of transverse diaphragms within the box will, however, minimize cross sectional distortion. The above two conditions are also satisfied by solid or voided cross sections, so that a space frame analysis is also valid for bridges with such cross sections. Bassi et al. (4), have confirmed this and have used three dimensional frame analysis for solid, curved sections.

Various authors have confirmed the validity of space frame analysis for curved box girder bridges. Scordelis and Larsen (39), in a theoretical and experimental investigation of a two span, multi box section curved bridge have confirmed the accuracy of a space frame modelling. They emphasised, however, that a separate analysis is required to determine the transverse distribution of internal forces and moments within the individual plate elements of the box section. The results of the space frame analysis were compared with finite strip and general finite element analyses, and sufficiently close correlation was obtained between the three methods to

indicate that space frame analysis is adequate for design purposes. Other authors who have confirmed the satisfactory use of space frame modelling for curved bridge structures are Van Zyl and Scordelis (46), and El-Amin and Brotton (15).

In a recent publication Scordelis et al. (38), have stated that for certain box girder types, beam theory assumptions may be "seriously in error". However, the curved bridges to be discussed in the present analysis satisfy the conditions previously outlined, regarding span to width ratio of the bridge and distortional properties of the cross section. Therefore, a space frame modelling is certainly satisfactory in this case.

2.3 Available Beam Finite Elements

2.3.1 Introduction - In modelling a curved bridge as an assemblage of beam elements the most simple approach is to model the geometry with straight chord elements. A sufficiently fine mesh of straight 12 d.o.f. bar elements, Figure 2.1(a), will produce accurate results in many situations. However, for more complex bridge geometries it becomes increasingly difficult to accurately model the

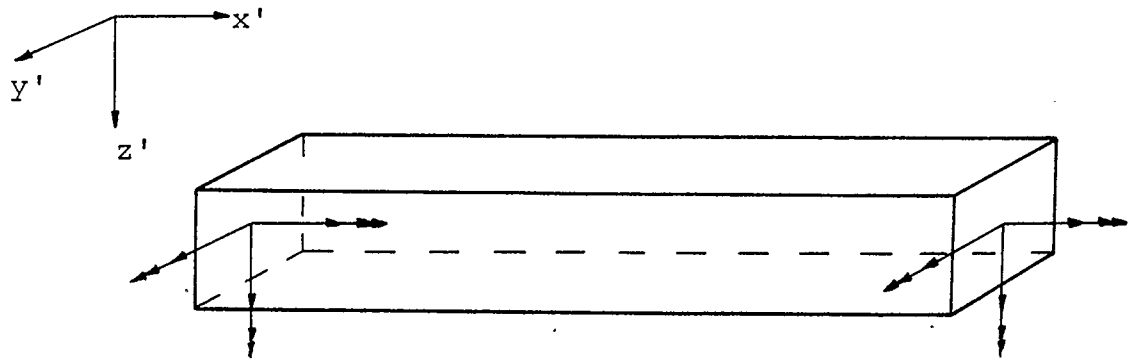

(a) Local axes and element degrees of freedom for straight bar element

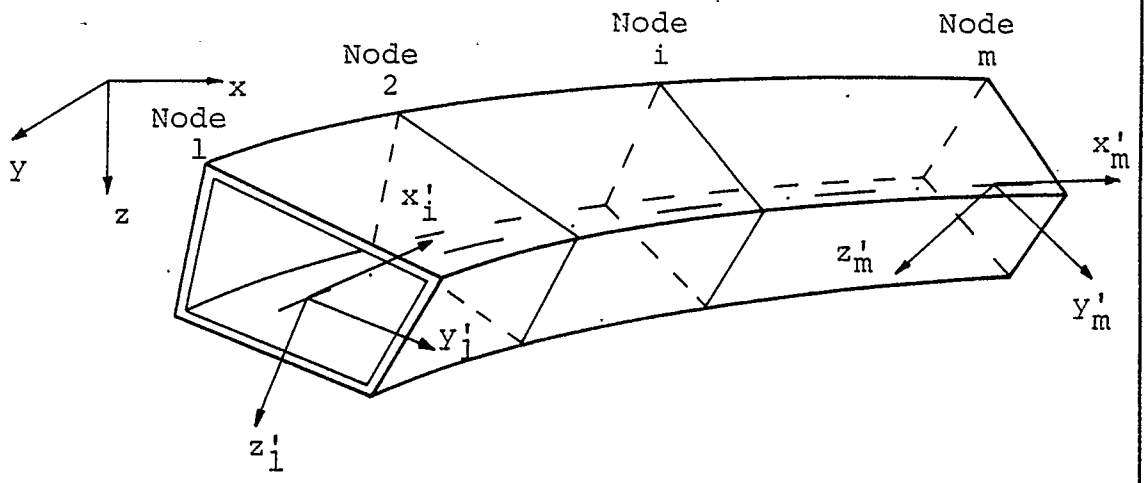

(b) Local axes for multinoded curved beam element of Jirousek

Figure 2.1 Available Beam Elements in the Computer Program SFRAME

bridge with straight elements. In particular, for the analysis of a structure with vertical as well as horizontal curvature, with varying superelevation or with varying cross sectional properties along its length, a more complex element is required.

2.3.2 Curved Beam Elements - A variety of curved beam element formulations exists. The most basic of these are horizontally curved circular elements, such as the element of Thornton and Master (45), derived using a direct stiffness formulation. Such elements, however, offer few advantages over a basic straight bar element. When used to model structures with varying curvature or with varying superelevation a relatively fine mesh must be used for satisfactory results.

An alternative formulation for curved beam elements is as a special form of a three dimensional isoparametric element, Ferguson and Clark (17). This element is superior to the circular element above in that it is of arbitrary geometry in space and of variable cross sectional area. The element is particularly useful as a shell stiffening element and may also be used as a stand alone beam element. However, the element cross section, though of variable area, must be rectangular. This limits the element's usefulness in the analysis of many typical bridge cross sections. In addition, because the element is derived as a

modified form of a three dimensional element it does not exactly model beam behaviour under certain types of loading. Jirousek (25), noted that the element is not successful in representing the torsional and shear response of a beam. It is preferable, therefore, that an element which is used to model assumed beam like behaviour be based on the appropriate beam theory rather than be derived as a special form of a continuum element. For this reason the elements of Buragohain (10), and Surana (42), in addition to the above element of Ferguson and Clark (17), are not considered further.

Albuquerque (3), developed a curved "Semiloof" beam element, based on Timoshenko beam theory, for use with shell elements. Though based on Timoshenko beam theory, the element is not suitable for use as a stand alone beam element, because it contains special rotational degrees of freedom at internal "Loof" nodes to ensure compatibility of deformation with a shell element. Therefore, it was decided to adopt the element formulation outlined by Jirousek (25), instead. This latter curved element is also based on Timoshenko beam theory, but unlike the Semiloof element, the Jirousek element follows more closely standard isoparametric finite element methodology. An additional advantage was that this element presented greater potential for automatic computation of prestressing forces. The

element, Figure 2.1, is multinoded and in the form programmed for the present analysis may contain from three to six nodes, (eighteen to thirty six degrees of freedom). The appropriate order element may be chosen according to the complexity of the geometry to be modelled. Difficult bridge geometries may be satisfactorily modelled with relatively few elements and arbitrary variation in cross sectional properties is easily catered for. Thus the element is extremely versatile in character and general in application.

Bazant and El-Nimeiri (6), developed a straight, skew ended, two noded beam element with eight degrees of freedom at each node. In addition to the usual translational and rotational degrees of freedom, the authors included a longitudional warping and a transverse distortional degree of freedom. Though the element is straight the skew ends enable it to model curved geometries more closely than an assemblage of 12 d.o.f. bar elements. Van Zyl and Scordelis (46), used the element in the analysis of curved prestressed segmental bridges. Even though the element did not appear as versatile, in the opinion of the present author, as the Jirousek element in modelling complex geometries, nevertheless, the skew ends would be advantageous in analysing curved bridges with skew supports. In the present thesis, however, only curved

bridges with radial supports are considered. It would be an interesting follow through to the present work to compare results obtained using the Jirousek element with those obtained using the Bazant/El Nimeiri element in order to measure the actual warping and distortional effects.

2.4 Computation of Prestressing Forces

In a paper by Salse (37), equivalent nodal loads due to prestressing were computed by hand. This, however, becomes a very laborious proposition for a curved bridge in which there may be a number of cables with both vertical and horizontal components of curvature. Thus in any detailed computer analysis of curved bridges it becomes necessary to incorporate the automatic calculation of equivalent nodal loads due to prestressing into the computer program. Van Zyl and Scordelis (46), indicate that the computer program developed in that particular analysis automatically computed prestressing loads, but give no indication of the method used. Scordelis et al. (38), however, give a detailed account of the automatic prestressing options in finite element and finite strip programs developed at the University of California, Berkeley. In this formulation, cable coordinates may be input directly or, alternatively, the cable profile may be parametrically defined. Short term prestressing losses due

to friction and anchor slip are computed. The cable is discretized into an assemblage of straight segments and the equivalent nodal loads due to each segment are computed.

Jirousek et al. (8,26), have developed a method of automatic computation of prestressing loads in thick shell elements by defining the cable profile within each element isoparametrically. The principal advantage of this technique, over that outlined above, is that the forces are computed due to the actual curved cable rather than for an equivalent, approximate subdivision into linear segments. The isoparametric formulation, outlined for shell elements, is adapted in the present analysis for use with the multi node curved beam element of Jirousek.

2.5 Torsion due to Prestressing in Curved Bridges

Vreden (49), used the flexibility method to compute torsional moments due to prestressing in curved beams. It was shown by this author that no torsional moments are induced by prestressing in statically determinate curved beams, but that torsional moments are generated by the redundant reactions of indeterminate structures. Egger (14), developed techniques for the minimization of combined torsional moments resulting from external loads and prestressing. Two techniques were outlined: firstly the vertical profiles of the cables on each side of the beam

may be altered, thus producing unequal balancing forces due to each cable, Figure 2.2. The unequal upward forces generate a twisting moment which may be used to partially or completely balance the torsion produced by the external loads and by the horizontal radial forces due to prestressing. An analytical technique was presented for computing cable profiles and prestressing forces required to simultaneously balance both bending and torsion at all points along the beam. Alternatively, a second technique produces the same effect by applying different prestressing forces on each side of the beam. For two identical cable profiles two different prestressing forces will produce unequal upward balancing forces. This latter technique has the disadvantage of introducing transverse bending moments in the beam; however, in many situations significant transverse moments may be sustained by box girder or solid sections.

Salse (37), developed governing equations of equilibrium for curved beams subject to prestressing forces and identified a method for balancing both bending and torsion by using prestressing cables with both vertical and horizontal eccentricities, Figure 2.3. However it was pointed out that complete balancing of torsional moments is, in many cases, not practically feasible; since the

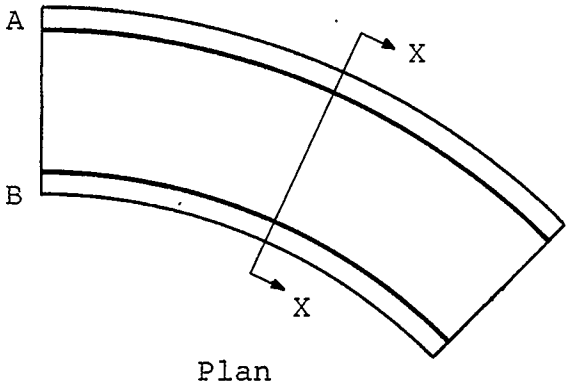

Plan

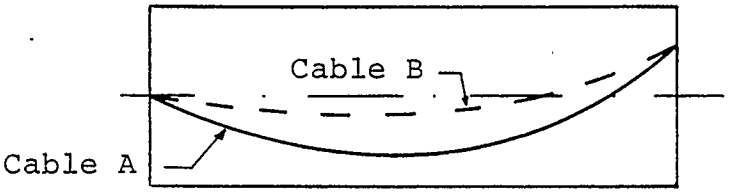

Developed Elevation

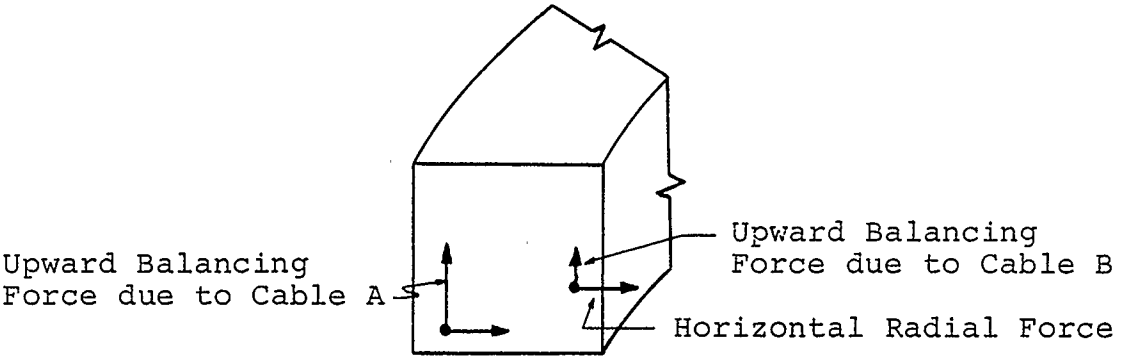

Section XX

Figure 2.2 Unbalanced Forced due to Cables of Different Sag

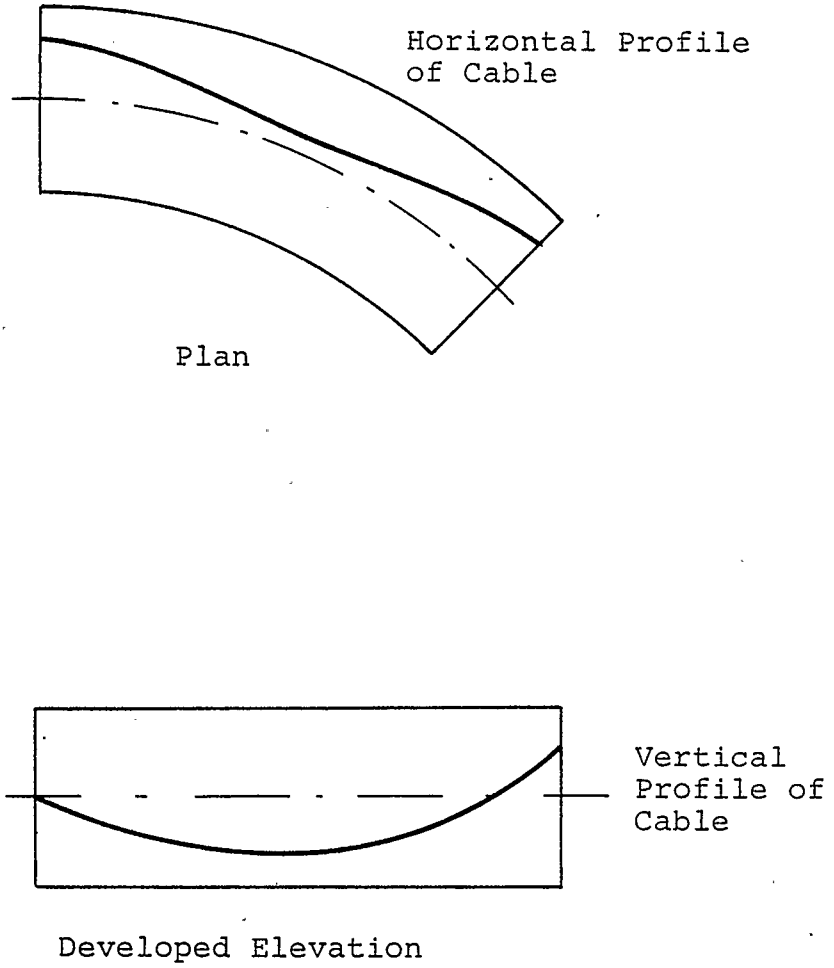

Figure 2.3 A Prestressing Cable with Both Horizontal and Vertical Eccentricities

required horizontal eccentricities may lie outside a reasonably sized section. In addition, the technique is not suitable for box sections since the prestressing cables, in this case, are constrained to lie within a particular web. However, it may be applied to solid or voided sections.

Campbell and Chitnuyanondh (11), proposed a semi-numerical technique to determine a cable profile that balances a proportion of the torsional moments in curved beams. Like Salse's technique, horizontal eccentricities were introduced in the cable profile to counteract the torsional moments due to the applied dead load. A second method was also proposed, involving the use of eccentric intermediate supports. The eccentric supports introduce a concentrated torque at the supports, opposite in sign to the torsional moments induced by external loads and prestressing.

CHAPTER THREE

CURVED ELEMENT DEVELOPMENT

3.1 Introduction

3.1.1 General - As already discussed in Chapter Two a number of curved beam element formulations exist in the literature. For the reasons outlined the element formulation presented by Jirousek (25), was deemed most appropriate for the present analysis. The element is based on Timoshenko beam theory and is developed using isoparametric finite element methodology. In Jirousek's formulation the element may be used either as a stand alone beam element or as a thick shell stiffening element. For the stand alone beam element there is no generalised displacement compatibility requirement between the beam and shell elements, and thus the formulation of the element stiffness matrix is correspondingly simplified. This simpler procedure is adopted in the present work.

3.1.2 Timoshenko Beam Theory - Euler beam theory does not include , directly, the effects of shear deformation; although shear effects can be included in the stiffness matrix (20). Timoshenko beam theory, on the other hand, directly incorporates shear effects in the displacement

function (40). The total slope of the beam centreline is given by the sum of the effects due to bending and shear deformation.

In Figure 3.1 it can be seen that the effect of pure bending is to rotate the cross section, ab, through an angle θ. In the case of pure shear it is assumed that any cross section ab, normal to the beam centreline in the undeformed state, remains vertical after deformation. Line elements tangent to the centreline rotate through an angle γ, corresponding to the shear strain. The total slope of the beam centreline is given by:

$$\frac{dw}{dx} = \gamma(x) + \theta(x) \tag{3.1}$$

where w is the displacement. The shear deformation is:

$$\gamma(x) = \frac{dw}{dx} - \theta(x) \tag{3.2}$$

At any cross section it is assumed that the shear strain is the same throughout the depth of the beam (40), Figure 3.2. Thus $\gamma(x)$, the shear angle, is constant over the cross section. This implies that the shear stress is constant over the beam cross section, which of course is not true. However, the error resulting from this

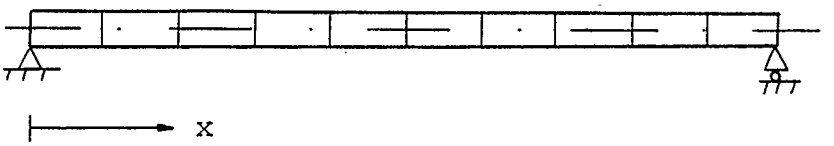

Undeformed Beam

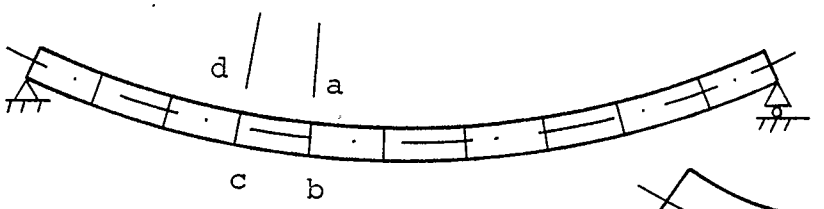

Pure Bending

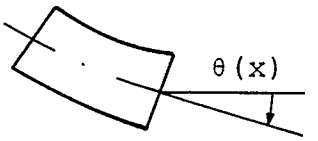

Section abcd

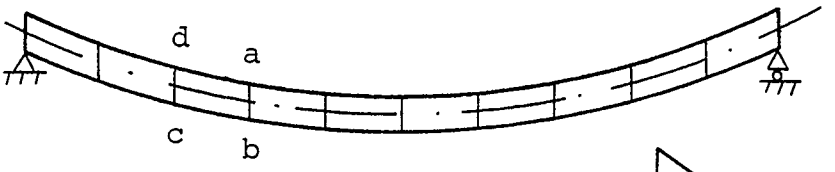

Pure Shear

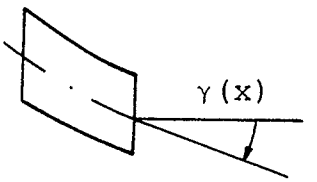

Section abcd

Figure 3.1 A Simple Beam Subject to Pure Bending and Pure Shear

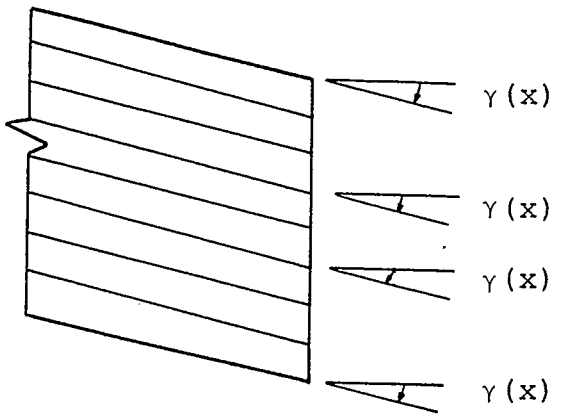

Figure 3.2 Assumed Constant Shear Strain Through a Cross Section

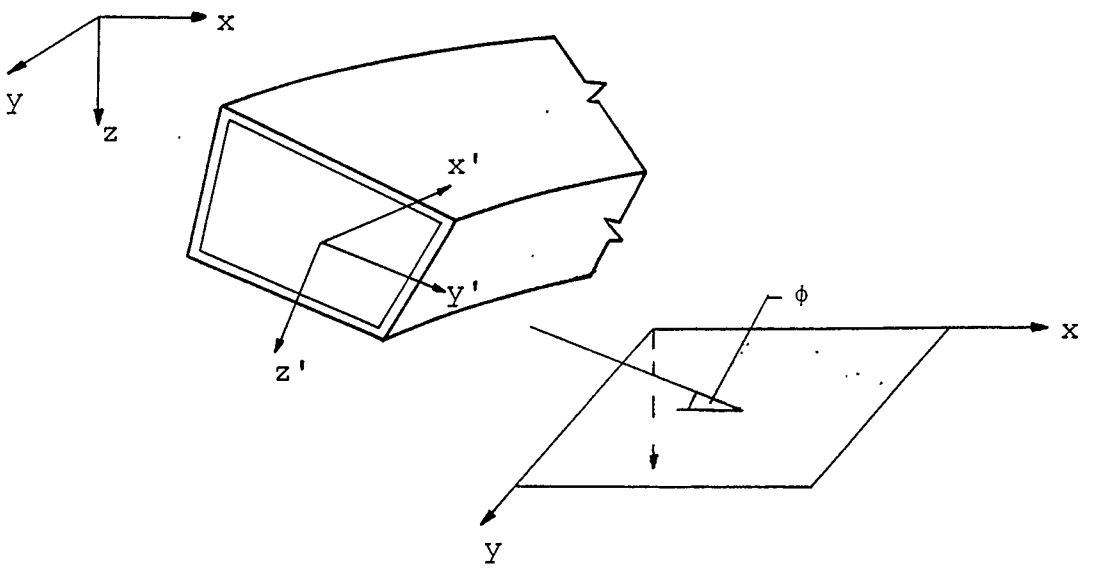

Figure 3.3 Description of Local Axes for the Jirousek Curved Element

assumption is catered for by using the appropriate reduced cross sectional area (20).

The shear force causing the shear strain is given by:

$$V = GA_r \left(\frac{dw}{dx} - \theta\right) \tag{3.3}$$

where V is the shear force, G is the shear strain and A_r is the reduced shear area. The bending relation is the same as for Euler beam theory:

$$M = EI\kappa = EI \frac{d\theta}{dx} \tag{3.4}$$

where M is the bending moment, E is Young's modulus, I is the moment of inertia and κ is the curvature. In this case, however, the rotation is not given by the first derivative of the displacement function. Thus, because the bending rotation and displacement functions are independent they must therefore be interpolated independently in any finite element formulation. This matter is discussed further in Section 3.2.2.

3.1.3 Isoparametric Element Formulation - The development of any general curved element necessitates the use of the isoparametric formulation (5,12). Isoparametric

elements are obtained by mapping from local or natural element coordinates to the global, cartesian coordinate system. This mapping is defined by the Jacobian of transformation. The natural coordinate system of the element will be one, two or three dimensional, depending on the element. In the case of a beam element a single coordinate is required. The geometry of the element is interpolated in the same way as displacements, using shape functions. If the order of the shape functions defining geometry and displacement are the same then the element is said to be isoparametric. If the geometry is interpolated with shape functions of higher order than those defining the displacement function, the element is super-parametric. Conversely, if the shape functions defining geometry are of lower order than those defining the displacement field the element is sub-parametric. The present element development uses the same order of interpolation for both geometry and displacement.

3.2 Theoretical Formulation

3.2.1 Element Geometry - The global and local coordinate systems are shown in Figure 3.3. The element may contain from three to six nodes with each node defining a point on the beam centroidal axis. A three node element describes a quadratic curve in space and similarly a six

node element describes a quintic curve. Following standard isoparametric methodology a natural curvilinear coordinate, ξ, may be defined, varying from -1 at the first element node to +1 at the element end node. Any point on the element centroidal axis is defined by:

$$\begin{Bmatrix} x_c(\xi) \\ y_c(\xi) \\ z_c(\xi) \end{Bmatrix} = \sum_{i=1}^{m} N_i(\xi) \begin{Bmatrix} x_{ci} \\ y_{ci} \\ z_{ci} \end{Bmatrix} \tag{3.5}$$

where $N_i(\xi)$ is a Lagrangian interpolation function given by:

$$N_i(\xi) = \frac{(\xi-\xi_1)(\xi-\xi_2)..(\xi-\xi_{i-1})(\xi-\xi_{i+1})..(\xi-\xi_m)}{(\xi_i-\xi_1)(\xi_i-\xi_2)..(\xi_i-\xi_{i-1})(\xi_i-\xi_{i+1})..(\xi_i-\xi_m)} \tag{3.6}$$

Each shape function, N_i is a polynomial of degree m-1 and has the property that $N_i = 1$ for $\xi = \xi_i$ and $N_i = 0$ at all other nodes. The terms x_{ci}, y_{ci} and z_{ci} in Equation 3.5 are the global x,y and z coordinates respectively, of node i. The subscript c refers to the element centroidal axis.

3.2.2 Displacement Functions - The element displacements are interpolated with the same shape

functions used to define the element geometry (isoparametric):

$$\begin{Bmatrix} u_c(\xi) \\ v_c(\xi) \\ w_c(\xi) \end{Bmatrix} = \sum_{i=1}^{m} N_i(\xi) \begin{Bmatrix} u_{ci} \\ v_{ci} \\ w_{ci} \end{Bmatrix} \tag{3.7a}$$

$$\begin{Bmatrix} \theta_x(\xi) \\ \theta_y(\xi) \\ \theta_z(\xi) \end{Bmatrix} = \sum_{i=1}^{m} N_i(\xi) \begin{Bmatrix} \theta_{xi} \\ \theta_{yi} \\ \theta_{zi} \end{Bmatrix} \tag{3.7b}$$

where u,v,w are the displacements in the global x,y and z directions respectively of the element centroidal axis, and $\theta_x, \theta_y, \theta_z$ are the corresponding global rotations. It can be seen that the above interpolation does not use Hermitian shape functions, as would be used in the case of Euler beam theory. With Hermitian functions the displacement at any point along the beam is a function of the nodal displacements and of the first derivatives of displacements. With Timoshenko beam theory the rotation no longer corresponds to the first derivative of the total displacement and thus the displacements and rotations must be interpolated independently using Lagrangian interpolation functions.

3.2.3 Coordinate Transformation - The local and global components of displacement are related as follows:

$$\begin{Bmatrix} u'_c \\ v'_c \\ w'_c \end{Bmatrix} = [T] \begin{Bmatrix} u_c \\ v_c \\ w_c \end{Bmatrix} \tag{3.8a}$$

$$\begin{Bmatrix} \theta'_x \\ \theta'_y \\ \theta'_z \end{Bmatrix} = [T] \begin{Bmatrix} \theta_x \\ \theta_y \\ \theta_z \end{Bmatrix} \tag{3.8b}$$

where the primed terms refer to the local axes and the unprimed terms to the global axes. The above equations may be written in condensed form as:

$$\{u'\} = [H]\{u\} \tag{3.8c}$$

$$[H] = \begin{bmatrix} [T] & 0 \\ 0 & [T] \end{bmatrix} \tag{3.9}$$

The matrix of transformation, [T] , cannot be uniquely defined by the global nodal coordinates alone. Several approaches are possible in defining the information

required to generate this matrix. A common method is to give the direction cosines of the local y' or z' axes with respect to the global axes; however it is not possible to interpolate nodal direction cosines to any required point on the beam. For this reason an alternative approach is adopted in the present development. The angle, ϕ, between the local y' axis and the global xy plane is defined at each node, Figure 3.4. The magnitude of the angle may be computed at any point along the beam by interpolating between the nodal values. Thus:

$$\phi(\xi) = \sum_{i=1}^{m} N_i(\xi)\phi_i \tag{3.10}$$

Given the value $\phi(\xi)$, the transformation matrix, [T], may be defined at any point along the element. The method of computation outlined here follows closely the derivation in Jirousek's paper (25).

The matrix, [T], may be written:

$$[T] = \begin{bmatrix} \lambda_{x'x} & \lambda_{x'y} & \lambda_{x'z} \\ \lambda_{y'x} & \lambda_{y'y} & \lambda_{y'z} \\ \lambda_{z'x} & \lambda_{z'y} & \lambda_{z'z} \end{bmatrix} = \begin{bmatrix} \{\lambda_{x'}\} \\ \{\lambda_{y'}\} \\ \{\lambda_{z'}\} \end{bmatrix} \tag{3.11}$$

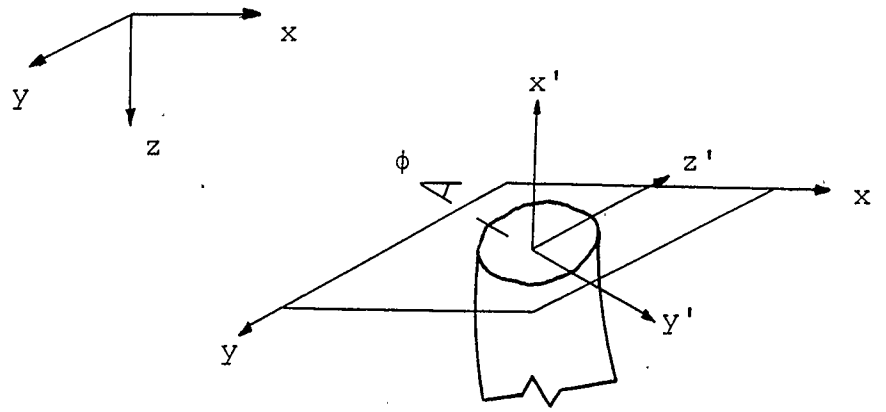

Figure 3.4 Definition of ϕ Value when a Cross Section Lies in the Global xy Plane

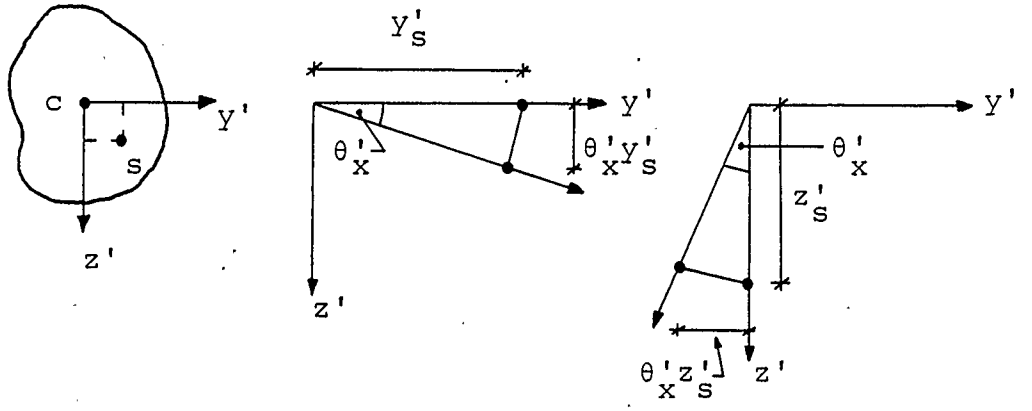

Figure 3.5 Relative Translation of the Shear Centre and Centroid due to Twisting of the Cross Section

where $\{\lambda_{x'}\}$ is the vector of direction cosines of the local x' axis with respect to the global axes. The vectors $\{\lambda_{y'}\}$ and $\{\lambda_{z'}\}$ are similarly defined. The vector $\{\lambda_{x'}\}$ is given by:

$$\{\lambda_{x'}\} = \frac{\{\hat{t}\}}{t} \tag{3.12}$$

where $$\{\hat{t}\} = \begin{Bmatrix} t_x \\ t_y \\ t_z \end{Bmatrix} = \sum_{i=1}^{m} \frac{dN_i}{d\xi} \begin{Bmatrix} x_{ci} \\ y_{ci} \\ z_{ci} \end{Bmatrix} \tag{3.13}$$

and $$t = \sqrt{t_x^2 + t_y^2 + t_z^2} \tag{3.14}$$

The method of computing $\{\lambda_{y'}\}$ depends upon the orientation of the member cross section. When t_x and t_y are not simultaneously equal to zero $\{\lambda_{y'}\}$ is computed as follows:

$$\lambda_{y'z} = \sin \phi \tag{3.15}$$

$$\lambda_{y'y} = \frac{-b \pm \sqrt{b^2 - 4ac}}{2a} \tag{3.16}$$

with $+\sqrt{}$ if $t_x > 0$ and $-\sqrt{}$ if $t_x < 0$

where $a = (t_x^2 + t_y^2)$; $b = 2t_y t_z$

and $c = t_z^2 \sin^2\phi - t_x^2 \cos^2\phi$

If $t_x \neq 0$

$$\lambda_{y'x} = -\frac{1}{t}\,(t_y\lambda_{y'y} + t_x\lambda_{y'z}) \tag{3.17a}$$

If $t_x = 0$

$$\lambda_{y'x} = \pm\sqrt{\cos^2\phi - (\lambda_{y'y})^2} \tag{3.17b}$$

with $+\surd$ if $t_y < 0$ and $-\surd$ if $t_y > 0$

For the situation where $t_x = 0$ and $t_y = 0$ the cross section is parallel to the global xy plane, Figure 3.4, and the local y'-axis lies in the xy plane. In this case ϕ must be redefined as the angle between the local y'-axis and the global x-axis. For this condition:

$$\left.\begin{aligned} \lambda_{y'x} &= \cos\phi \\ \lambda_{y'y} &= \sin\phi \\ \lambda_{y'z} &= 0 \end{aligned}\right\} \tag{3.18}$$

Having computed the vectors $\{\lambda_{x'}\}$ and $\{\lambda_{y'}\}$, the third vector of direction cosines, $\{\lambda_{z'}\}$, is computed from the vector (cross) product of the other two.

3.2.4 Cross Section Properties - The present element is valid for any compact cross section. Cross sections in which warping deformations are significant are not accurately modelled by this element. The element may be of any shape, subject to satisfying the above condition, and the cross sectional properties may vary along its length. The element cross section is normal to the centroidal axis and thus skew sections are not considered in the analysis. In formulating the element stiffness matrix the following quantities are required:

(1) Cross sectional area, A.

(2) Reduced shear areas, $A_{y'}$ and $A_{z'}$.

(3) Torsional constant, $J_{x'}$.

(4) Principal moments of inertia, $I_{y'}$ and $I_{z'}$.

(5) Local (section) coordinates of the section shear centre, y'_s and z'_s.

The above values are specified at the nodes and are interpolated to give the respective quantities at any section along the member. Thus, for cross scctional area:

$$A(\xi) = \sum_{i=1}^{m} N_i(\xi) A_i \qquad (3.19)$$

Other quantities are interpolated in the same manner.

3.2.5 Strain / Displacement Relation - The vector of generalised strains at any section in a curved beam is given by:

$$\{\varepsilon\} = \begin{Bmatrix} u'_{c,x'} \\ v'_{s,x'} - \theta'_z \\ w'_{s,x'} + \theta'_y \\ \theta'_{x,x'} \\ \theta'_{y,x'} \\ \theta'_{z,x'} \end{Bmatrix} \qquad (3.20)$$

where the subscripts c and s refer to the centroidal axis and shear centre respectively, and ,x' denotes differentiation with respect to the cross section normal. The above strain/ displacement relationship incorporates shear effects and assumes that the cross section is normal to the centroidal axis. The generalised stresses are obtained by multiplying the generalised strains by the elasticity matrix, [D], so that:

$$\{\sigma\} = [D]\{\varepsilon\} \qquad (3.21)$$

$$\text{where} \quad \{\sigma\} = \begin{Bmatrix} N_{x'} \\ V_{y'} \\ V_{z'} \\ M_{x'} \\ M_{y'} \\ M_{z'} \end{Bmatrix}$$

$$\text{and} \quad [D] = \begin{bmatrix} EA & & & & & \\ & GA_{y'} & & & & \\ & & GA_{z'} & & & \\ & & & GJ_{x'} & & \\ & & & & EI_{y'} & \\ \text{Elements not shown are zero} & & & & & EI_{z'} \end{bmatrix}$$

The term $N_{x'}$ is the axial force; $V_{y'}$ and $V_{z'}$ are shear forces in the local y' and z' directions respectively; $M_{x'}$ is the torsional moment about an axis through the shear centre, and $M_{y'}$ and $M_{z'}$ are bending moments about the local y' and z' axes respectively. The terms of the [D] matrix are as previously defined.

The strain vector in Equation 3.20 is given in terms of displacements in the local coordinate system. These are

obtained via Equation 3.8. The terms v'_s and w'_s are given by the following relation, see also Figure 3.5:

$$\begin{Bmatrix} v'_s \\ w'_s \end{Bmatrix} = \begin{Bmatrix} v'_c \\ w'_c \end{Bmatrix} + \theta'_x \begin{Bmatrix} -z'_s \\ y'_s \end{Bmatrix} \tag{3.22}$$

Inspection of the strain vector reveals that the differentiation of the displacements is with respect to the cross section normal x'; however, the displacement at any point along the beam is known only as a function of the natural coordinate, ξ. Thus for this element, as for all elements based on the isoparametric formulation, a scaling factor or Jacobian of transformation between the coordinate systems must be defined. Invoking the chain rule of differentiation yields:

$$\frac{d}{dx'} = \frac{d\,\xi}{dx'}\,\frac{d}{d\,\xi} = \frac{1}{t}\,\frac{d}{d\,\xi} \tag{3.23}$$

$$\text{where} \quad t = \sqrt{t_x^2 + t_y^2 + t_z^2} \tag{3.24}$$

$$\text{and} \quad \begin{Bmatrix} t_x \\ t_y \\ t_z \end{Bmatrix} = \sum_{i=1}^{m} \frac{dN_1(\xi)}{d\xi} \begin{Bmatrix} x_{ci} \\ y_{ci} \\ z_{ci} \end{Bmatrix} \tag{3.25}$$

It can be seen that Equations 3.24 and 3.25 are identical to Equations 3.14 and 3.15 respectively.

The terms of the strain matrix are now expanded. The dependence upon ξ has been omitted for clarity and simplicity. Using Equations 3.7 and 3.8:

$$\begin{Bmatrix} u'_c \\ v'_c \\ w'_x \end{Bmatrix} = [T] \sum_{i=1}^{m} N_i \begin{Bmatrix} u_{ci} \\ v_{ci} \\ w_{ci} \end{Bmatrix} \tag{3.26}$$

$$\text{Therefore} \quad \begin{Bmatrix} u'_{c,x'} \\ v'_{c,x'} \\ w'_{c,x'} \end{Bmatrix} = \frac{1}{t} [T] \sum_{i=1}^{m} \frac{dN_1}{d\xi} \begin{Bmatrix} u_{ci} \\ v_{ci} \\ w_{ci} \end{Bmatrix} \tag{3.27}$$

$$\text{Also} \quad \begin{Bmatrix} \theta'_x \\ \theta'_y \\ \theta'_z \end{Bmatrix} = [T] \sum_{i=1}^{m} N_i \begin{Bmatrix} \theta_{xi} \\ \theta_{yi} \\ \theta_{zi} \end{Bmatrix} \tag{3.28}$$

From Equation 3.22:

$$v'_s = v'_c - \theta'_x z'_s$$

$$v'_{s,x'} = \frac{dv'_c}{dx'} - \frac{d}{dx'}(\theta'_x z'_s)$$

$$= v'_{c,x'} - (\theta'_x z'_{s,x'} + z'_s \theta'_{x,x'}) \tag{3.29}$$

From Equation 3.28 may be written:

$$\theta'_x = \{\lambda_{x'}\} \sum_{i=1}^{m} N_i \begin{Bmatrix} \theta_{xi} \\ \theta_{yi} \\ \theta_{zi} \end{Bmatrix} \tag{3.30}$$

where $\{\lambda_{x'}\}$ has been previously defined in Equation 3.11.

Thus:

$$\theta'_{x,x'} = \frac{1}{t}\{\lambda_{x'}\} \sum_{i=1}^{m} \frac{dN_i}{d\xi} \begin{Bmatrix} \theta_{xi} \\ \theta_{yi} \\ \theta_{zi} \end{Bmatrix} \tag{3.31}$$

From Equation 3.19 z'_s is given by:

$$z'_s = \sum_{i=1}^{m} N_i z'_{si} \tag{3.32}$$

and thus

$$z'_{s,x'} = \frac{1}{t} \sum_{i=1}^{m} \frac{dN_i}{d\xi} z'_{si} \tag{3.33}$$

The above derivation is repeated in the following:

$$w'_s = w'_c + \theta'_x y'_s$$

$$w'_{s,x'} = w'_{c,x'} + (\theta'_x y'_{s,x'} + y'_s \theta'_{x,x'}) \tag{3.34}$$

From Equation 3.19:

$$y'_s = \sum_{i=1}^{m} N_i y'_{si} \tag{3.35}$$

$$y'_{s,x'} = \frac{1}{t} \sum_{i=1}^{m} \frac{dN_i}{d\xi} y'_{si} \tag{3.36}$$

The strain displacement relation is given by:

$$\{\varepsilon\} = [B]\{u\} \tag{3.37}$$

where $\{u\}$ is the vector of nodal displacements. Using Equations 3.27 to 3.36 the strain displacement matrix may be written in expanded form as:

$$[B] = \begin{bmatrix} \begin{array}{cc} \begin{array}{cc} \qquad\qquad\qquad i = 1 & \qquad\qquad\qquad i = 2 \end{array} \\ \begin{bmatrix} \begin{bmatrix} \\ \frac{dN_2}{d\xi}[T] \\ \\ \end{bmatrix}_{3x3} & \begin{bmatrix} 0 \\ -t\,N_1[\lambda_{z'}] - \frac{dz_{s'}}{d\xi} N_1 [\lambda_{x'}] - z_{s'} \frac{dN_1}{d\xi} [\lambda_{x'}] \\ t\,N_1[\lambda_{y'}] + \frac{dy_{s'}}{d\xi} N_1 [\lambda_{x'}] + y_{s'} \frac{dN_1}{d\xi} [\lambda_{x'}] \end{bmatrix}_{3x3} \\ \begin{bmatrix} 0 \end{bmatrix}_{3x3} & \begin{bmatrix} \frac{dN_1}{d\xi}[T] \end{bmatrix}_{3x3} \end{bmatrix} & \begin{bmatrix} \\ \\ \\ \end{bmatrix} \end{array} \cdots \end{bmatrix} \tag{3.38}$$

3.2.6 <u>Element Stiffness Matrix</u> - The element stiffness matrix is computed in standard finite element fashion:

$$[S] = \int_0^{\ell} [B]^T [D] [B] \, d\ell \tag{3.39}$$

or $$[S] = \int_{-1}^{+1} [B]^T [D] [B] \, t d\xi \tag{3.40}$$

Numerical integration is required to integrate the expression above. Gaussian quadrature is used, the order of which depends on the order of the shape functions in the [B] matrix. In the present analysis the highest order term resulting from the product $[B]^T[D][B]$ is $N_i N_j$. Thus for

example, in the case of a five node element $N_i(\xi)$ is quartic and the term $N_i N_j$ is eighth order. Gaussian integration using k sample points can exactly integrate a polynomial of order 2k - 1 (12), so that for exact integration of an eighth order function five point integration is required.

In certain cases a reduced order of integration may give results which are as accurate, or even more accurate than exact integration (5). This is the result of the softening effect of reduced integration countering the inherent over-stiffness of a finite element discretization. While an order of integration one less than that required for exact integration gave exact results with the present element, a reduction of two in the order of integration in many cases gave completely erroneous results. It is felt that the extra computing cost of exact integration in the present element is minimal, and that there is therefore no benefit in using a reduced order of integration.

3.2.7 Consistent Nodal Load Vector - Consistent nodal loads are computed in the usual way. In the case of distributed forces or couples, the consistent load vector is given by:

$$\{F\} = \int_{-1}^{+1} \{N(\xi)\}\, q(\xi)\, t\, d\xi \qquad (3.41)$$

The vector $\{N(\xi)\}$ is a vector of nodal interpolation functions at the appropriate Gauss point, and $q(\xi)$ is the magnitude of the distributed load at that point. For simplicity, the same order of quadrature is used in computing the consistent load vector as is used to generate the element stiffness matrix, even though a lower order of integration would be adequate.

The consistent load vector due to a concentrated force or couple, f, applied to any point on the element is given by:

$$\{F\} = \{N(\xi)\}\ f \qquad (3.42)$$

where $\{F\}$ and $\{N(\xi)\}$ are as previously defined.

3.3 Prestressing Effects

3.3.1 Introduction - In the analysis of any prestressed bridge it is necessary to include the forces induced by prestressing. Ideally a computer program should be able to compute automatically the loads due to different arrangements of cables so that the design engineer may analyse different cable profiles, with different prestressing forces, without having to recompute loads for each individual case. In the present computer program the effects of prestressing are modelled as element nodal

loads. The following assumptions are adopted (8,26):

(1) The cross sectional areas of cables, cable ducts and non prestressed steel are not considered when computing cross section properties.

(2) The cable forces are not affected by instantaneous or time dependent shortening of the structure.

The first assumption means that the element stiffness matrix is unaffected by the number of and location of the prestressing cables, or the non prestressed steel. Thus different cable layouts are analysed as separate load cases without having to recompute the structural stiffness matrix for each alternative cable profile.

The method of computing prestressing forces that is used in the present analysis is more general than the traditional load balancing technique (29). As demonstrated by Rozvany (36), the load balancing technique does not give a rigourous mathematical solution but is satisfactory for shallow beams. For deeper beams it becomes less accurate to assume that the radial forces due to the cable curvature are vertical, Figure 3.6. According to Leonhardt (28), the non verticality of the distributed cable forces should be considered where the sag to span ratio exceeds 1:12. In the present analysis no such limitation exists because the exact loads due to prestressing are computed from first principles.

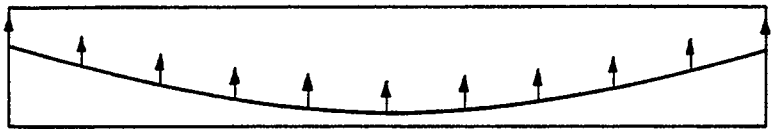

Commonly Assumed Vertical Load Distribution

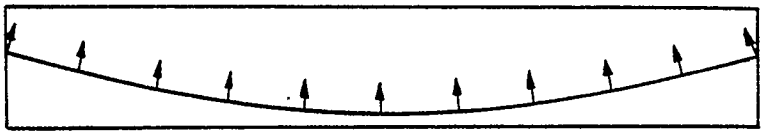

Actual Radial Load Distribution Adopted in Present Work

Figure 3.6 Assumed and Actual Force Distribution due to Curvature of a Prestressing Cable

3.3.2 Geometric Description - When computing forces due to prestressing on a curved beam element, the first problem is to define the cable's location in space and its location relative to the centroidal axes of the element. If the global coordinates of the cable at the element nodal cross sections are known, the cable may be defined in space by the relation:

$$\begin{Bmatrix} x_p \\ y_p \\ z_p \end{Bmatrix} = \sum_{i=1}^{m} N_i(\chi) \begin{Bmatrix} x_{pi} \\ y_{pi} \\ z_{pi} \end{Bmatrix} \tag{3.43}$$

where the subscript p refers to the prestressing cable. The shape functions $N_i(\xi)$ are the same polynomials defined by Equation 3.6. If the cable passes through the end cross sections of the element, Figure 3.7a, the natural coordinate, χ, of the cable corresponds to ξ, the natural coordinate of the beam centroid. This correspondence is assumed in the following development and thus ξ is used throughout. Cables not anchored at element ends are not considered in the analysis, Figure 3.7b.

In the computer program SFRAME (19), the eccentricities of the cable with respect to the principal axes of the section are given in the input data at each node. The global coordinates may be computed using the following relation:

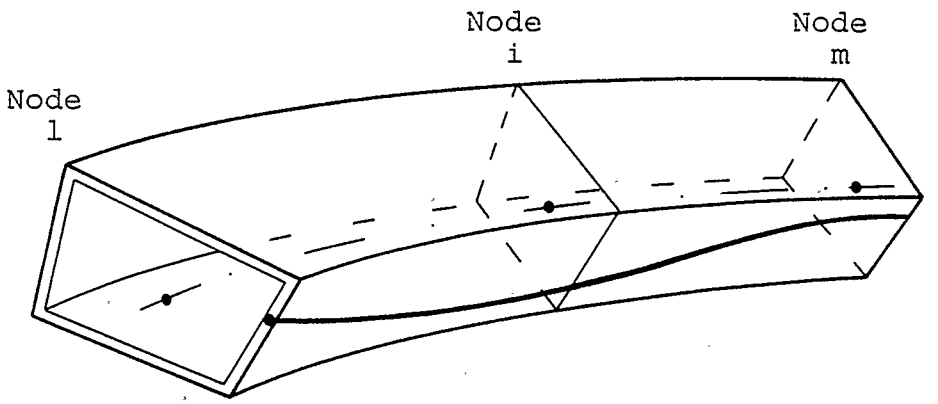

(a) Permissible Cable Profile

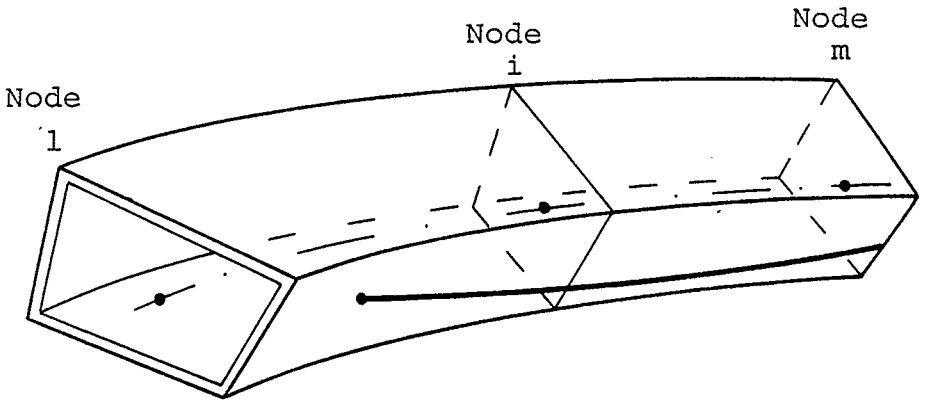

(b) Invalid Cable Profile (Cable Anchorage Point does not coincide with the end node of an element)

Figure 3.7 A Cable Profile to be Used with the Jirousek Curved Beam Element

$$\begin{Bmatrix} x_{pi} \\ y_{pi} \\ z_{pi} \end{Bmatrix} = \begin{Bmatrix} x_{ci} \\ y_{ci} \\ z_{ci} \end{Bmatrix} + [K]_i \begin{Bmatrix} e'_{yi} \\ e'_{zi} \end{Bmatrix} \qquad (3.44)$$

where $\begin{Bmatrix} x_{pi} \\ y_{pi} \\ z_{pi} \end{Bmatrix}$ are the global coordinates of the cable at node i,

$\begin{Bmatrix} x_{ci} \\ y_{ci} \\ z_{ci} \end{Bmatrix}$ are the global coordinates of the element centroidal axis at node i,

and $\begin{Bmatrix} e'_{yi} \\ e'_{zi} \end{Bmatrix}$ are the cable eccentricities in the y' and z' directions at node i.

The matrix of transformation [K] is a 3x2 matrix given by:

$$[K]_i = \begin{bmatrix} \lambda_{y'x} & \lambda_{z'x} \\ \lambda_{y'y} & \lambda_{z'y} \\ \lambda_{y'z} & \lambda_{z'z} \end{bmatrix} = [\{\lambda_{y'}\} \{\lambda_{z'}\}] \qquad (3.45)$$

where $\{\lambda_{y'}\}$ and $\{\lambda_{z'}\}$ are the vectors of direction cosines of the local y' and z' axes at the given section, as previously defined in Equation 3.11.

The shape functions $N_i(\xi)$ are also used to define the prestressing force in the cable at any point along the cable length. The cable force is defined at each element node and is interpolated in the usual manner:

$$P(\xi) = \sum_{i=1}^{m} N_i(\xi) P_i \qquad (3.46)$$

where P represents the absolute value of the prestressing force.

3.3.3 Cable Anchorage Loads - The element loads due to prestressing consist of:

(1) Point loads at anchorages and,

(2) Distributed line loads along the cable

Any element within the structure may contain anchorage points. These points must coincide with an external node of the element. The anchorage loads are tangential to the cable axis at the nodal cross section and may be resolved into global components using the relation:

$$\{F\}_i = \begin{Bmatrix} F_1 \\ F_2 \\ F_3 \end{Bmatrix}_i = P_i \{\lambda_{ct}\}_i \tag{3.47}$$

where the subscript i refers to the ith node and $\{\lambda_{ct}\}$ is a unit vector tangential to the cable at the appropriate node. It is obtained from the following equations:

$$\{\hat{t}\} = \begin{Bmatrix} t_x \\ t_y \\ t_z \end{Bmatrix} = \sum_{i=1}^{m} \frac{dN_i}{d\xi} \begin{Bmatrix} x_{pi} \\ y_{pi} \\ z_{pi} \end{Bmatrix} \tag{3.48}$$

$$t = \sqrt{t_x^2 + t_y^2 + t_z^2} \tag{3.49}$$

$$\{\lambda_{ct}\} = \frac{\{\hat{t}\}}{t} \tag{3.50}$$

The vector of nodal forces may be transformed into local coordinates using the familiar relation:

$$\begin{Bmatrix} F'_1 \\ F'_2 \\ F'_3 \end{Bmatrix}_i = [T]_i \begin{Bmatrix} F_1 \\ F_2 \\ F_3 \end{Bmatrix}_i \tag{3.51}$$

where [T] is the transformation matrix given by Equation 3.11.

The nodal moments are computed using the following equations, see Figure 3.8:

$$\left.\begin{aligned} F'_{4(1)} &= - F'_{2(1)}\ e'_{z1} + F'_{3(1)}\ e'_{y1} \\ F'_{5(1)} &= F'_{1(1)}\ e'_{z1} \\ F'_{6(1)} &= - F'_{1(1)}\ e'_{y1} \end{aligned}\right\} \tag{3.52a}$$

$$\left.\begin{aligned} F'_{4(m)} &= - F'_{2(m)}\ e'_{zm} + F'_{3(m)}\ e'_{ym} \\ F'_{5(m)} &= F'_{1(m)}\ e'_{zm} \\ F'_{6(m)} &= -F'_{1(m)}\ e'_{ym} \end{aligned}\right\} \tag{3.52b}$$

where the subscripts 1 and m refer to the first and last nodes, respectively, of the cable. The forces and moments at the anchorage nodes are transformed back into global

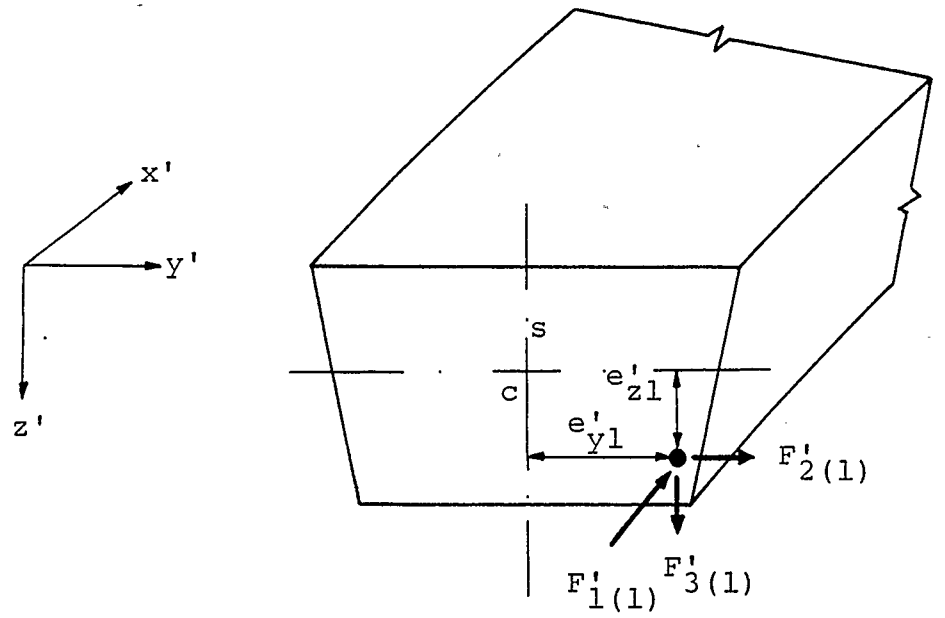

(a) Cable Anchorage Point at the First Node of an Element

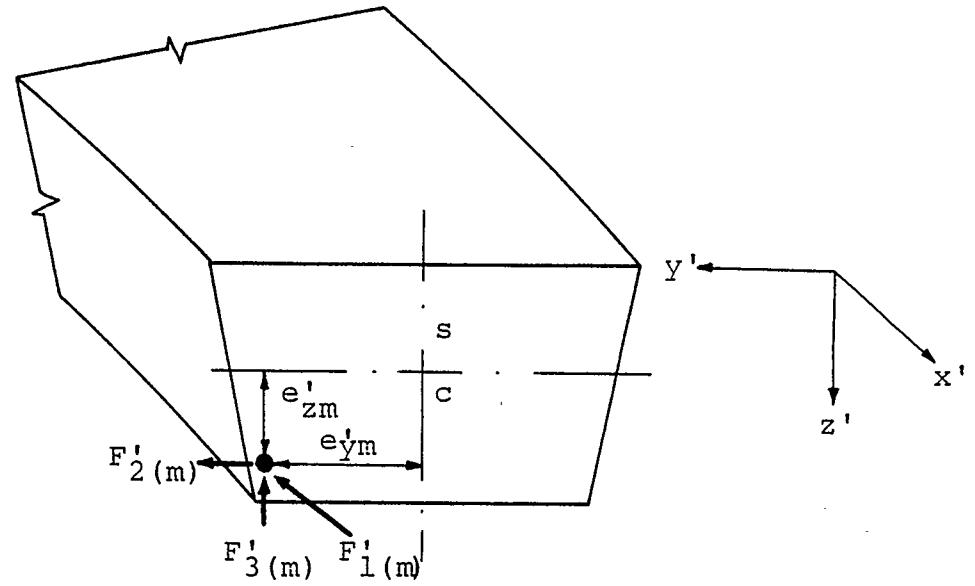

(b) Cable Anchorage at the End Node of an Element

Figure 3.8 Forces at Cable Anchorage Points

components for assembly in the overall load vector by the equation:

$$\{F\} = [L]\{F'\} \tag{3.53}$$

where $\{F\}$ and $\{F'\}$ are the vectors of anchorage forces and moments in the global and local coordinate systems respectively; and

$$[L] = \begin{bmatrix} [T]^T & 0 \\ 0 & [T]^T \end{bmatrix}$$

3.3.4 Distributed Forces Due to Prestressing - The distributed load due to the effects of a prestressing cable has two components, tangential and normal. The tangential component is due to the variation in prestressing force along the cable length and is given by (8):

$$P_t = \frac{dP}{ds} \tag{3.54}$$

The normal component is due to the curvature of the cable and is given by:

$$P_n = \frac{P}{R} \tag{3.55}$$

where R is the radius of principal curvature, in space, of the cable at the point in question.

The basic equations in the following analysis may be found in standard analytic geometry texts (34,44). The expression for the tangential component of distributed load at a point may be expanded to give:

$$\frac{dP}{ds} = \frac{d\xi}{ds}\frac{dP}{d\xi} = \frac{1}{t}\frac{dP}{d\xi} \tag{3.56}$$

where t is the magnitude of the tangent vector to the cable at the given point. Using Equation 3.44 the expression may be further expanded to give the value of tangential force/unit length due to prestressing:

$$P_t = -\frac{1}{t}\frac{dP}{d\xi} = -\frac{1}{t}\sum_{i=1}^{m}\frac{dN_i}{d\xi}P_i \tag{3.57}$$

Calculation of the normal component of distributed load requires the computation of the radius of principal curvature at the point in question. The radius of principal curvature of a curve in space, at any point on the curve, is equal to the reciprocal of the magnitude of the principal normal vector at that point, Figure 3.9. The principal normal vector is obtained from the following equation:

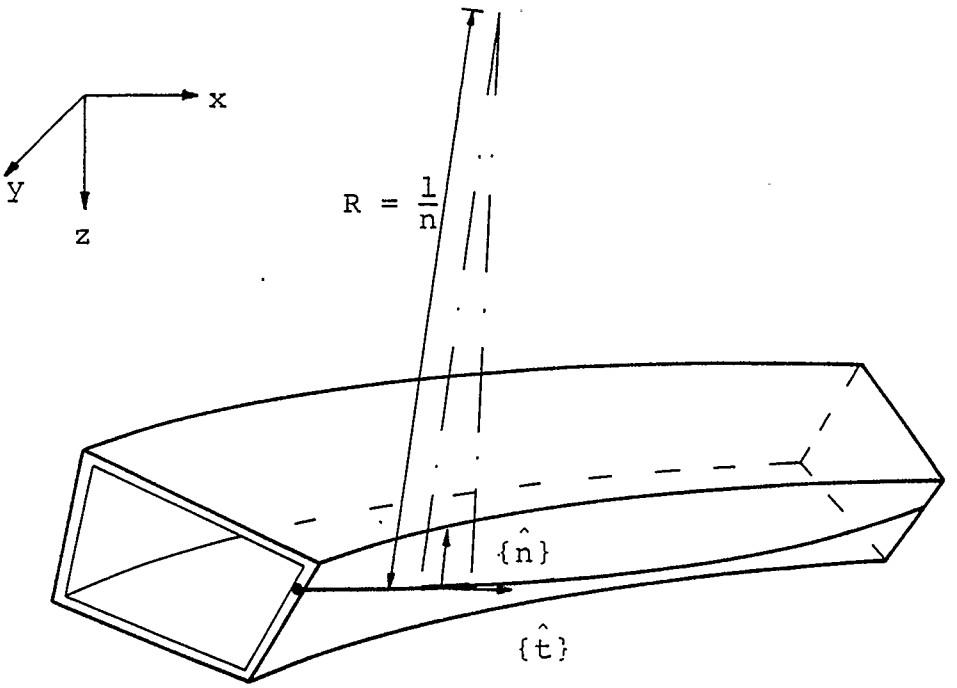

Figure 3.9 Principal Normal and Tangent Vectors to a Cable in Space

$$\{\hat{n}\} = \frac{1}{t^2}\left(\frac{d^2}{d\xi^2}\{X_p\} - \frac{a}{t^2}\frac{d}{d\xi}\{X_p\}\right) \tag{3.58}$$

where $$\{X_p\} = \begin{Bmatrix} x_p \\ y_p \\ z_p \end{Bmatrix}$$

the vector of global coordinates of the point on the cable. The coefficient a is defined by:

$$a = \frac{d^2}{d\xi^2}\{X_p\} \cdot \frac{d}{d\xi}\{X_p\} \tag{3.59}$$

which is the dot product of the first and second derivatives of the vector of global coordinates at the point. The magnitude of $\{n\}$ is denoted by n so that the unit normal vector is:

$$\{\lambda_{cn}\} = \frac{\{\hat{n}\}}{n} \tag{3.60}$$

The unit normal vector is orthogonal to the unit tangent vector, $\{\lambda_{c_t}\}$, defined in Equation 3.50. The normal component of distributed load may now be defined as:

$$P_n = \frac{P}{R} = nP \tag{3.61}$$

It is of interest to note that the above vectorial formulation yields identical results to the equation given in Rozvany's discussion of Lin's paper (36).

The global components of the distributed loads at the point may now be obtained as follows:

$$\{P\} = \begin{Bmatrix} P_x \\ P_y \\ P_z \end{Bmatrix} = P_t\{\lambda_{ct}\} + P_n\{\lambda_{cn}\} \tag{3.62}$$

The load vector is transformed into local coordinates at the section in question using Equation 3.51. Equation 3.52a may then be employed to compute the magnitude of the distributed moment vector at the section. Forces and moments are transformed back into global coordinates using Equation 3.53.

The equivalent nodal loads are computed via:

$$\{F\} = \int_{-1}^{+1} \{N(\xi)\}\ \{P(\xi)\}\ t\,d\xi \tag{3.63}$$

Numerical integration is again required to compute the above integral.

3.4 Short Term Prestress Losses

Short term prestress losses in post-tensioned beams derive from two sources; friction between the tendon and the duct, and anchorage slip at the time of jacking. Both factors are incorporated into the automatic prestressing option of SFRAME. The program assumes that all tendons are stressed simultaneously, and that therefore, there are no losses due to sequential tensioning.

3.4.1 Friction Loss - Frictional loss is made up of two components, the wobble effect and the curvature effect. The wobble effect is the amount of friction loss in an equivalent straight tendon and is due to misalignments and imperfections in the ducts or sheathing surrounding the tendon. Because of imperfections in the duct some friction exists between the tendon and the surrounding material.

The curvature effect results from the intended curvature of the tendons. The force in a tendon at a point j, a distance s along the cable from the jacking end, Figure 3.10, is given by (31):

$$P_j = P_o \, e^{-(\mu\alpha + \kappa s)} \qquad (3.64)$$

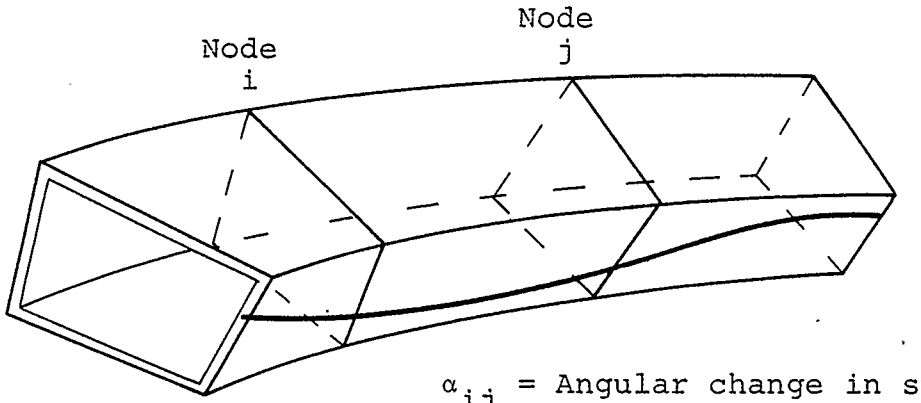

α_{ij} = Angular change in space between nodes i and j

s_{ij} = Distance, measured along cable between nodes i and j

Figure 3.10 Definition of Terms, α_{ij} and s_{ij}

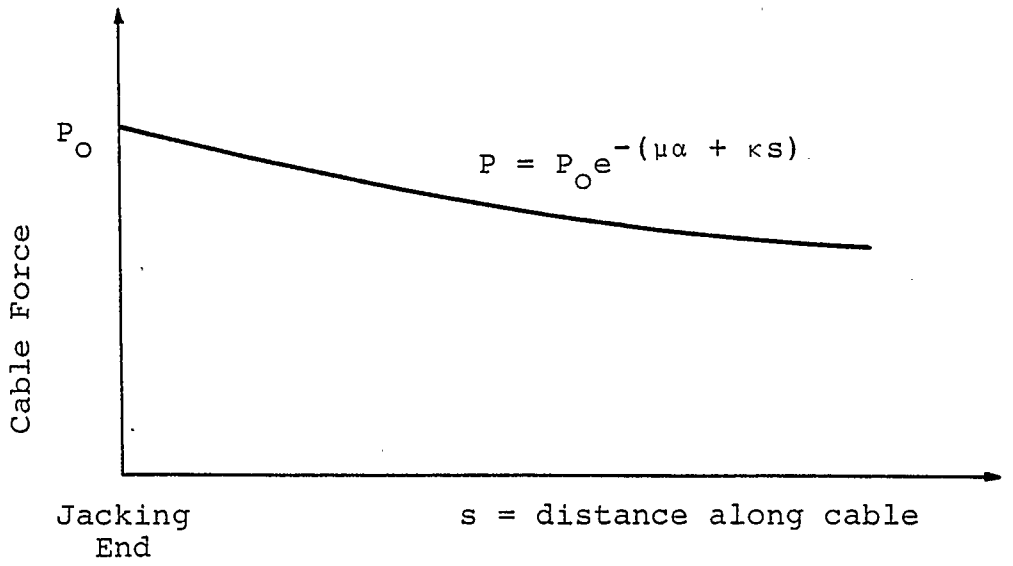

Figure 3.11 Typical Force Variation Along a Prestressing Cable

where P = jacking force

μ = curvature friction coefficient

α = angular change in radians between the anchorage and point j

k = wobble coefficient

In the present analysis the jacking force and friction coefficients are given as input data. The angle α, and distance s, along the cable are computed between each pair of nodal points, i and j, on the multi node beam element, Figure 3.10. The appropriate equations are:

$$\alpha_{ij} = \cos^{-1} (\{\lambda_{ct}\}_i \cdot \{\lambda_{ct}\}_j) \tag{3.65}$$

$$s_{ij} = \int_i^j ds \tag{3.66}$$

where the . refers to scalar product. The vector $\{\lambda_{ct}\}_i$, defined in Equation 3.50, is a unit tangent vector to the cable at point i. The individual components of the vector represent the direction cosines of the cable at the point. The product of the direction cosines of any two vectors gives the cosine of the angle in space between the vectors.

Two point Gaussian quadrature, adequate to exactly integrate a cubic function, is used in Equation 3.65.

Using Equation 3.64 the variation of prestressing force along the cable is computed. The resulting exponential curve, Figure 3.11, is a more accurate representation of the variation in force than is the stepped variation obtained using the method adopted by Scordelis et al. (38). This latter variation results from the angular changes in the cable being lumped at the ends of the straight chord segments used in the analysis.

A further point of interest relates to the recommendations which exist in some codes of practice regarding the computation of the total angle subtended in space by a prestressing cable. The Ontario Bridge Code (33), states that for a cable with both vertical and horizontal components of angular change, the components in the two planes should be summed vectorially. The ACI Bridge Code (2), and the ACI Manual of Concrete Practice (1), on the other hand state that the total angle is computed by summing directly the vertical and horizontal anglular change. This latter approach is invalid, as can be easily demonstrated by reference to Figure 3.12. The bridge shown is a simply supported box section with webs inclined at 30° to the vertical. On the basis of the ACI recommendations, the total change in angle along the cable is given by the sum of the vertical and horizontal angular changes, i.e.

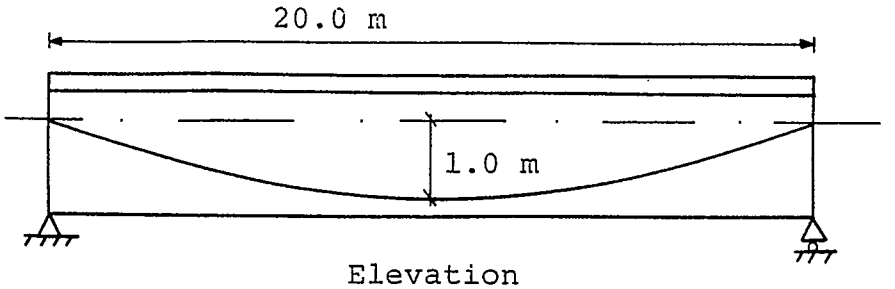

Elevation

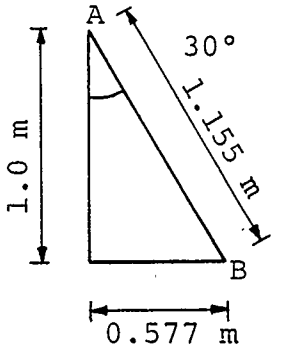

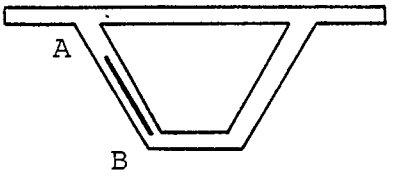

Section

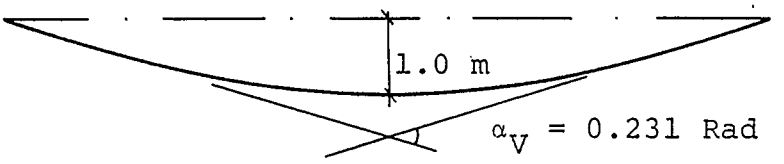

Vertical Projection of Cable

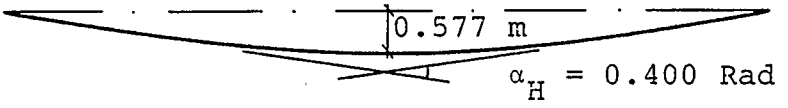

Horizontal Projection of Cable

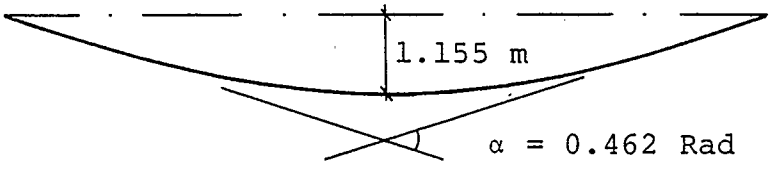

Profile of Cable in Plane AB

Figure 3.12 A Prestressing Cable with Both Vertical and Horizontal Components of Angular Change

$$\alpha = \alpha_V + \alpha_H$$

This gives a total change in angle of 0.631 radians, which is 37% greater than would be obtained by summing the angles vectorially as suggested in the Ontario code. A vectorial addition of the components obviously gives the same change in angle as would be obtained if the cable lay in a vertical plane. It is certainly erroneous to suggest that the magnitude of the angular change along a cable profile, within a particular plane, is altered by the rotation of the plane in space. This is the implication of the approach adopted in the ACI code.

In using SFRAME this obvious contradiction is not encountered, since the program computes exact angular changes automatically without the designer being required to calculate vertical and horizontal components. All that is required is that the designer input the required cable eccentricities at each node.

3.4.2 Anchorage Slip Losses - Losses due to anchor slip occur in post-tensioned members when the jacking force is transferred to the anchorage. A small slipping occurs before the development of full gripping of the tendon. The loss of prestress due to anchorage slip may be particularly severe in short members (31). When the anchor slips a

distance $\Delta\ell$ the jacking force drops and the frictional force reverses direction over the distance c shown in Figure 3.13. The exponential variation of prestressing force along the cable may be approximated with sufficient accuracy over the distance in question by a straight line. ΔP represents the drop in prestressing force at the anchorage. The lines AC and BC have equal and opposite slopes so that:

$$\Delta P' = 2cP' \tag{3.67}$$

where $P' = \frac{dP}{ds}$

The anchor slip may be approximated by:

$$\Delta\ell = \frac{1}{E_{ps} A_{ps}} \left(\frac{\Delta Pc}{2}\right) \tag{3.68}$$

where E_{ps} and A_{ps} are the Young's modulus and cross sectional area, respectively, of the prestressing steel. The term in brackets is equal to the area of the triangle ABC. Combining Equations 3.67 and 3.68 gives:

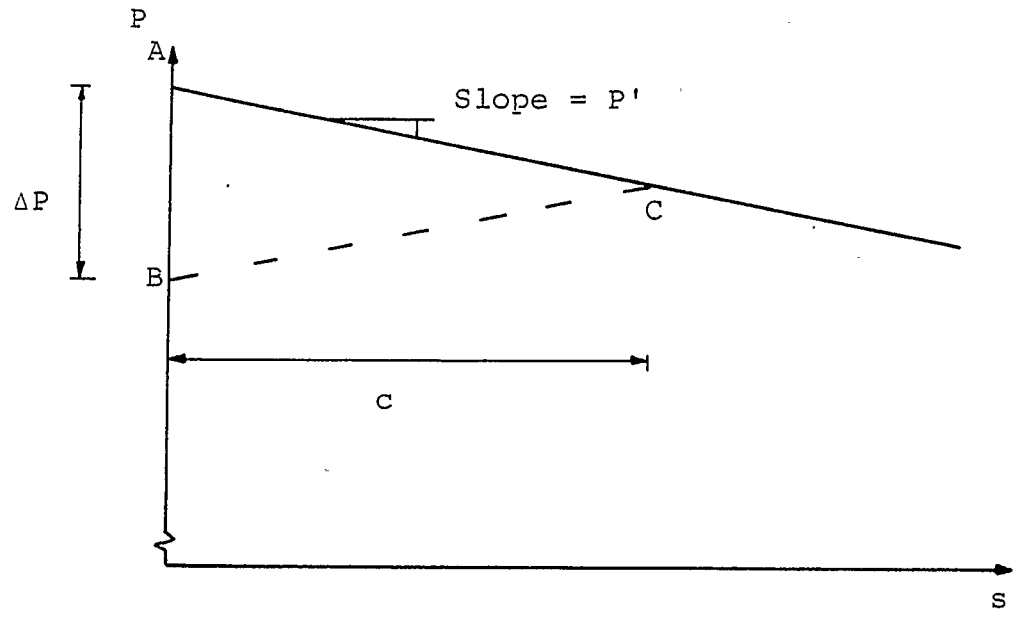

(a), $c < \ell$

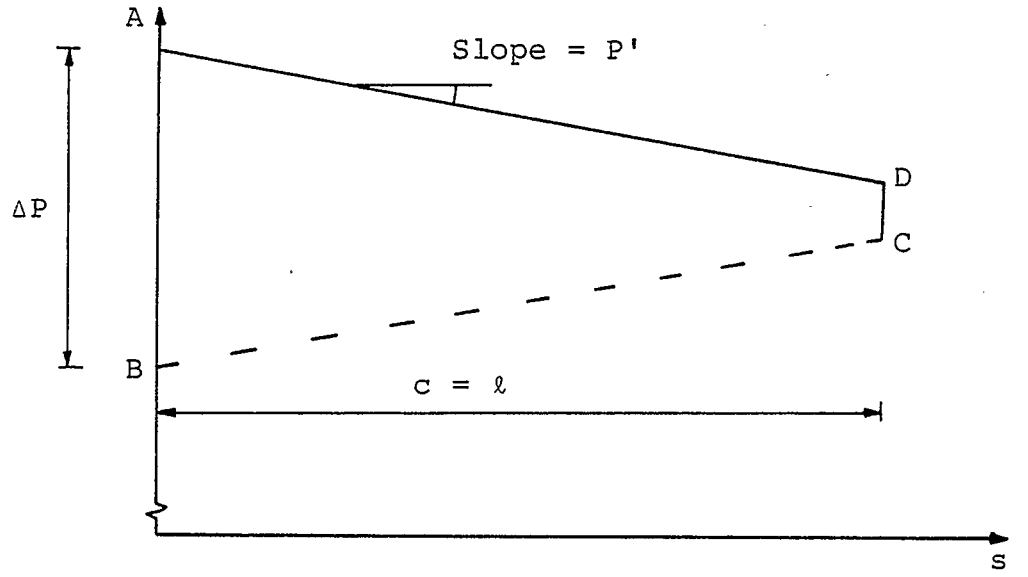

(b) $c = \ell$

Figure 3.13 Prestress Loss Due to Anchorage Slip

$$c = \sqrt{\frac{E_{ps} A_{ps} \Delta\ell}{2}} \tag{3.69}$$

If the tendon is short c may be greater than the total length, ℓ, of the tendon. In this case:

$$\Delta\ell = \frac{1}{E_{ps} A_{ps}} [(\Delta P - P'\ell)\ell] \tag{3.70}$$

where the term in square brackets is equal to the area ABCD, Figure 3.13b. The loss of prestressing force in this case is given by:

$$\Delta P = \frac{E_{ps} A_{ps} \Delta\ell}{\ell} + P'\ell \tag{3.71}$$

The procedure above is programmed in SFRAME. On computing ΔP the prestressing force at all points between the anchorage and point C are modified by the appropriate amount. The program can accomodate tendons which are jacked from either end or from both ends.

3.5 Concluding Remarks

In this chapter the development of the Jirousek beam element is outlined in detail. The use of Timoshenko beam theory and isoparametric finite element methodology are successfully combined to give an element which offers excellent potential for the analysis of curved bridge structures.

The element formulation has been extended to include the option of automatic computation of forces due to prestressing. Such an addition is vital for the analysis of curved prestressed bridges. The method adopted exactly models curved cable geometries, and as will be shown in Chapter Five gives very accurate results. Advantage is taken of the accurate geometric description of a cable in space to compute prestress frictional losses. Using this technique, no problems occur with respect to computing the vertical and horizontal components of angular change along a cable.

CHAPTER FOUR

VERIFICATION OF ELEMENT BEHAVIOUR

4.1 Introduction

The present chapter is a divergence from the principal direction of the thesis, in order to investigate the performance of the Jirousek beam element. The purpose of checking the element's behaviour is twofold. Firstly, it is important to verify that the formulation of the element stiffness matrix has been programmed correctly: this is achieved by demonstrating that the element gives exact results under simple load conditions. Secondly it is necessary to check that the element behaves in the manner expected, and to identify appropriate conditions for the suitable use of the element.

In its simplest form the isoparametric element reduces to a straight beam. To facilitate analysis by hand and comparison of results, the element behaviour is investigated using straight simply supported and cantilever beams. The following examples are considered, Figure 4.1:

(1) A 4 node single element cantilever, with a point load at the tip.

(2) A 5 node single element cantilever, with a point load at the tip.

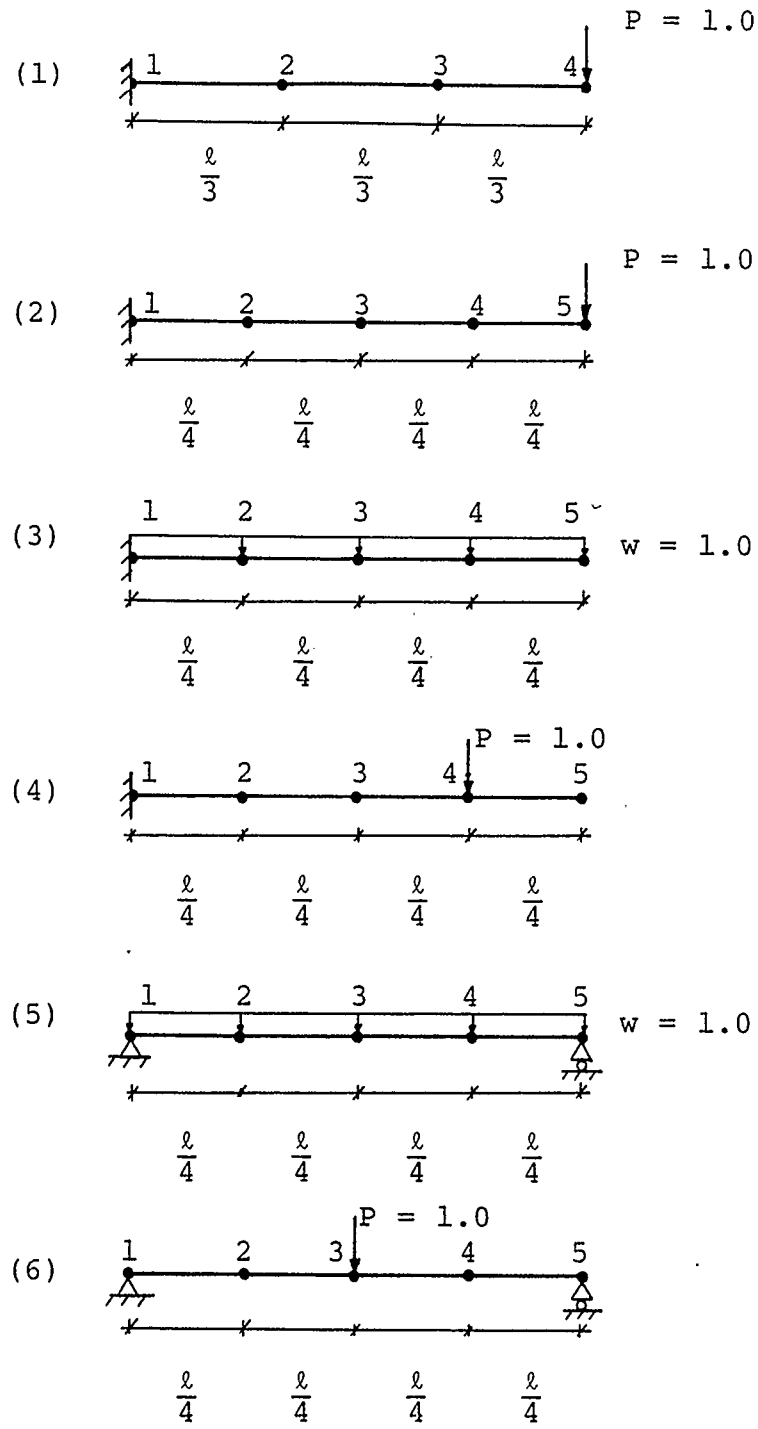

For all Cases

$\ell = 2.0$
$A_r = 1.0$
$I = 0.1$
$E = 1.0$
$\nu = 0.0$

Figure 4.1 Examples Used to Check Behaviour of Jirousek Element

(3) A 5 node single element cantilever, with a uniformly distributed load along its length.

(4) A 5 node single element cantilever, with a point load at the node next to the tip.

(5) A 5 node single element simple beam, with a uniformly distributed load along its length.

(6) A 5 node single element simple beam, with a point load at midspan.

The results of these examples are summarized in Tables 4.1 to 4.6.

4.2 Results of Single Element Examples

For Examples 1 and 2 (end loaded cantilevers) the results obtained are in exact agreement with the correct values. In the case of the 4 node cantilever the assumed deflection and rotation fields are cubic. The equation of the deflected beam is obtained from the computed displacements:

$$w = -1.667x^3 + 10.0x^2 + 2.0x \qquad (4.1)$$

where x is the distance from the left end to any section. The beam rotation equation may also be computed using the results in Table 4.1:

Node	Displacements		Stress Resultants	
	Deflection	Rotation	Shear	Moment
	Bar Elements			
1	0.	0.	1.0	-2.0
2	5.288	-11.116	1.0	-1.333
3	16.495	-17.778	1.0	-0.667
4	30.672	-20.0	1.0	0.0
	Jirousek Element			
1	0.0	0.0	1.0	-2.0
2	5.288	-11.116	1.0	-1.333
3	16.495	-17.778	1.0	-0.667
4	30.672	-20.0	1.0	0.0

Table 4.1 - 4 Node Cantilever, Example 1, Figure 4.1

Node	Displacements		Stress Resultants	
	Deflection	Rotation	Shear	Moment
	Bar Elements			
1	0.0	0.0	1.0	-2.0
2	3.292	-8.75	1.0	-1.5
3	10.334	-15.0	1.0	-1.0
4	19.875	-18.75	1.0	-0.5
5	30.672	-20.0	1.0	0.0
	Jirousek Element			
1	0.0	0.0	1.0	-2.0
2	3.292	-8.75	1.0	-1.5
3	10.334	-15.0	1.0	-1.0
4	19.875	-18.75	1.0	-0.5
5	30.672	-20.0	1.0	0.0

Table 4.2 - 5 Node Cantilever, Example 2, Figure 4.1

Node	Displacements		Stress Resultants	
	Deflection	Rotation	Shear	Moment
	Bar Elements			
1	0.0	0.0	2.0	-2.0
2	3.859	-7.708	1.5	-1.125
3	10.083	-11.667	1.0	-0.5
4	17.109	-13.125	0.5	-0.125
5	24.0	-13.333	0.0	0.0
	Jirousek Element			
1	0.0	0.0	2.0	-2.0
2	3.859	-7.708	1.5	-1.125
3	10.083	-11.667	1.0	-0.5
4	17.109	-13.125	0.5	-0.125
5	24.0	-13.333	0.0	0.0

Table 4.3 - 5 Node Cantilever, Example 3, Figure 4.1

Node	Displacements		Stress Resultants	
	Deflection	Rotation	Shear	Moment
	Bar Elements			
1	0.0	-3.333	1.0	0.0
2	2.234	-2.292	0.5	0.375
3	3.083	0.0	0.0	0.5
4	2.234	2.292	-0.5	0.375
5	0.0	3.333	-1.0	0.0
	Jirousek Element			
1	0.0	-3.333	1.0	0.0
2	2.234	-2.292	0.5	0.375
3	3.083	0.0	0.0	0.5
4	2.234	2.292	-0.5	0.375
5	0.0	3.333	-1.0	0.0

Table 4.4 - 5 Node Simple Beam, Example 5, Figure 4.1

Node	Displacements		Stress Resultants	
	Deflection	Rotation	Shear	Moment
	Bar Elements			
1	0.0	0.0	1.0	-1.5
2	2.667	-6.250	1.0	-0.5
3	7.833	-10.000	1.0	-0.5
4	14.250	-11.250	1.0	0.0
5	19.875	-11.250	0.0	0.0
	Jirousek Element			
1	0.0	0.0	0.864	-1.495
2	2.682	-6.286	1.072	-1.001
3	7.887	-9.952	0.961	-0.475
4	14.073	-11.252	0.581	-0.087
5	19.875	-11.250	-0.425	0.019

Table 4.5 - 5 Node Cantilever, Example 4, Figure 4.1

Node	Displacements		Stress Resultants	
	Deflection	Rotation	Shear	Moment
	Bar Elements			
1	0.	0.	1.0	-2.0
1	0.0	-2.50	0.5	0.0
2	1.646	-1.875	0.5	0.25
3	2.667	0.0	0.5	0.5
4	1.646	1.875	-0.5	0.25
5	0.0	2.50	-0.5	0.0
	Jirousek Element			
1	0.0	-2.50	0.313	-0.063
2	1.699	-1.836	0.566	0.289
3	2.50	0.0	0.0	0.406
4	1.699	1.836	-0.566	0.289
5	0.0	2.50	-0.313	-0.063

Table 4.6 - 5 Node Simple Beam, Example 6. Figure 4.1

$$\theta = 0.0x^3 + 5.0x^2 - 20.0x \qquad (4.2)$$

It can be seen that the assumed cubic rotation field reduces to the correct quadratic form. Differentiation of the deflection curve gives:

$$w' = -5.0x^2 + 20.0x + 2.0 \qquad (4.3)$$

This does not correspond in absolute value to the rotatation of the member; the difference being due to the shear deformation. The flexural deflection is always of higher order than the shear deflection. Since the rotation field is a function of the flexural deflection only; the rotation field for an exact solution, must be of order one less than the order of the deflection curve. Thus for all examples in which an exact solution is obtained the rotation field must always turn out to be of lower order than assumed by the element.

The results obtained for the 5 node cantilever are also exact. Solving between the displacements and rotations, respectively, in Table 4.2 gives the following equations:

$$w = -1.667x^3 + 10.0x^2 + 2.0x \tag{4.4}$$

$$\theta = 0.0x^3 + 5.0x^2 - 20.0x \tag{4.5}$$

These are seen to be identical to Equations 4.1 and 4.2 respectively. Thus the assumed quartic deflection and rotation fields reduce to the correct quadratic and cubic functions, respectively.

A cantilever with a uniform load has a quartic deflection and a cubic rotation field. Thus a 5 node element, with its assumed quartic deflection and rotation fields should perform satisfactorily. The results in Table 4.3 confirm this. A simple beam under a uniform load also has a quartic deflection and cubic deflection curve. Thus the element again gives exact results, Table 4.4.

Incorrect results, however, are obtained for the case of a 5 node cantilever, loaded at the node adjacent to the tip, and for the case of a simple beam under a point load at midspan, Tables 4.5 and 4.6. In the case of the cantilever, the true deflection is cubic between the load and the fixed end, and linear between the load and the free end. The solution with the isoparametric element

approximates this shape with one best fitting cubic curve. Thus the results are inexact.

For the case of a simple beam subjected to a point load at midspan, the true deflected shape is given by two cubic curves on each side of the point load. The Jirousek element passes a single cubic curve through all points and as a result t' e computed stress resultants are not exact.

4.2.1 Variable Section Cantilever - In order to check that the element gives correct results for variable cross sections, the beam in Figure 4.2 is considered. The cantilever is subjected to two loads, a unit axial force and a unit transverse force at the tip as shown. The cross sectional area, reduced shear area and moment of inertia are assumed to vary linearly, as shown, over the length of the beam.

The deflection of the beam under axial load is given by:

$$\delta_{axial} = \int_o^{\ell} \frac{P_1 dx}{EA}$$

which in this case gives:

$$\delta_{axial} = 0.5776$$

The computed deflection is also equal to 0.5776. The transverse deflection of the cantilever tip is given by:

$$\delta_{transverse} = \int_o^{\ell} \frac{M_1 M_1 \, dx}{EI} + \int_o^{\ell} \frac{V_1 V_1 \, dx}{GA_r}$$

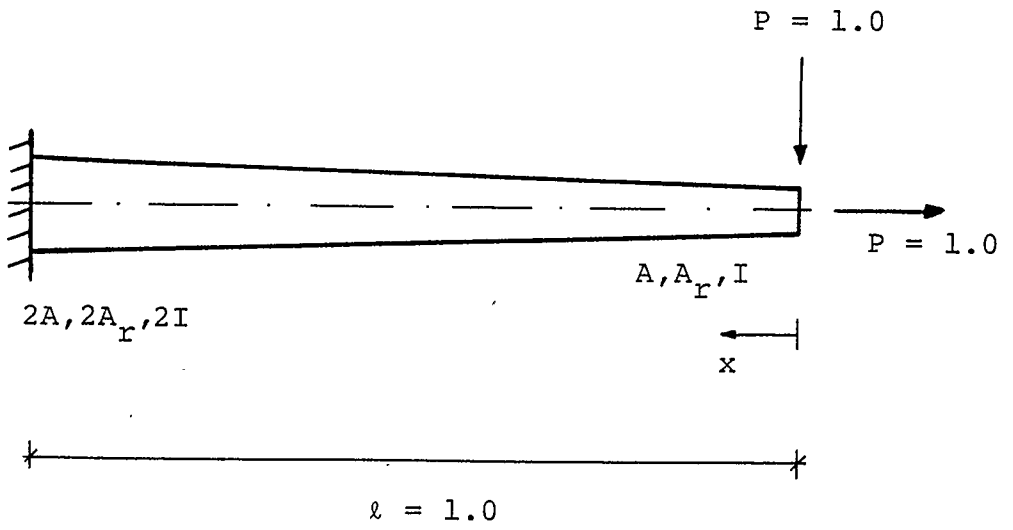

A = 1.2
A_r = 1.0
I = 0.1
E = 1.0
ν = 0.0

Figure 4.2 Cantilever Beam with Linearly Varying Cross Section Properties

where M and V refer to the bending moments and shear forces due to a unit transverse load at the tip. The deflections of the tip due to bending and shear are:

$$\delta_{flexural} = 1.9314 \quad ; \quad \delta_{shear} = 1.3864$$

Thus the total deflection is equal to 3.3178. The Jirousek element gives a value of 3.3177 which is slightly different. The source of the difference is the Jirousek's element modelling of the natural logarithmic term in the element's deflection field by a quartic polynomial. The correspondence is very close, but not quite exact. However, the difference is minimal and the element may be thus assumed to behave saisfactorily in modelling variable section beams.

4.3 Analysis of Element Stiffness Matrices

To investigate further the behaviour of the element, the stiffness matrix of the Jirousek element is compared, for a number of simple structures, to the stiffness matrix from a bar element modelling. It will be seen that while the stiffness matrices for the two element types are quite different, the flexibility matrices resemble one another closely. However, they are not exactly the same, and the

unexpected behaviour of the Jirousek element under certain loading conditions results from the differences between the two.

4.3.1 4 Node Cantilever - The structure is modelled using a four node Jirousek element and also using three bar elements, Figure 4.3. The eight degrees of freedom of the structure reduce to six as shown, when the boundary conditions are introduced. The 8x8 stiffness matrix of the Jirousek element is:

$$[S]_{\text{Jirousek}} = \begin{bmatrix} .925 & -.250 & -1.18 & -.356 & .338 & .150 & -.081 & -.044 \\ -.250 & .261 & .356 & -.177 & -.150 & .046 & .044 & -.005 \\ -1.18 & .356 & 2.70 & 0.0 & -1.86 & -.506 & .338 & .150 \\ -.356 & -.177 & 0.0 & .926 & .506 & -.419 & -.150 & .046 \\ .338 & -.150 & -1.86 & .506 & 2.70 & 0.0 & -1.18 & -.356 \\ .150 & .046 & -.506 & -.419 & 0.0 & .926 & .356 & -.177 \\ -.081 & .044 & .338 & -.150 & -1.18 & .356 & .925 & .250 \\ -.044 & -.005 & .150 & .046 & -.356 & -.177 & .250 & .261 \end{bmatrix} \qquad (4.6)$$

Application of the boundary conditions by eliminating rows and columns 1 and 2 gives the reduced, non singular stiffness matrix:

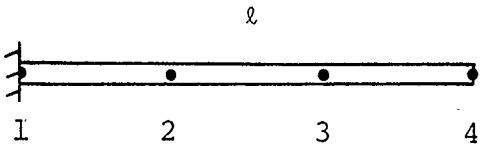

A Four Node Jirousek Element

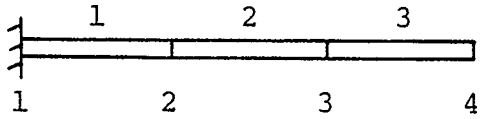

$\ell = 2.0$
$A_r = 2.0$
$I = 0.1$
$E = 1.0$
$\nu = 0.0$

Three Bar Elements

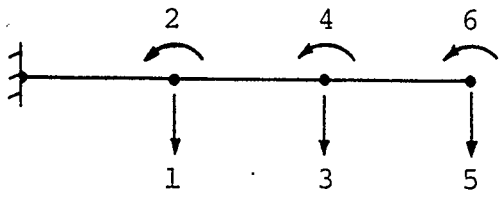

Degrees of freedom corresponding to the appropriate rows and columns of the stiffness and flexibility matrices, Equations 4.7, 4.9, 4.10 and 4.11.

Figure 4.3 Bar and Jirousek Element Models of the Four Node Cantilever, Figure 4.1

$$[S]_{Jirousek} = \begin{bmatrix} 2.70 & 0.0 & -1.86 & -.506 & .338 & .150 \\ 0.0 & .926 & .506 & -.419 & -.150 & .046 \\ -1.86 & .506 & 2.70 & 0.0 & -1.18 & -.356 \\ -.506 & -.419 & 0.0 & .926 & .356 & -.177 \\ .338 & -.150 & -1.18 & .356 & .925 & .250 \\ .150 & .046 & -.356 & -.177 & .250 & .261 \end{bmatrix} \quad (4.7)$$

The 8x8 stiffness matrix of the three bar elements is given by:

$$[S]_{Bar} = \begin{bmatrix} .633 & -.211 & -.633 & -.211 & & & & \\ -.211 & .220 & .211 & -.080 & & & & \\ -.633 & .211 & 1.27 & 0.0 & -.633 & -.211 & & \\ -.211 & -.080 & 0.0 & .441 & .211 & -.080 & & \\ & & -.633 & .211 & 1.27 & 0.0 & -.633 & -.211 \\ & & -.211 & -.080 & 0.0 & .441 & .211 & -.080 \\ & & & & -.633 & .211 & .633 & .211 \\ & & & & -.211 & -.080 & .211 & .220 \end{bmatrix} \quad (4.8)$$

The reduced matrix is:

$$[S]_{Bar} = \begin{bmatrix} 1.27 & 0.0 & -.633 & -.211 & & \\ 0.0 & .441 & .211 & -.080 & & \\ -.633 & .211 & 1.27 & 0.0 & -.633 & -.211 \\ -.211 & -.080 & 0.0 & .441 & .211 & -.080 \\ & & -.633 & .211 & .633 & .211 \\ & & -.211 & -.080 & .211 & .220 \end{bmatrix} \quad (4.9)$$

The stiffness matrices corresponding to the two models are obviously quite different. That of the bar element is typically banded in character whereas the Jirousek element matrix is not. In addition, the magnitude of corresponding terms in each matrix differ quite significantly from each other. Inverting both matrices gives the respective flexibility matrices:

$$[f]_{Jirousek} = \begin{bmatrix} 2.01 & -2.18 & 3.81 & -2.35 & 5.29 & -2.22 \\ -2.18 & 5.67 & -6.54 & 6.93 & -11.1 & 6.67 \\ 3.81 & -6.54 & 10.3 & -8.93 & 16.5 & -8.88 \\ -2.35 & 6.93 & -8.93 & 12.3 & -17.8 & 13.3 \\ 5.29 & -11.1 & 16.5 & -17.8 & 30.7 & -20.0 \\ -2.22 & 6.67 & -8.88 & 13.3 & -20.0 & 20.0 \end{bmatrix} \quad (4.10)$$

$$[f]_{Bar} = \begin{bmatrix} 2.32 & -2.22 & 3.80 & -2.22 & 5.29 & -2.22 \\ -2.22 & 6.67 & -6.67 & 6.67 & -11.1 & 6.67 \\ 3.80 & -6.67 & 10.6 & -8.89 & 16.5 & -8.88 \\ -2.22 & 6.67 & -8.89 & 13.3 & -17.8 & 13.3 \\ 5.29 & -11.1 & 16.5 & -17.8 & 30.7 & -20.0 \\ -2.22 & 6.67 & -8.88 & 13.3 & -20.0 & 20.0 \end{bmatrix} \quad (4.11)$$

The flexibility matrices, though not identical, are very similar. A particular column of the flexibility matrix is equal to the displacement at each coordinate, due to a unit load at the coordinate corresponding to the column. For example, column 6 in Equations 4.10 and 4.11 above corresponds to the displacements at each coordinate due to a unit force at coordinate 6 of the structure, Figure 4.2 Thus:

$$\{u\} = [f]\{F\} \quad (4.12)$$

where $\{F\} = \begin{Bmatrix} 0 \\ 0 \\ 0 \\ 0 \\ 0 \\ 1 \end{Bmatrix}$

Inspection of the flexibility matrices for the models indicates that exact correspondence between the two occurs only in columns 5 and 6, representing the displacements at each coordinate due to a unit force and a unit couple, respectively, at the cantilever tip. For the case of a concentrated couple applied at node 3 (coordinate 4) the resulting displacement vector for the Jirousek element is given by:

$$\{u\} = \begin{Bmatrix} -2.35 \\ 6.93 \\ -8.93 \\ 12.3 \\ -17.8 \\ 13.3 \end{Bmatrix} \qquad (4.13)$$

The exact result, given by the bar element modelling is:

$$\{u\} = \begin{Bmatrix} -2.22 \\ 6.67 \\ -8.89 \\ 13.3 \\ -17.8 \\ 13.3 \end{Bmatrix} \qquad (4.14)$$

Deflections only agree at the end node (coordinates 5 and 6). Agreement occurs here because of the symmetry of the flexibility matrix. At all other nodes errors occur in the computed deflections and rotations. Figure 4.4 shows the true displacement and rotation field along the cantilever under the applied load. The deflection is quadratic from node 1 to node 3 and linear from node 3 to node 4. The rotation is linear from node 1 to node 3 and constant between nodes 3 and 4. The errors occuring in the Jirousek beam modelling are due to the fact that the four node element tries to model the beam deflection as a single cubic curve. Obviously this modelling will yield incorrect results. According to the principle of minimum potential energy (12,40), the beam will adopt a deflected shape which minimizes the total potential energy in the system. In this case the "system" means the structure and the forces that act on it. While the cubic deflection and rotation curves corresponding to a configuration of minimum potential energy may agree quite closely with the true displacement functions they will not give exact results.

4.3.2 5 Node Cantilever - The stiffness matrices corresponding to the coordinates shown in Figure 4.5, for Jirousek and bar elements respectively are given by:

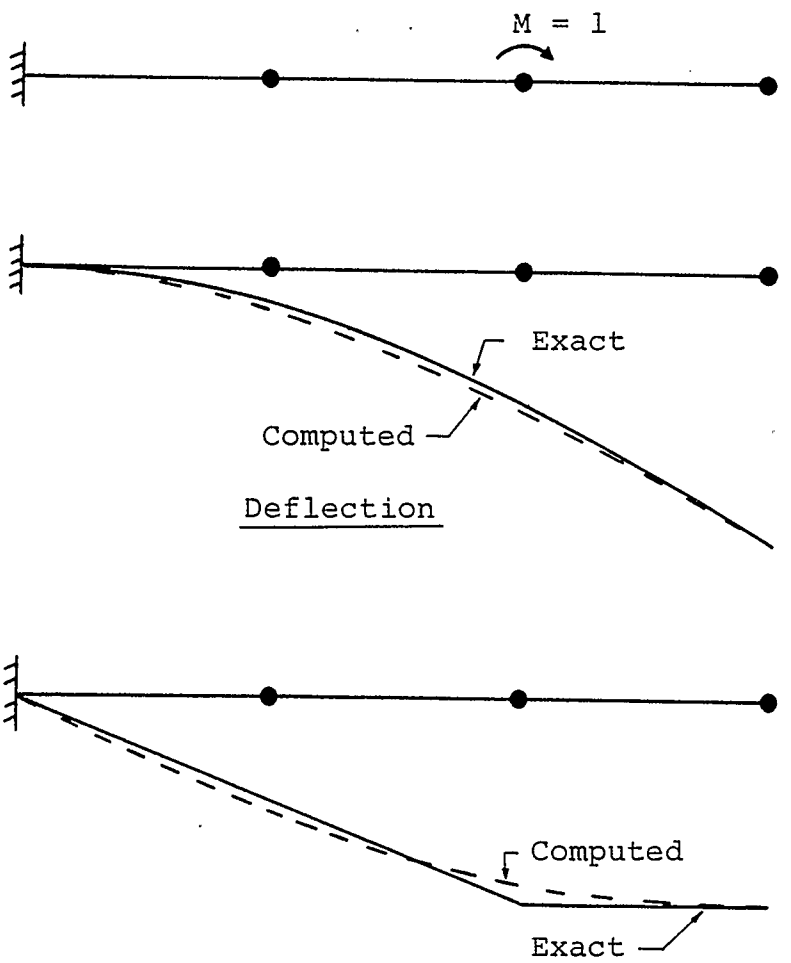

Figure 4.4 Exact and Computed Deflections and Rotations Using a Four Node Jirousek Element

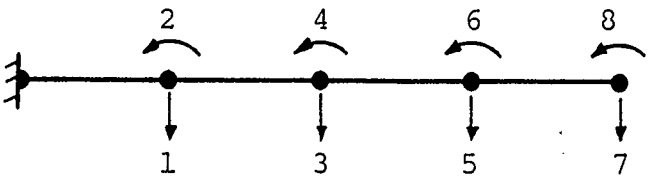

Figure 4.5 Degrees of Freedom of the Five Node Cantilever, Figure 4.1

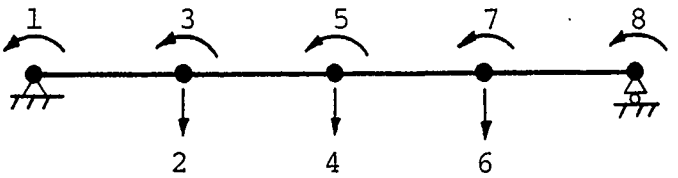

Figure 4.6 Degrees of Freedom of the Five Node Simple Beam, Figure 4.1

$$[S]_{Jirousek} = \begin{bmatrix} 4.40 & 0.0 & -3.76 & -.559 & 1.56 & .271 & -.389 & -.102 \\ 0.0 & 1.19 & .559 & -.820 & -.271 & .357 & .102 & -.068 \\ -3.76 & .559 & 5.91 & 0.0 & -3.76 & -.559 & .806 & .213 \\ -.559 & -.820 & 0.0 & 1.51 & .559 & -.820 & -.213 & .131 \\ 1.56 & -.271 & -3.76 & .559 & 4.40 & 0.0 & -1.81 & -.389 \\ .271 & .357 & -.559 & -.820 & 0.0 & 1.19 & .389 & -.310 \\ -.389 & .102 & .806 & -.213 & -1.81 & .389 & 1.30 & .250 \\ -.102 & -.068 & .213 & .131 & -.389 & -.310 & .250 & .312 \end{bmatrix} \quad (4.15)$$

$$[S]_{Bar} = \begin{bmatrix} 2.13 & 0.0 & -1.07 & -.267 & & & & \\ 0.0 & .533 & .267 & -.133 & & & & \\ -1.07 & .267 & 2.13 & 0.0 & -1.07 & -.267 & & \\ -.267 & -.133 & 0.0 & .533 & .267 & -.133 & & \\ & & -1.07 & .267 & 2.13 & 0.0 & -1.07 & -.267 \\ & & -.267 & -.133 & 0.0 & .533 & .267 & -.133 \\ & & & & -1.07 & .267 & 1.07 & -.267 \\ & & & & -.267 & -.133 & -.267 & .267 \end{bmatrix} \quad (4.16)$$

The corresponding flexibility matrices are:

$$[f]_{Jirousek} = \begin{bmatrix} 1.24 & -1.24 & 2.09 & -1.29 & 2.68 & -1.21 & 3.29 & -1.25 \\ -1.24 & 4.25 & -3.71 & 5.21 & -6.29 & 4.99 & -8.75 & 5.00 \\ 2.09 & -3.71 & 5.16 & -5.00 & 7.89 & -5.04 & 10.3 & -5.00 \\ -1.29 & 5.21 & -5.00 & 9.26 & -9.95 & 10.2 & -15.0 & 10.0 \\ 2.68 & -6.29 & 7.89 & -9.95 & 14.1 & -11.3 & 19.9 & -11.3 \\ -1.21 & 4.99 & -5.04 & 10.2 & -11.3 & 14.3 & -18.8 & 15.0 \\ 3.29 & -8.75 & 10.3 & -15.0 & 19.9 & -18.8 & 30.7 & -20.0 \\ -1.25 & 5.00 & -5.00 & 10.0 & -11.3 & 15.0 & -20.0 & 20.0 \end{bmatrix} \quad (4.17)$$

$$[f]_{Bar} = \begin{bmatrix} 1.41 & -1.25 & 2.04 & -1.25 & 2.67 & -1.25 & 3.29 & -1.25 \\ -1.25 & 5.00 & -3.75 & 5.00 & -6.25 & 5.00 & -8.75 & 5.00 \\ 2.04 & -3.75 & 5.33 & -5.00 & 7.83 & -5.00 & 10.3 & -5.00 \\ -1.25 & 5.00 & -5.00 & 10.0 & -10.0 & 10.0 & -15.0 & 10.0 \\ 2.67 & -6.25 & 7.83 & -10.0 & 14.3 & -11.3 & 19.9 & -11.3 \\ -1.25 & 5.00 & -5.00 & 10.0 & -11.3 & 15.0 & -18.8 & 15.0 \\ 3.29 & -8.75 & 10.3 & -15.0 & 19.9 & -18.8 & 30.7 & -20.0 \\ -1.25 & 5.00 & -5.00 & 10.0 & -11.3 & 15.0 & -20.0 & 20.0 \end{bmatrix} \quad (4.18)$$

It can be seen that only for the case of a point load or couple applied at the cantilever tip (coordinates 7 and 8) are exact results obtained. For a point load at coordinate 5 the results obtained differ from the exact solution.

$$\{u\}_{\text{Jirousek}} = \begin{Bmatrix} 2.68 \\ -6.29 \\ 7.89 \\ -9.95 \\ 14.1 \\ -11.3 \\ 19.9 \\ -11.3 \end{Bmatrix} ; \quad \{u\}_{\text{Bar}} = \begin{Bmatrix} 2.67 \\ -6.25 \\ 7.83 \\ -10.0 \\ 14.3 \\ -11.3 \\ 19.9 \\ -11.3 \end{Bmatrix} \qquad (4.19)$$

The Jirousek element models the discontinuous deflection fields as a continuous quartic curve. Hence the results obtained are inexact. It can be seen ,however, that the two sets of results correspond more closely than in the case of the four node cantilever. It may be assumed, therefore, that increasingly more accurate results are obtained with increased numbers of nodes.

4.3.3 5 Node Simple Beam - The flexibility matrices corresponding to the coordinates shown in Figure 4.6 are for the Jirousek and bar element modelling respectively:

$$[f]_{Jirousek} = \begin{bmatrix} 7.67 & -2.19 & 3.29 & -2.50 & .167 & -1.56 & -1.71 & -2.33 \\ -2.19 & 1.51 & -1.25 & 1.70 & .265 & .995 & 1.29 & 1.56 \\ 3.29 & -1.25 & 3.17 & -1.84 & 1.01 & -1.29 & -1.09 & -1.71 \\ -2.50 & 1.70 & -1.84 & 2.50 & 0.0 & 1.70 & 1.84 & 2.50 \\ .167 & .265 & 1.01 & 0.0 & 1.92 & -.265 & 1.01 & .167 \\ -1.56 & .995 & -1.29 & 1.70 & -.265 & 1.51 & 1.25 & 2.19 \\ -1.71 & 1.29 & -1.09 & 1.84 & 1.01 & 1.25 & 3.17 & 3.29 \\ -2.33 & 1.56 & -1.71 & 2.50 & .167 & 2.19 & 3.29 & 7.67 \end{bmatrix}$$

(4.20)

$$[f]_{Bar} = \begin{bmatrix} 7.67 & -2.19 & 3.29 & -2.50 & .167 & -1.56 & -1.71 & -2.33 \\ -2.19 & 1.69 & -1.25 & 1.65 & .313 & .979 & 1.25 & 1.56 \\ 3.29 & -1.25 & 3.92 & -1.88 & .792 & -1.25 & -1.08 & -1.71 \\ -2.50 & 1.65 & -1.88 & 2.67 & 0.0 & 1.65 & 1.88 & 2.50 \\ .167 & .313 & .792 & 0.0 & 2.67 & -.313 & .792 & .167 \\ -1.56 & .979 & -1.25 & 1.65 & -.313 & 1.69 & 1.25 & 2.19 \\ -1.71 & 1.25 & -1.08 & 1.88 & .792 & 1.25 & 3.92 & 3.29 \\ -2.33 & 1.56 & -1.71 & 2.50 & .167 & 2.19 & 3.29 & 7.67 \end{bmatrix}$$

(4.21)

It can be seen that exact correlation occurs only in the first and eighth columns. These represent the deflections due to unit couples at the support nodes. Under such a loading configuration the beam deflects as a cubic curve with a quadratic rotation field. This is exactly modelled by the element. For loads applied at internal coordinates,

however, inexact results are obtained. Nevertheless, it is possible to obtain a loading configuration in which the combined effects of several loads produce a correct solution.

4.3.4 Uniform Load on a 5 Node Cantilever - The flexibility matrix corresponding to the coordinates in Figure 4.5 is given by Equation 4.15 for a Jirousek element and by Equation 4.16 for a bar element modelling. Though different, both matrices exhibit an exact response to a uniformly distributed load. The consistent nodal load vectors are for the Jirousek and bar element respectively:

$$\{F\}_{\text{Jirousek}} = \begin{Bmatrix} .711 \\ 0.0 \\ .267 \\ 0.0 \\ .711 \\ 0.0 \\ .156 \\ 0.0 \end{Bmatrix}; \quad \{F\}_{\text{Bar}} = \begin{Bmatrix} 0.5 \\ 0.0 \\ 0.5 \\ 0.0 \\ 0.5 \\ 0.0 \\ 0.25 \\ 0.02 \end{Bmatrix} \tag{4.22}$$

These are again different but when multiplied by the appropriate flexibility matrix, the terms combine to give exact results; though individually each lumped load, for the Jirousek element, produces an incorrect result.

4.4 Conclusions

The Jirousek element has been seen to give exact results when the appropriate order element is subjected to certain loads. In particular, when subjected to point loads at end node coordinates, or to distributed loads, the element gives excellent results. However inaccuracies occur when concentrated forces are applied to internal element degrees of freedom. The errors in the computed displacements, though small, produce more significant errors in the computed element stresses. The source of the error is the element's attempt to model discontinuous deflection and rotation fields by single continuous functions. The differences between the exact flexibility matrix and the Jirousek element flexibility matrix are much smaller than those occuring between the corresponding stiffness matrices.

Overall the Jirousek beam element behaves very well. The element's excellent response under end nodal loading, and under distributed loads, in addition to its ability to accurately model curved geometries, make it particularly suited to the analysis of curved prestressed bridges.

CHAPTER FIVE

TORSION CONTROL IN CURVED CONTINUOUS BRIDGES

5.1 Introduction

Torsional effects are in many cases very significant in curved bridges, even when the applied external load and prestressing are symmetrical about the centreline of the section. In the case of single span, statically determinate curved beams no torsional moments are induced by prestressing, provided the resultant force lies in a vertical cylindrical surface through the beam centroid, (49). However, for continuous curved beams the redundant reactions produce a combination of bending and torsion in the beam.

The torsional moments due to prestressing may be significant. Moreover, the torsion induced by prestressing and the torsion due to dead load tend to be additive. Thus while a typical parabolic profile as shown in Figure 5.1 will tend to balance out the bending moments due to dead load, the torsional moments induced by the prestressing will add to the dead load torsion. In addition to the increased torsional moments along the bridge, the torsion induced by prestressing may substantially increase the tendency for lifting at the bearings. Figure 5.2 is a

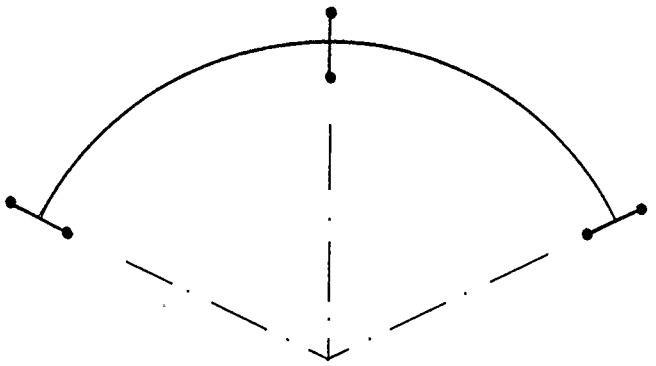

Schematic Plan of Two Span Circular Curved Beam Torsionally Restrained at All Supports

Parabolic Cable Profile

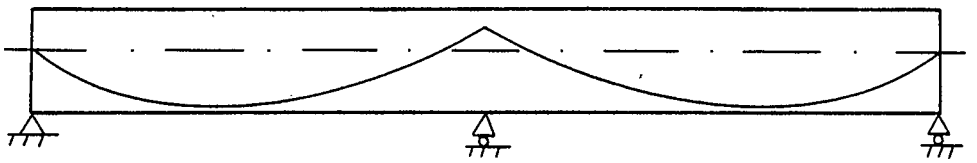

Developed Elevation

Figure 5.1 Two Span Circular Curved Beam

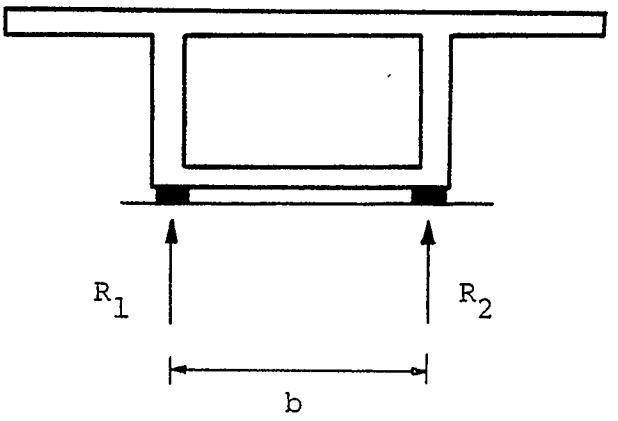

$$\text{Torque} = \frac{b}{2} (R_1 - R_2)$$

Figure 5.2 Torsional Support

schematic representation of a typical torsion resisting support. Where large torsional restraint exists, there is a tendency for one bearing to lift under the effect of dead load. The problem is aggravated by the prestressing in situations where the torsional moments due to dead load and due to prestressing are additive. In many situations lifting of the bearings may be the deciding criterion in establishing what proportion of the maximum torsional moment should be balanced out.

5.2 Demonstration Example

Referring to Figure 5.3, the two span continuous bridge is analysed to demonstrate the essence of the problem. The given simplified cross section is adopted purely for demonstration purposes and it is not intended that it be interpreted as a practical size or shape. The bridge is torsionally restrained at all three supports and is subjected to a uniformly distributed load. This applied loading represents the load balanced by the given cable profile in an equivalent straight beam of the same span. The example serves to demonstrate the additive property of the dead load and prestressing torsional effects, and also as a check on the accuracy of SFRAME in modelling the structure.

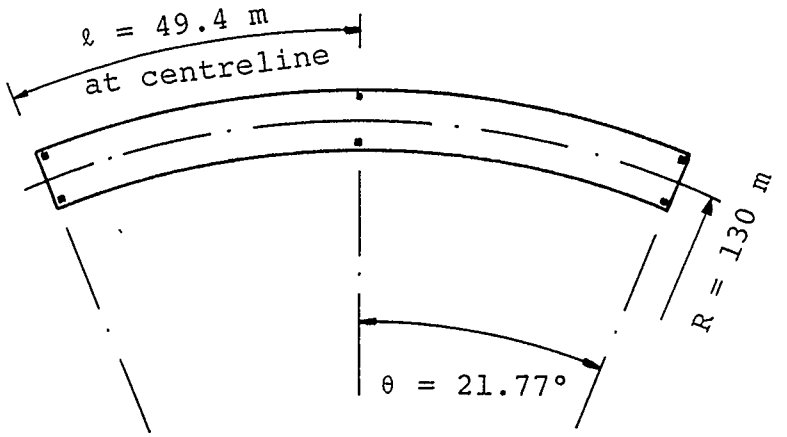

Plan

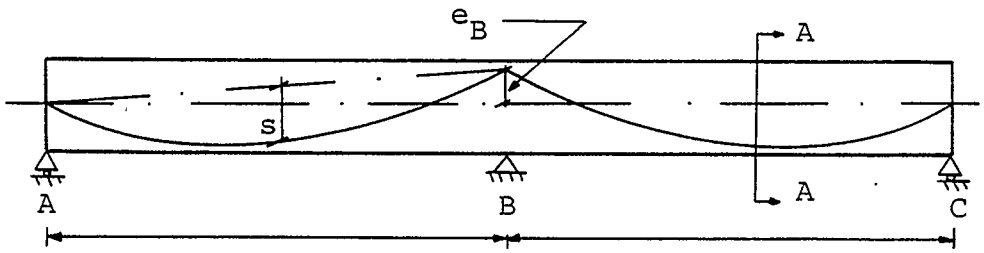

Developed Elevation

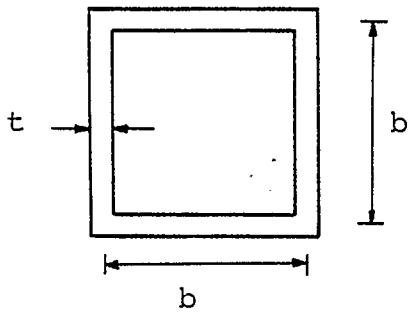

X Section AA

Square Box Section

$I = 0.67tb^3$
$J = tb^3$
$E = 1.0$
$\nu = 0.2$
$b = 1.0$ m
$e_B = 0.4$ m
$s = 0.6$ m

Symmetric Pre-Stressing in Each Web

Figure 5.3 Two Span Circular Bridge

P = 1.0 MN

$w = 8Ps/\ell^2 = 0.001967$ MN/m

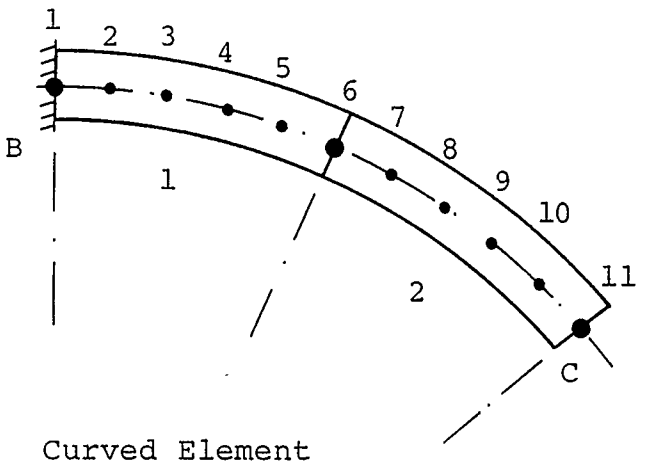

Curved Element Modelling of the Bridge

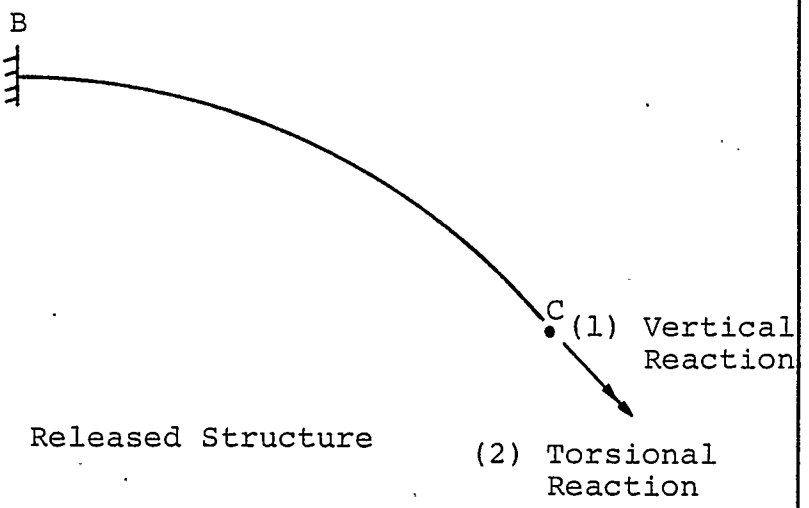

Released Structure

Figure 5.3 (continued)

The bridge was analysed by hand using the force method (20). Advantage was taken of the structural symmetry so that only a single span was considered, Figure 5.3. The structure was reduced to statically determinate form by the introduction of releases as follows:

(1) Vertical reaction at C.

(2) Torsional reaction at C.

Symmetry was also availed of in the computer analysis. The single span beam was modelled using two 6 noded curved elements, Figure 5.3. Shear effects are not included in either case. As can be seen from Table 5.1 this mesh gave results which were almost identical to the closed form solution. Thus the program SFRAME closely models the curved beam behaviour under the external distributed load and the prestressing loads. The bending and torsional moments in Table 5.1 are plotted in Figure 5.4. It can be seen that the prestressing almost exactly balances the bending moments due to the external uniform load. This is in agreement with the conclusions of Witecki (50), who noted that bending moments are largely unaffected by the curvature of a bridge. It is evident, however, that the torsion due to prestressing adds to the torsion induced by the external load. Furthermore, the maximum ordinates of the two torsion diagrams are of the same order of

Node	Bending Moments (MNm)		Torsional Moments (MNm)	
	Closed Form	Computer	Closed Form	Computer
Dead Load				
1	-0.61042	-0.61042	0.00099	0.00101
2	-0.33319	-0.33292	-0.01678	-0.01683
3	-0.10330	-0.10313	-0.02492	-0.02496
4	0.07872	0.07884	-0.02524	-0.02527
5	0.21264	0.21284	-0.01955	-0.01957
6	0.29826	0.29838	-0.00969	-0.00973
7	0.33547	0.33558	0.00251	0.00250
8	0.32419	0.32427	0.01520	0.01519
9	0.26445	0.26450	0.02654	0.02652
10	0.15633	0.15637	0.03468	0.03467
11	0.0	0.0	0.03781	0.03780

Table 5.1 - Comparison of Closed Form and Computer Results For the Beam in Figure 5.3

Node	Bending Moments (MNm)		Torsional Moments (MNm)	
	Closed Form	Computer	Closed Form	Computer
Prestressing				
1	0.59678	0.59717	-0.02531	-0.02536
2	0.32282	0.32273	-0.01815	-0.01815
3	0.09568	0.09568	-0.01172	-0.01172
4	-0.08377	-0.08360	-0.00602	-0.00602
5	-0.21542	-0.21531	-0.00106	-0.00106
6	-0.30421	-0.29919	0.00314	0.00314
7	-0.33522	-0.33517	0.00659	0.00660
8	-0.32331	-0.32323	0.00929	0.00929
9	-0.26349	-0.26347	0.01120	0.01121
10	-0.15573	-0.15559	0.01236	0.01237
11	0.0	0.0	0.01274	0.01274

Table 5.1. - continued.

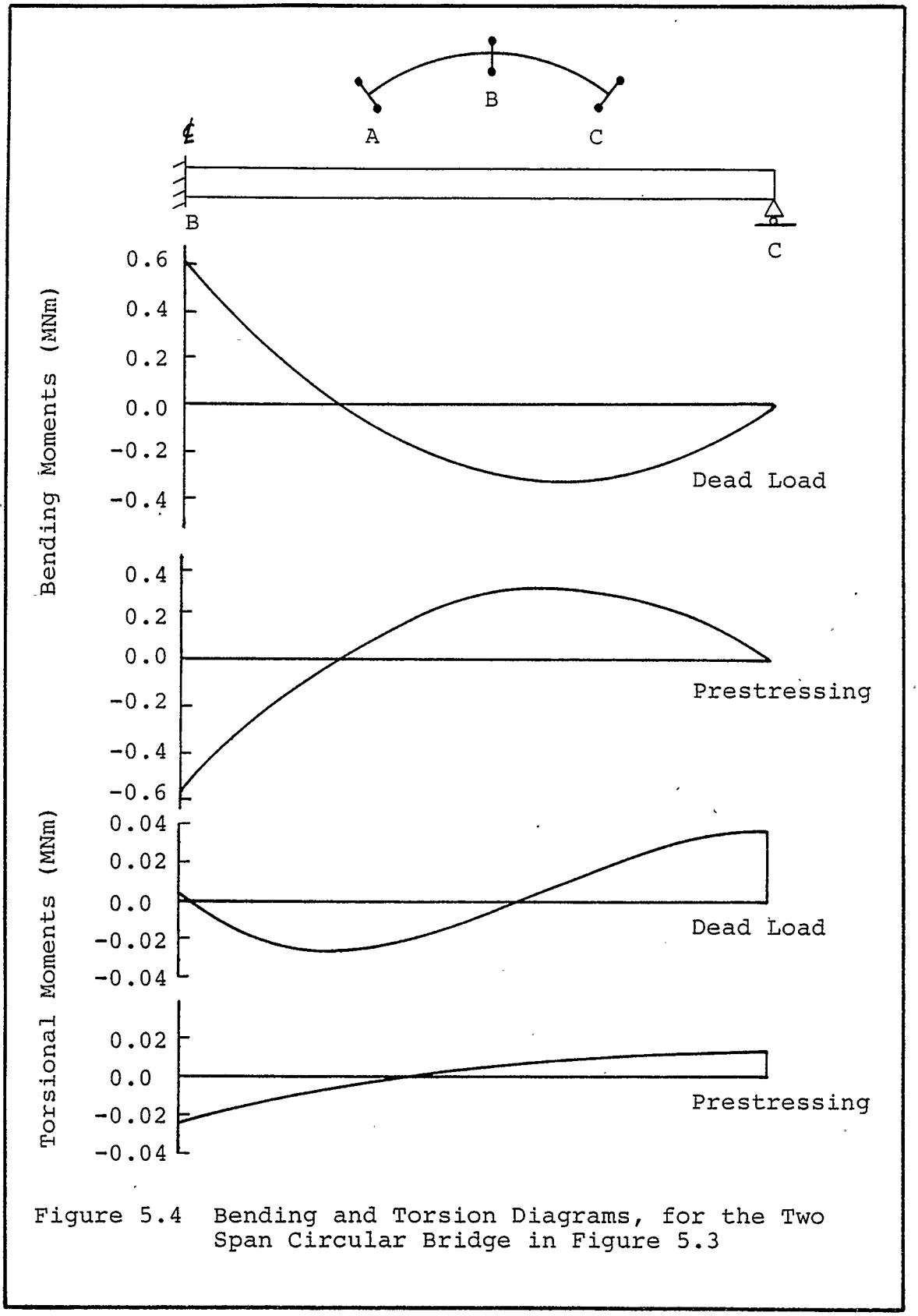

Figure 5.4 Bending and Torsion Diagrams, for the Two Span Circular Bridge in Figure 5.3

magnitude; thus there is a substantial increase in torsional moments along the beam.

In the example considered above all three supports are torsionally restrained. Many continuous curved bridges are constructed with some or all of the internal supports torsionally free. This has the effect of increasing the torque arm of the structure and results in an increase in the magnitude of the torsional moments. For the example just considered; the bending and torsional moment diagrams when the intermediate support is torsion free are shown in Figure 5.5. Little change occurs in the distribution of bending or torsional moments due to external loads. However, in the case of torsion induced by prestressing the torsional moment at the external support increases substantially. The combined torque at this point, as a result, increases by over 40%.

5.2.1 Parameters Affecting Behaviour - Two parameters which govern the torsional response of a curved beam are the radius of curvature, R, and the ratio of bending to torsional stiffness EI/GJ. For a given span length, $R\theta$, where θ is the angle subtended by the span it is reasonable to expect that torsional moments should increase in magnitude as the curvature increases (radius of curvature decreases). Thus for a straight beam ($R=\infty$) under

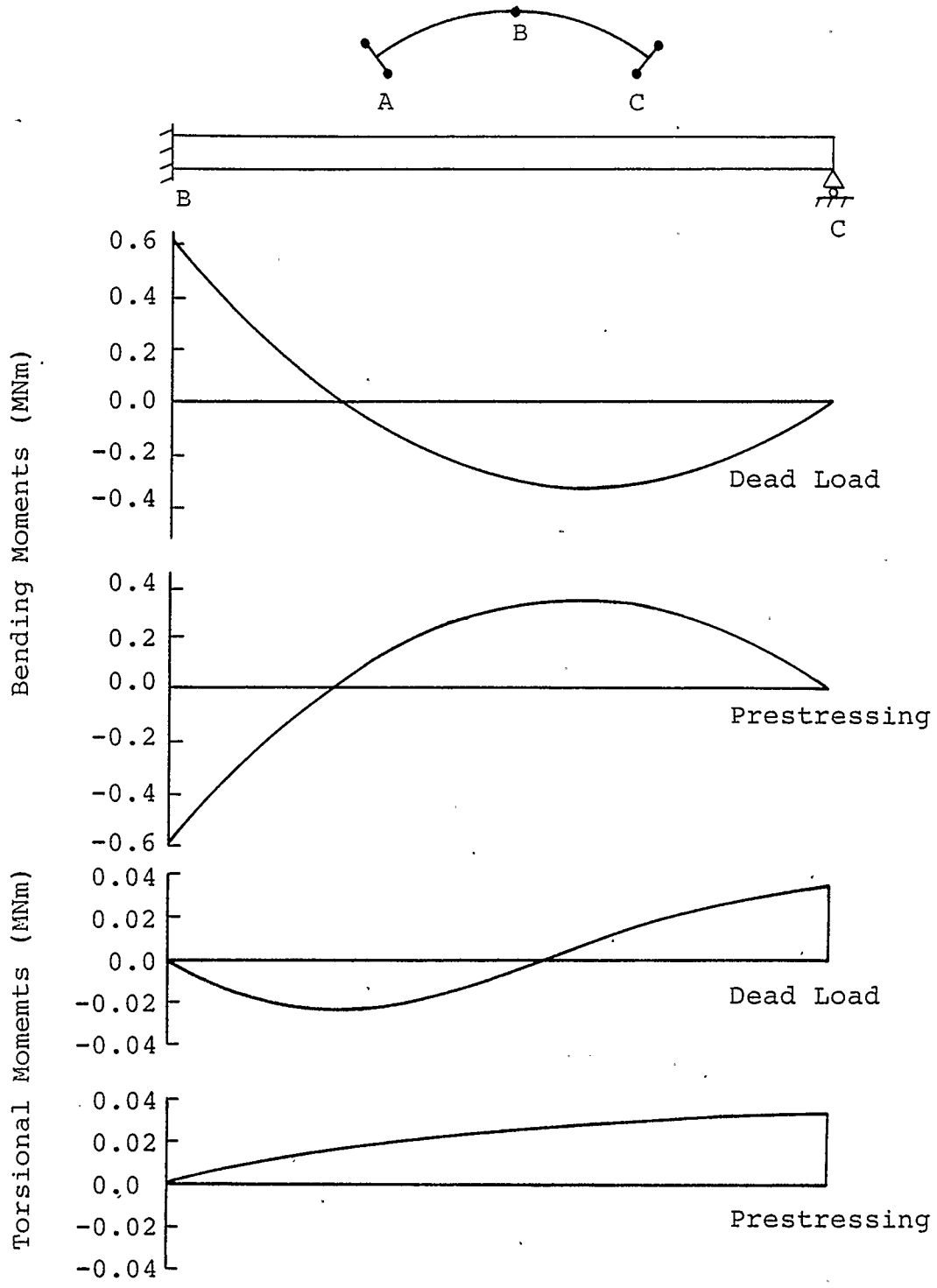

Figure 5.5 Bending and Torsional Moments When Torsional Rotation is Free to Occur at the Central Support of the Beam in Figure 5.3

symmetric prestressing and external loads no torsional moments are induced. For progressively smaller radii of curvature the magnitude of the torsional moments increases. This is demonstrated in Figure 5.6. It can be seen that the increase in torsional moments with increased curvature is almost exactly linear over the range in question.

The ratio of bending to torsional stiffness also affects the response of a curved beam. In Figure 5.7 the torsion moment diagrams, under external loads and prestressing, are plotted for the ratios I/J = 0.2 and I/J = 5.0, for a radius of curvature of 130m. Most box sections in practical use fall well within these limits. It can be seen that very little change occurs in the torsional moments; in fact, only a slight reduction occurs over a twenty five fold decrease in torsional stiffness relative to bending stiffness. This agrees with the conclusions of Bassi et al. (4), who noted that the magnitude of the torsional stiffness only affects the distribution of torsional moments at very low values of torsional stiffness. However, the reduction is more noticeable for more sharply curved geometries. For a radius of curvature of 65m, Figure 5.8, a somewhat greater variation in the torsional response occurs with varying I/J. However, such a large curvature is unlikely to be encountered in practice. Indeed Scordelis and Larsen (39),

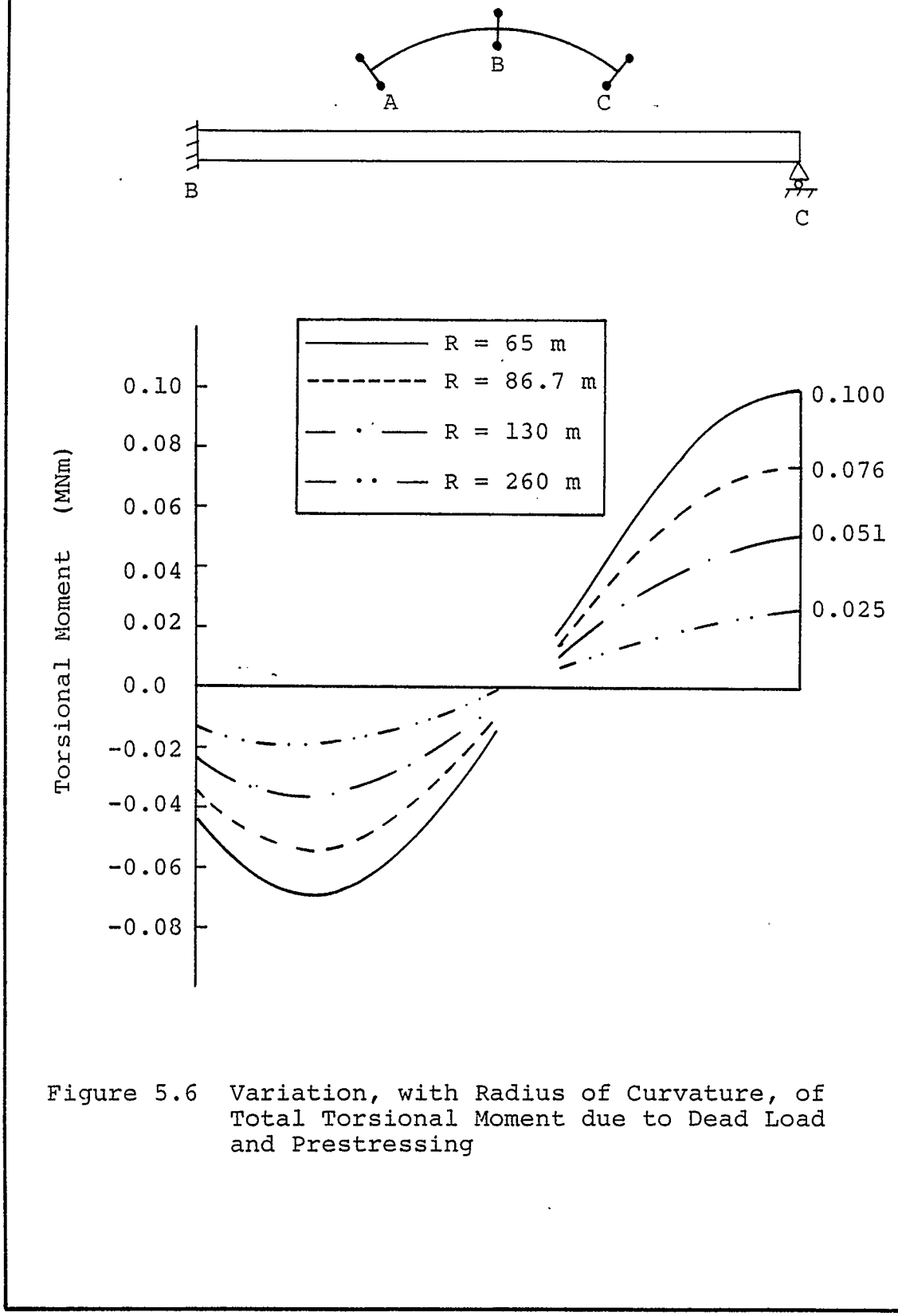

Figure 5.6 Variation, with Radius of Curvature, of Total Torsional Moment due to Dead Load and Prestressing

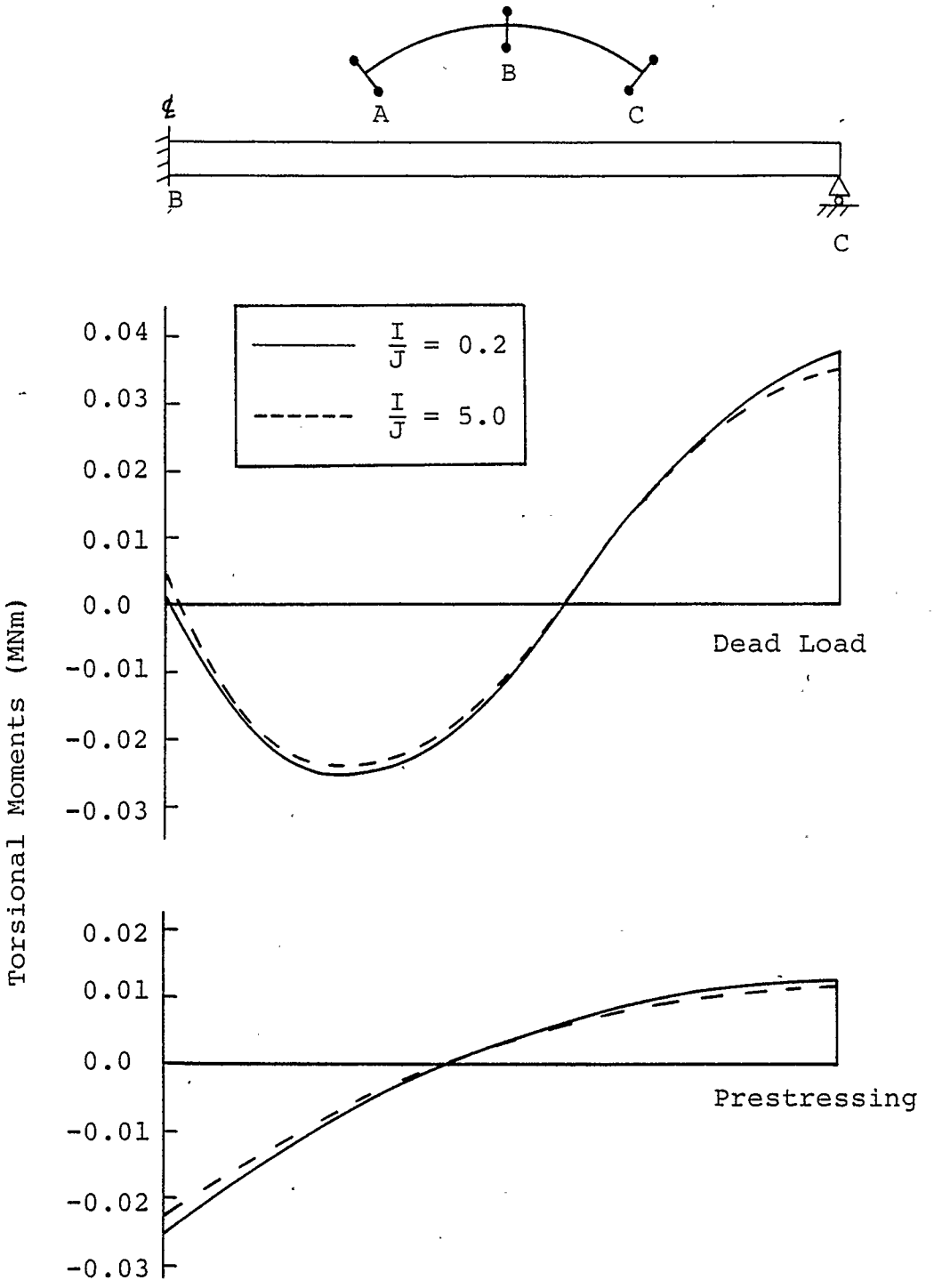

Figure 5.7 Variation in Torsional Moments with $\frac{I}{J}$ Ratio, for the Bridge in Figure 5.3, for R = 130 m

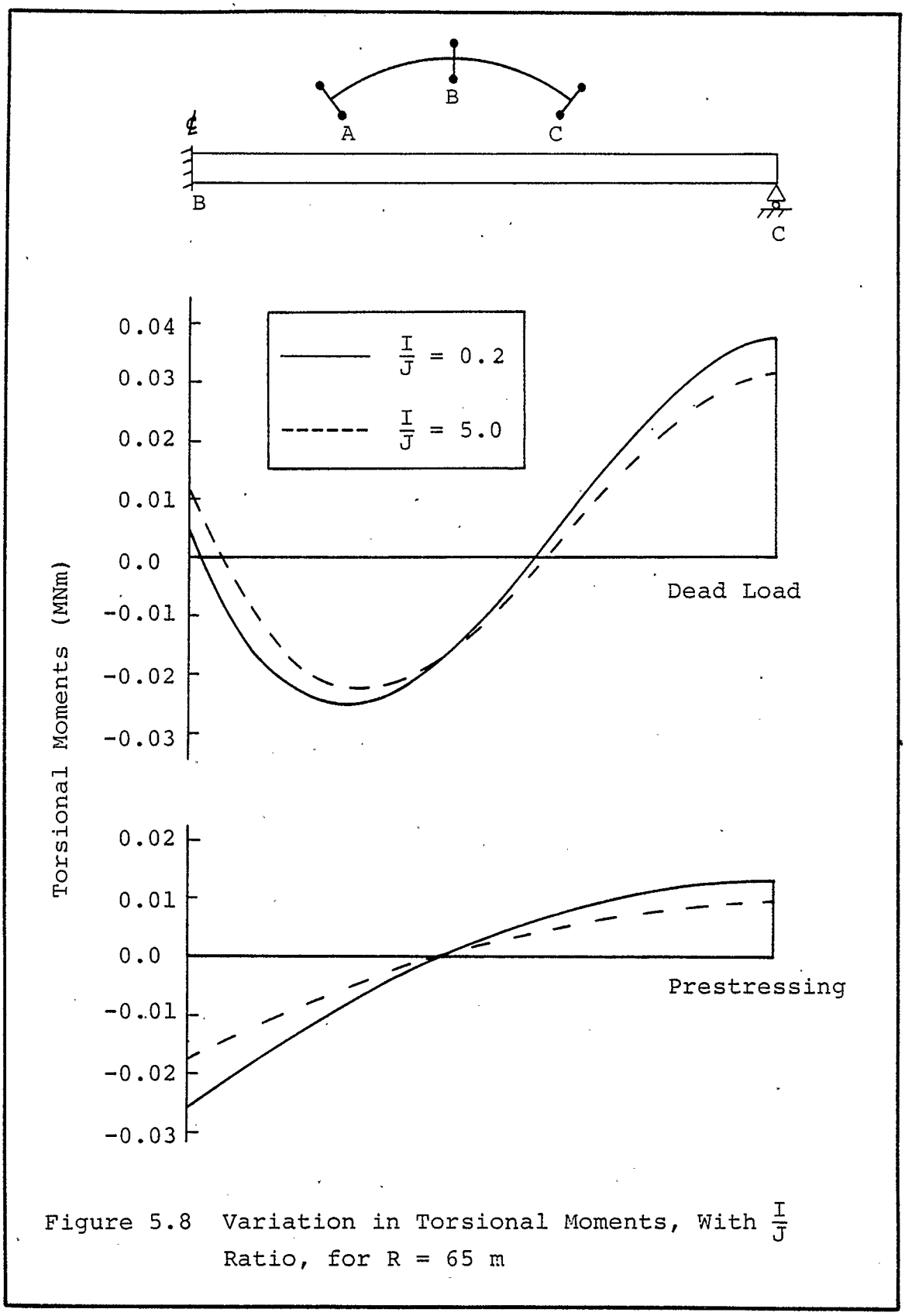

Figure 5.8 Variation in Torsional Moments, With $\frac{I}{J}$ Ratio, for R = 65 m

have quoted a figure of 85m - 90m as being the minimum radius likely to be used. Thus, in the remainder of this thesis no further consideration need be given to the effects of varying the I/J ratio.

5.3 A Method for Control of Bending and Torsion

A method is presented below for computing the profile of prestressing tendons to control the bending and torsional moments in a curved bridge to any desired amount. A basic cable profile is first assumed and subsequently adjusted by the addition of profiles of higher order. The basic cable profile(s) may be chosen to balance the dead load bending moments for an equivalent straight beam of length equal to the developed length of the curved beam. For a box girder of uniform cross section, the basic cable profile is parabolic in each web. The magnitude of the prestressing force is chosen to balance any desired portion of the dead load. The chosen prestressing force, and the basic tendon profile, in combination with the dead load, produce high torsional moments; small bending moments may also occur.

Additional shape functions are superimposed on the basic cable profile(s) to reduce the torsional moments to a desired amount, while maintaining the bending moments at a low level. The additional shape functions are chosen as

quadratic, cubic or quartic Lagrangian interpolation functions, Figure 5.9. These are the same shape functions employed in the formulation of the isoparametric element in Chapter Three. The eccentricity of any cable after adjustment will be given by:

$$e = e_{basic} + \sum_{i=1}^{n} \eta_i N_i \qquad (5.1)$$

Here e refers to the eccentricity with respect to the principal axes, y' or z', of the beam cross section, (Figure 3.8). N_i is a shape function, Figure 5.9, and η_i is a scaling factor applied to this shape function.

In Section 5.4 a procedure will be presented for computing the best set of parameters $\{\eta\}$ such that the objective of reducing torsional moments without increasing the bending is achieved, as closely as possible with the chosen shape functions (least squares fitting).

5.4 Superposition of Eccentricities

Consider a prestressing tendon coincident with the centroidal axis of a curved beam. ($e_{y'} = e_{z'} = 0$), Figure 5.10. Let the value of any action due to the prestressing be A. The eccentricty of the tendon is changed either in the z' or y' direction, or both, such that:

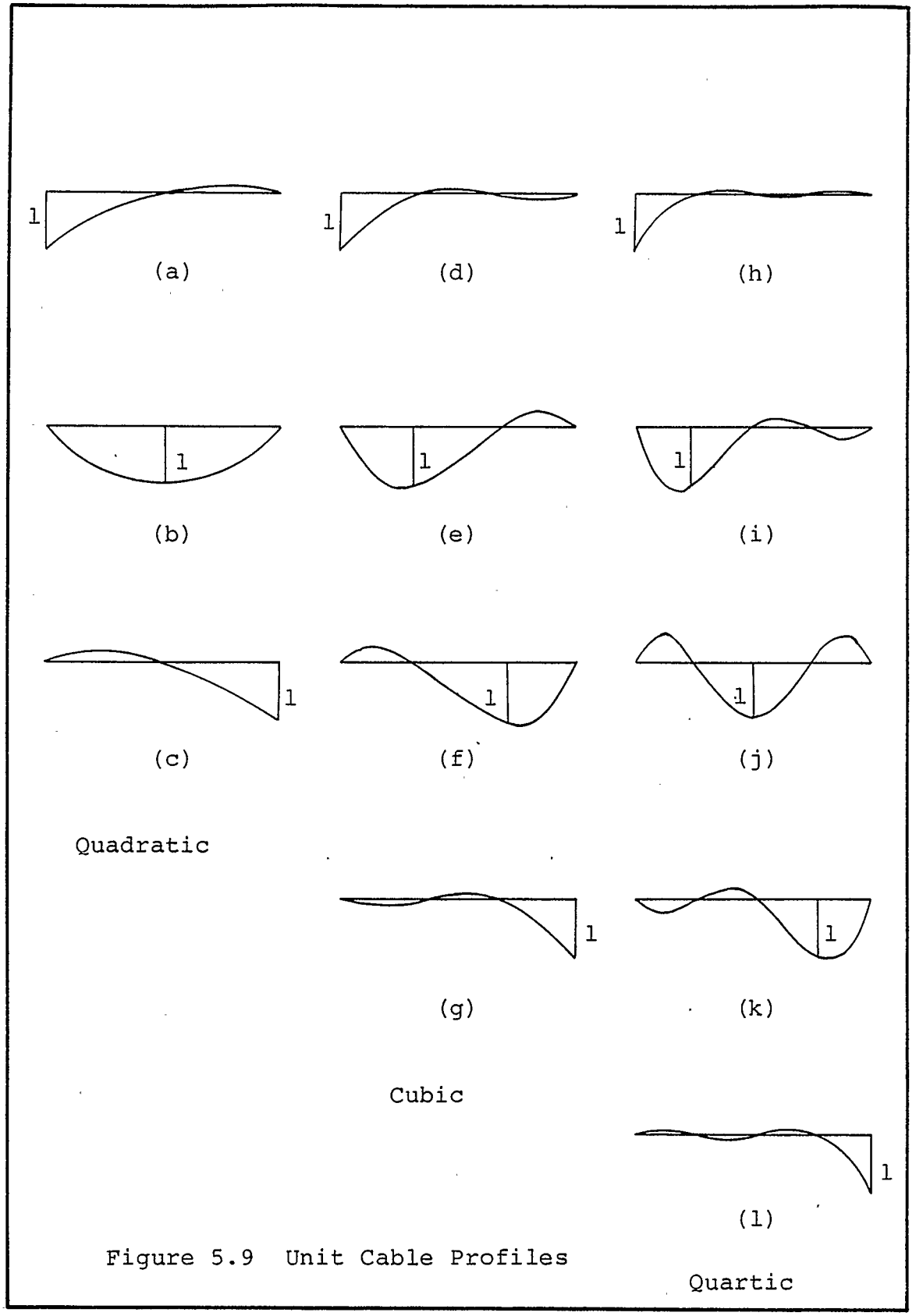

Figure 5.9 Unit Cable Profiles

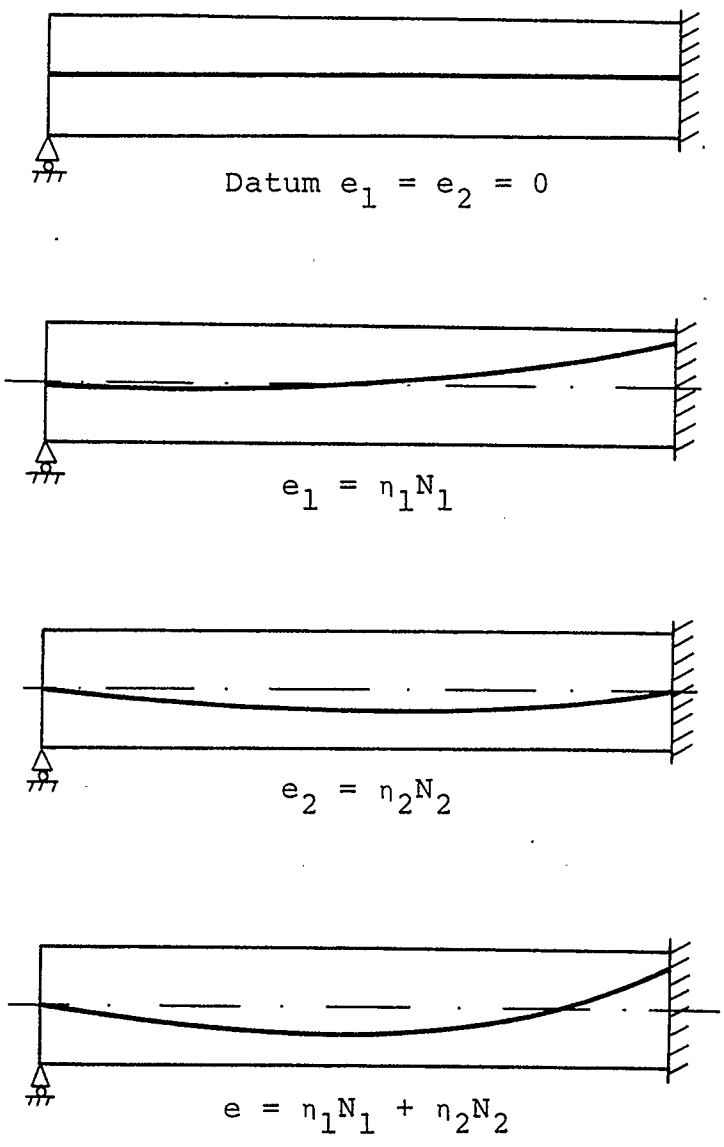

Figure 5.10 Superposition of Unit Cable Profiles

$$\Delta e_1 = \eta_1 N_1 \tag{5.2}$$

where η and N are as defined in the preceeding section. The change in the magnitude of the action due to the above change in eccentricity is ΔA. If the curvature of the tendon can be approximated by the second derivative of the eccentricity, then:

$$\kappa = \frac{d^2 e}{d s^2} \tag{5.3}$$

where s is the distance measured along the cable profile. In this case a linear relationship exists between the curvature and the eccentricity. Since the distributed force generated by a prestressing tendon is proportional to the curvature, for a given prestressing force the change in action must be directly proportional to the change in eccentricity. Furthermore, an inverse linear relationship exists between the prestressing force ,P, and the eccentricity, e. For example, if the eccentricity is doubled, and the prestressing force halved, the same transverse forces are generated by the cable.

If a second change in eccentricity is applied to the cable, Figure 5.10, we may write:

$$\Delta e_2 = \eta_2 N_2 \tag{5.4}$$

The corresponding change in action is equal to ΔA_2. A linear relationship again exists between Δe_2 and ΔA_2. The eccentricities e_1 and e_2 may be applied simultaneously such that the total change in eccentricity is given by:

$$\Delta e = \Delta e_1 + \Delta e_2 \tag{5.5}$$

Since a linear relationship exists between the changes in eccentricity, when applied individually, and the respective changes in action, the change in action due to the combined change in eccentricity, $\Delta e_1 + \Delta e_2$, is equal to $\Delta A_1 + \Delta A_2$, provided the curvature of the combined cable is again small. The direct superposition of the actions due to different changes in eccentricity is also true when the changes occur in different planes. In this case the resultant change in eccentricity is obtained by the vector sum of the individual changes; the resulting actions are added directly.

As will be discussed in Section 5.7 the adjusted cable profiles, obtained using the present technique, may be

constrained to lie within the bridge cross section. For most practical cross sections, this ensures that the cable curvatures are sufficiently small that superposition of cable actions is valid.

5.5 Formulation of the Method

The formulation of a method for controlling torsion in curved bridges is explained in this section. The box girder bridge in Figure 5.11 is considered and the objective is to find a cable profile and prestressing force in each web that control bending and torsional moments to a desired amount. In the present development of the method certain assumptions are made so as to simplify the explanation. It is assumed that cable profiles extend from one end of the bridge to the other; however this need not be so. It is also assumed that the prestressing force is constant in each cable. However, once the desired cable profiles are obtained, the actual prestressing force along the tendon may be used to compute the bending and torsional moments. Alternatively, the actual prestressing force, at each nodal point, taking account of friction and anchorage slip losses, may be used in the analysis. However, if superposition of eccentricities is to be valid, the force at a given section must be the same for all unit shape function profiles and for the basic cable profile.

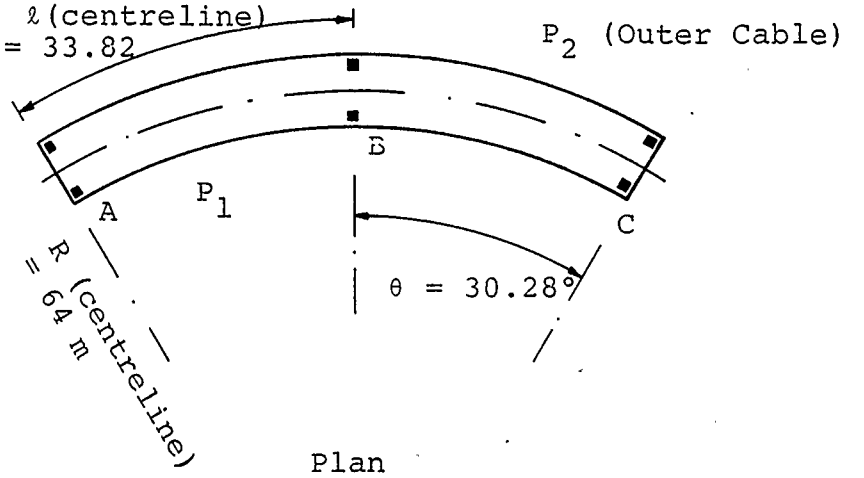

Plan

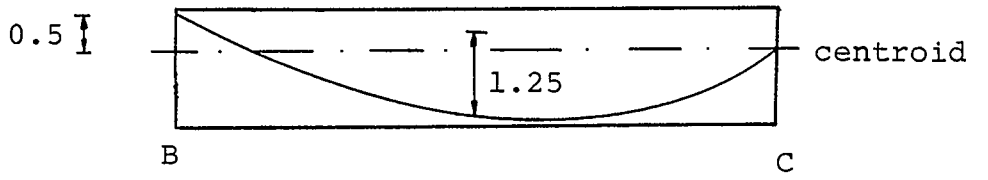

Basic Cable Profile

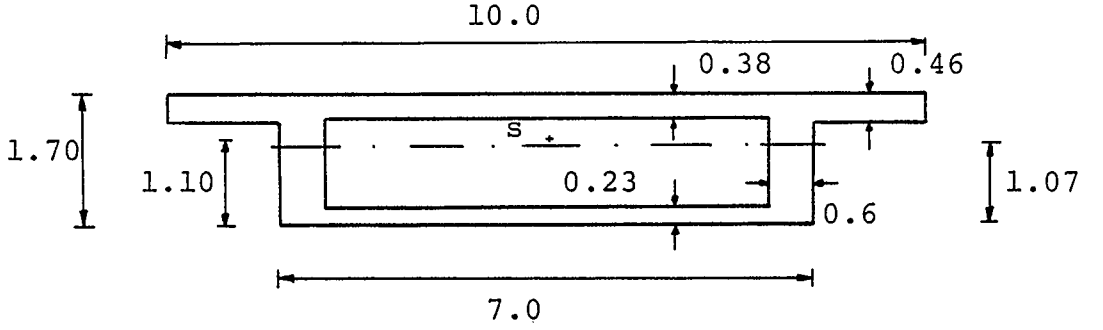

Cross Section

Note: All dimensions in meters

$I_{y'} = 2.38\ m^4$

$I_{z'} = 56.51\ m^4$

$J_{x'} = 56.65\ m^4$

$A = 6.96\ m^2$

Figure 5.11 Two Span Circular Bridge

The control of torsional moments is achieved in two ways. Firstly, the eccentricity of the cable profile is adjusted by the addition of appropriate shape function terms. Secondly, if required, the magnitude of the prestressing force, which minimizes the adjusted values of bending and torsion, is obtained. The procedure for calculating the adjusted cable profile is given by the following six steps.

(1) A basic cable profile is selected. A suitable choice is to use the cable profile for a straight bridge, of developed length equal to the developed length of the curved bridge. The magnitude of the prestressing force is selected to balance a fraction of the dead load bending moments as desired.

(2) Calculate the bending and torsional moments at a number of sections, m. These may be chosen at the nodal points of the Jirousek curved elements, employed in the idealization of the curved beam BC, Figure 5.12.

(3) If the bending and torsional moments obtained are considered satisfactory, no further calculations are necessary. If not, the moments may be adjusted by the equation:

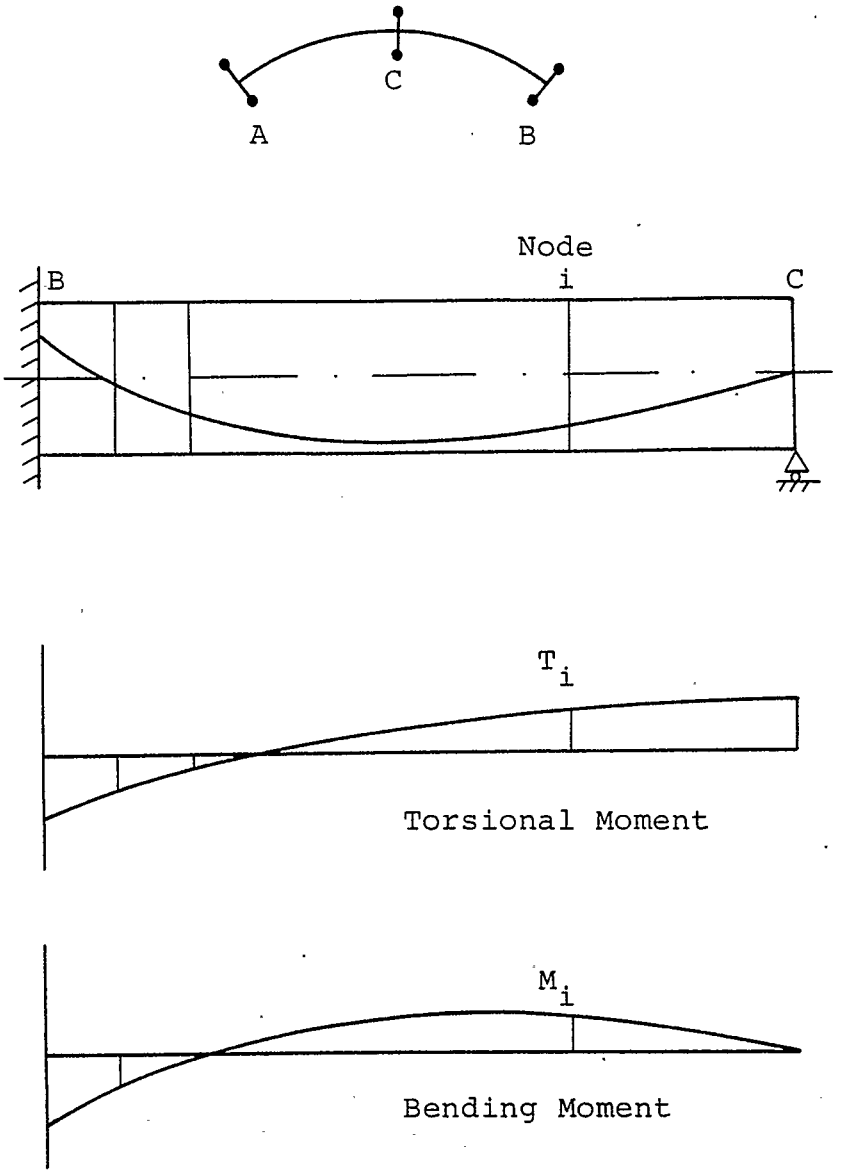

Figure 5.12 Computation of Bending and Torsional Moments at Nodal Points

$$\{\Delta M\}_{basic} + \{\Delta M\} = \{\Delta M\}_{adjusted} \qquad (5.6)$$

The symbol M refers to the vectors of 2m moment values, both bending and torsion. The vector $\{\Delta M\}$ represents the changes in moment values to be achieved by the adjustment of the cable profiles, or by the change in magnitude of the prestressing forces in the two webs. The objective is to achieve a solution which satisfies the condition:

$$\{\Delta M\}_{adjusted} = \{0\} \qquad (5.7)$$

However, this only needs to be approximately achieved, as will be done below.

(4) Select the N-functions, specifying the adjustment in cable eccentricity over span BC, Figure 5.11. Let the number of shape functions for each web be n. The parabolic profile, Figure 5.9(b), and the cubic profiles, Figure 5.9(e) and (f) are the most useful. The other parabolic and cubic profiles may also be used but they alter the eccentricity at the cable ends, which in many cases may not be desirable. Quartic shapes, Figure 5.9(i), (j) and (k) may also be added if the vector of moments $\{\Delta M\}_{adjusted}$ is

to be brought closer to zero. In the remainder of the development, the shape functions in Figure 5.9 will be refered to as unit cable profiles.

(5) Unit cable profiles corresponding to the shape functions chosen in the previous step are introduced separately in each web. The magnitude of the prestressing force is the same as in the basic cables in Step (1). The values of bending and torsional moments for each unit profile are determined at the node points of the Jirousek elements and are listed in a column of a matrix $[\Delta A_u]$.

(6) The following superposition equation may be written:

$$[\Delta A_u]\{\eta\} = \{\Delta M\} \qquad (5.8)$$

The vector $\{\eta\}$ has 2n elements, representing the scaling factors for the shape functions in the two webs. When 2n = 2m the solution of Equation 5.8 gives the values of $\{\eta\}$ which will bring the bending and torsional moments to zero at the sections considered. As mentioned earlier, exact balancing is not necessary and the number of unit profiles can be smaller than the number of sections ($n<m$). In this case there are more equations than unknowns, $\{\eta\}$, in the above set of superposition equations. Thus the set is

said to form an inconsistent system. Since n<m there is no vector $\{\eta\}$ which exactly satisfies Equation 5.8 (27); in this case an approximate solution to the equation must be obtained. Premultiplying both sides by $[\Delta A_u]^T$ gives

$$[\Delta A_u]^T[\Delta A_u]\{\eta\} = [\Delta A_u]^T\{\Delta M\} \quad (5.9)$$

or $$[U]\{\eta\} = \{B\} \quad (5.10)$$

The square matrix [U] has dimensions 2nx2n and the equation may thus be solved for the unknown parameters $\{\eta\}$. It can be shown that the above procedure gives a least squares approximation to Equation 5.7 (21). In other words, optimum use is made of the chosen shape functions to bring the sum of the squares of the elements of the vector $\{\Delta M\}$ to a minimum.

The individual unit cable profiles in each web are factored by the corresponding terms of the vector $\{\eta\}$. The resulting cable profiles may be satisfactory, in which case the analysis is completed by computing the resulting bending and torsional moments due to these profiles. More often, however, the computed profiles may be undesirable

from two standpoints. Firstly, a web cable profile may extend below the depth of the beam; alternatively, the cable profile in one web may have a very small eccentricity, thus having a potentially adverse effect on the ultimate flexural strength of the section. If the cable eccentricity is too large, the prestressing force in the web may be increased and the cable eccentricity proportionately decreased. However, this also causes a change in eccentricity of the cable at internal supports, something which may not be desirable.

Instead of adjusting the cable profile in this manner, constraint equations may be incorporated directly into the analysis to constrain the cable profiles in each web to lie within the depth of the beam. This will be outlined in Section 5.7.

5.6 Residual Moments

As discussed in the preceeding section, Equation 5.10 gives a least squares approximation to a condition of exactly balanced bending and torsional moments. In this case $\{\Delta M\}_{adjusted}$ is not equal to $\{0\}$. Residual bending and torsional moments, $\{R\}$, occur at each section, and ΣR_i^2 is a minimum for the chosen unit cable profiles and prestressing forces. In general, the greater the number of unit cable profiles used, the smaller is the value of ΣR_i^2.

Using Equation 5.9 the following relationship may be written:

$$I = \Sigma R_i^2 = \{R\}^T\{R\} = \text{minimum}$$

$$= \{ [\Delta A_u]\{\eta\} - \{\Delta M\} \}^T \{ [\Delta A_u]\{\eta\} - \{\Delta M\} \}$$

$$I = \{\eta\}^T[\Delta A_u]^T[\Delta A_u]\{\eta\} - \{\eta\}^T[\Delta A_u]^T\{\Delta M\} - \{\Delta M\}^T[\Delta A_u]\{\eta\} + \{\Delta M\}^T[\Delta A_u] = \text{minimum}$$

$$I = \{\eta\}^T[\Delta A_u]^T[\Delta A_u]\{\eta\} - 2\{\eta\}^T[\Delta A_u]^T\{\eta\} + \{\Delta M\}^T\{\Delta M\} \qquad (5.11)$$

If $\frac{\partial I}{\partial \{\eta\}} = \{0\}$

then $[\Delta A_u]^T[\Delta A_u]\{\eta\} - [\Delta A_u]^T\{\Delta M\} = \{0\}$

Therefore $[U]\{\eta\} - \{B\} = \{0\}$

which is Equation 5.10.

Thus Equation 5.10 minimizes the sum of the squared residual bending and torsional moments.

5.7 Geometrical Constraint of the Cable Profile

The adjusted cable profile in each web may be constrained, using the Lagrange multiplier technique (12), to lie within the depth of the bridge cross section. The eccentricity of the adjusted cable profile is constrained at required sections along the bridge. At any point, c,

the adjustment in cable eccentricity in a given web may be set equal to a specified value, e_c. For example, the eccentricity of the basic cable profile at midspan may be such that it cannot be exceeded without going outside the beam depth. In this case the sum of the ordinates of the unit cable profiles, factored by the appropriate terms of the vector $\{\eta\}$ may be set to zero, so that no change in the basic cable profile occurs at this section. This can be expressed as follows:

$$[\ N_1(c)\ N_2(c)\ \ldots\ ]\ \{\eta\} \quad = \quad e_c \tag{5.12}$$

where $N_1(c)$, $N_2(c)$, ... are the ordinates of the unit cable profiles at the section and $\{\eta\}$ is the vector of computed scaling factors. Where there are more than one constraint this equation may be written in matrix form as:

$$[C]\ \{\eta\} \quad = \quad \{Q\} \tag{5.13}$$

There are generally more unit cable profiles than constraint equations so [C] is a rectangular matrix with more columns than rows.

The above equation may be multiplied by the row vector $2\{\lambda\}^T$. This vector contains as many Lagrange multipliers as there are constraint equations. Thus:

$$2\{\lambda\}^T([C]\{\ \} - \{Q\}\ ) \quad = \quad \{0\} \tag{5.14}$$

The above term may be added to the functional equation, 5.11, in the previous section without altering its value, thus:

$$\begin{aligned} I \quad = \quad & \{\eta\}^T[U]\{\eta\} - 2\{\eta\}^T\{B\} + \{\Delta M\}^T\{\Delta M\} \\ & - 2\{\lambda\}^T([C]\{\eta\} - 2\{Q\}\ ) \end{aligned} \tag{5.15}$$

The stationary value of I is found via:

$$\frac{\partial I}{\partial\{\eta\}} = \{0\} \ ; \quad \frac{\partial I}{\partial\{\lambda\}} = \{0\} \tag{5.16}$$

This yields:

$$\begin{bmatrix} [U] & [C]^T \\ [C] & [0] \end{bmatrix} \begin{Bmatrix} \{\eta\} \\ \{\lambda\} \end{Bmatrix} \quad = \quad \begin{Bmatrix} \{B\} \\ \{Q\} \end{Bmatrix} \tag{5.17}$$

The equation may be solved for the unknown parameters, $\{\eta\}$, and the Lagrange multipliers $\{\lambda\}$. The zero diagonal terms

in the above equation cause no problem as they become non zero in the Gaussian elimination process.

5.8 Method of Torsional Moment Control, Applied to a Two Span Bridge

The bridge geometry is shown in Figure 5.11. The centreline radius is 64.0 m and the span angle is 30.28°. The bridge is symmetric and thus, as for the example shown in Figure 5.3, only a single span is analysed. Two six node Jirousek elements (a total of eleven nodes), are used to model the bridge. The bridge section is not symmetric about the y' axis, and thus the shear centre does not coincide with the centroid. The method for locating the shear centre is outlined in Appendix A.

A basic cable profile, as shown, is adopted in the analysis. A dead load of 164 kN/m, corresponding to the self weight of the cross section is to be balanced. For the chosen profile, the required total prestressing force is given as

$$P = \frac{w\ell^2}{8s}$$

where w is the dead load, ℓ is the developed length of the span, and s is the cable sag as shown. This gives P = 18.70 MN; equal prestressing is assumed in both webs, so

that $P_{inner} = P_{outer} = 9.35$ MN. The above represents Step (1) of the analysis outlined in Section 5.5. The torsional moment diagram due to the dead load and basic prestressing is shown in Figure 5.13. The computed bending and torsional moments at the eleven nodes of the structure are listed in the vector $\{\Delta M\}$, Step (2).

$$\{\Delta M\} = \begin{Bmatrix} -3.236 \\ -3.360 \\ -3.021 \\ -2.320 \\ -1.357 \\ -0.232 \\ 0.944 \\ 2.078 \\ 3.060 \\ 3.788 \\ 4.164 \\ -1.160 \\ -0.774 \\ -0.483 \\ -0.264 \\ -0.099 \\ 0.024 \\ 0.111 \\ 0.162 \\ 0.169 \\ 0.121 \\ 0.000 \end{Bmatrix} \text{ MNm} \qquad (5.18)$$

The first eleven terms in this vector represent the torsional moments at the eleven points. The bending moments are given by the second eleven terms of the vector. As can be readily seen these are small; thus the basic prestressing balances closely the dead load bending moments. The value of I is equal to $86.75\,(\text{MNm})^2$.

5.8.1 Profile Adjustment - Assuming that the computed torsional moments are excessive, we now proceed to Step

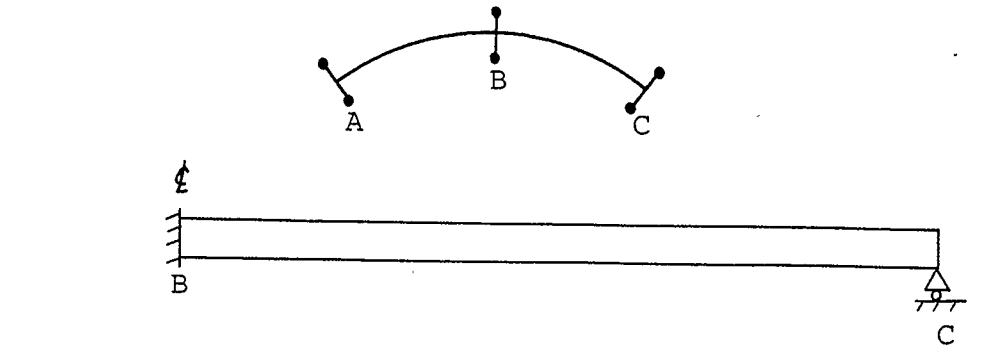

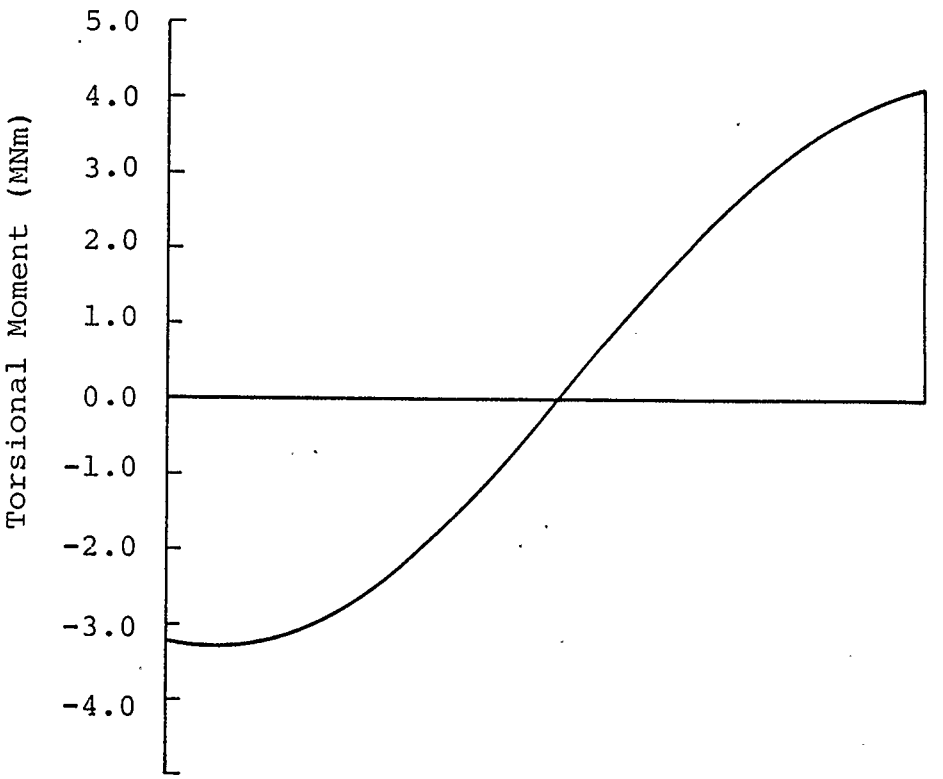

Figure 5.13 Torsional Moment Diagram due to Dead Load and Basic Prestressing, for the Two Span Example, Figure 5.11

(3), in which the basic cable profile is adjusted by the addition of unit cable profiles. The method outlined in Section 5.5 is applied using three combinations of unit cable profiles. Firstly the analysis is carried out with only a single quadratic term applied to each web, Figure 5.9(b). The procedure is repeated with the quadratic plus two cubic terms, Figure 5.9 (e) and (f) superimposed in each web. The analysis is further extended to include the quartic terms (i), (j) and (k) of Figure 5.9. This represents Step (4) of the procedure. The unit cable profiles are numbered as is shown in Figure 5.14.

The bending and torsional moments corresponding to these unit cable profiles are computed at each nodal point of the structure. The moments due to each unit profile are listed in the corresponding column of the matrix $[\Delta A_u]$. The matrices $[\Delta A_u]$ generated for quadratic only, and for quadratic and cubic unit profiles are given below. Space restrictions preclude the listing of $[\Delta A_u]$ for quadratic, cubic and quartic terms added to the basic profiles. In this case there would be twelve columns, corresponding to six unit cable profiles in each web. For the quadratic unit cable profiles:

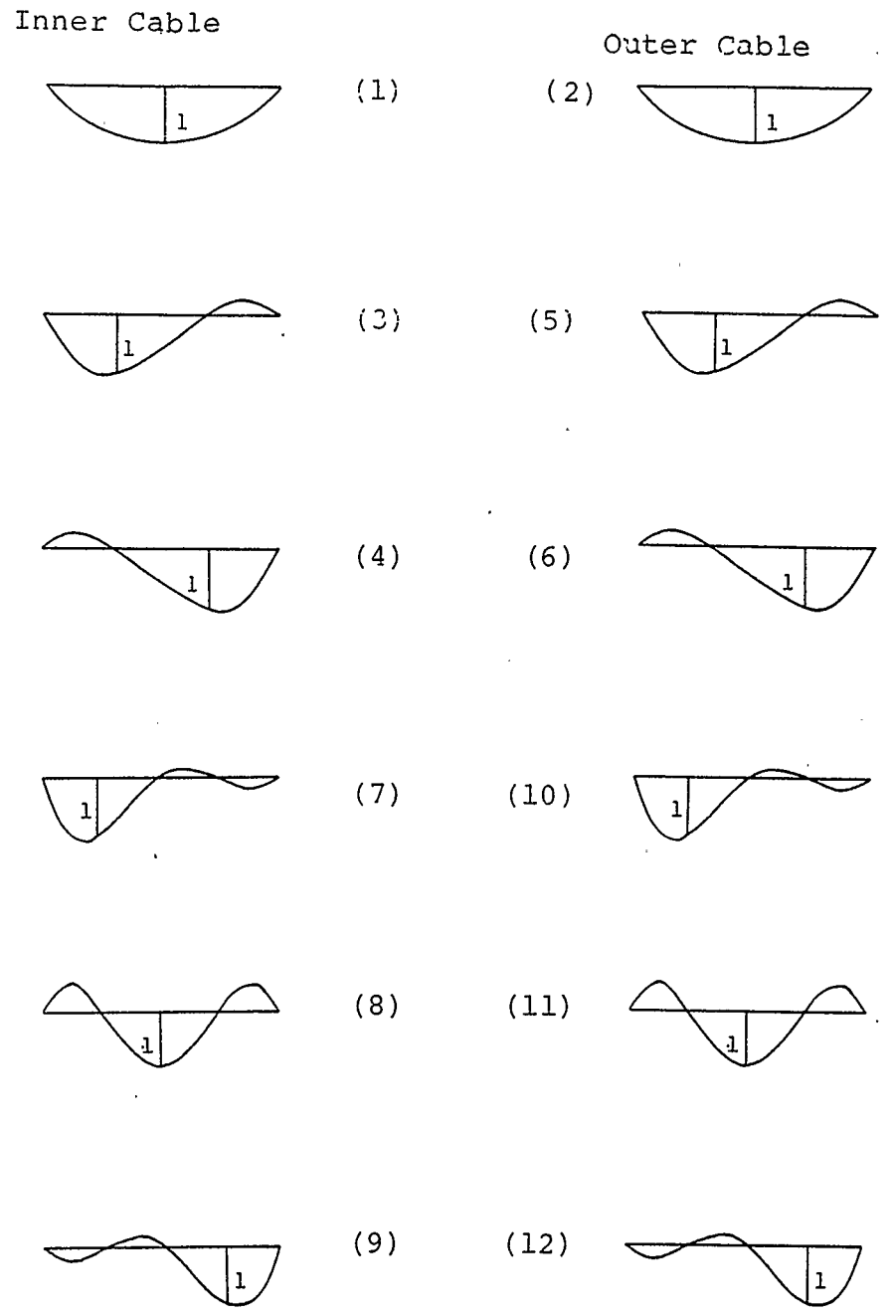

Figure 5.14 Unit Cable Profiles, Quadratic, Cubic and Quartic

$$[\Delta A_u] = \begin{bmatrix} -5.542 & 1.581 \\ -4.303 & 1.396 \\ -3.107 & 1.166 \\ -1.957 & 0.891 \\ -0.853 & 0.569 \\ 0.203 & 0.200 \\ 1.210 & -0.217 \\ 2.167 & -0.683 \\ 3.074 & -1.199 \\ 3.930 & -1.763 \\ 4.735 & -2.377 \\ 9.129 & 9.000 \\ 4.760 & 4.978 \\ 1.152 & 1.644 \\ -1.693 & -1.001 \\ -3.772 & -2.956 \\ -5.080 & -4.216 \\ -5.619 & -4.776 \\ -5.380 & -4.636 \\ -4.658 & -3.796 \\ -2.574 & -2.251 \\ 0.000 & 0.000 \end{bmatrix} \quad (5.19)$$

For the quadratic plus cubic profiles the matrix is

$$[\Delta A_u] = \begin{bmatrix} -5.542 & 1.581 & -10.221 & 4.301 & 5.728 & -3.879 \\ -4.303 & 1.396 & -5.725 & 1.175 & 2.963 & -1.234 \\ -3.107 & 1.166 & -2.298 & -1.038 & 0.567 & 0.845 \\ -1.957 & 0.891 & 0.442 & -2.519 & -1.085 & 2.188 \\ -0.853 & 0.569 & 2.358 & -3.185 & -2.132 & 2.867 \\ 0.203 & 0.200 & 3.428 & -3.046 & -2.571 & 2.887 \\ 1.210 & -0.217 & 3.668 & -2.109 & -2.401 & 2.238 \\ 2.167 & -0.683 & 3.080 & 0.363 & -1.626 & 0.889 \\ 3.074 & -1.199 & 1.639 & 2.196 & -0.253 & -1.059 \\ 3.930 & -1.763 & -0.375 & 2.991 & 1.723 & -4.206 \\ 4.735 & -2.377 & -2.092 & 4.535 & 7.706 & -14.059 \\ 9.129 & 9.000 & 8.325 & 4.983 & 7.971 & 2.604 \\ 4.760 & 4.978 & 0.774 & 3.571 & 1.143 & 4.787 \\ 1.152 & 1.644 & -3.149 & 3.913 & -2.466 & 4.480 \\ -1.693 & -1.001 & -4.316 & 2.319 & -3.488 & 2.401 \\ -3.772 & -2.956 & -3.469 & -0.432 & -2.686 & -0.712 \\ -5.080 & -4.216 & -1.398 & -3.542 & -0.782 & -4.144 \\ -5.619 & -4.776 & 1.097 & -6.226 & 1.502 & -7.182 \\ -5.380 & -4.636 & 3.242 & -7.689 & 3.452 & -9.101 \\ -4.658 & -3.796 & 4.236 & -7.124 & 4.357 & -9.179 \\ -2.574 & -2.251 & 3.270 & -4.110 & 3.502 & -6.606 \\ 0.000 & 0.000 & 0.000 & 0.000 & 0.000 & 0.000 \end{bmatrix} \quad (5.20)$$

As in the case the vector $\{\Delta M\}$ the first eleven terms of each column represent the torsional moments. The second eleven terms are the bending moments. Individual columns correspond to the unit profiles numbered in Figure 5.14. The solution of Equation 5.10 is initially carried out

without geometric constraint of the prestressing cables. The computed cable eccentricities, residual moments and scaling factors, $\{\eta\}$, are given in Tables 5.2 to 5.4; for the case of quadratic terms only, quadratic plus cubic, and quadratic, cubic plus quartic terms respectively added to the basic cable profiles.

It can be seen that the greater the number of unit cable profiles added, the closer to an exactly balanced configuration are the adjusted moments. In all cases the adjusted outer cable profiles have eccentricities which are too large at midspan. On the other hand the inner cable eccentricities are decreased by the factored unit cables. Obviously the eccentricities in the outer web are unsatisfactory. However, because the forces due to a given cable profile are proportional to the product Pe we may change the cable profile and prestressing force provided the product Pe remains constant. While this may contravene the principle of superposition outlined in Section 5.4, the resulting cable profile is a useful first approximation to a satisfactory solution. The exact distribution of moments, resulting from this set of profiles, may be obtained by re-analysing the structure using SFRAME. For each of the three sets of computed cable profiles in Tables 5.2 to 5.4, the prestressing force in the outer web may be increased until the outer web cable lies entirely within the beam depth. However, decreasing the cable eccentricity at midspan also has the undesirable effect of decreasing the eccentricity over the internal support, Figure 5.15.

P_{inner} = 9.35 MN	T_{max} = 1.033 MNm
P_{outer} = 9.35 MN	I = 2.40 $(MNm)^2$

Node	Residual Moments (MNm)		Cable Eccentricities (m)	
	Bending	Torsion	Inner	Outer
1	-0.023	1.003	-0.500	-0.500
2	-0.013	0.071	-0.205	0.252
3	0.021	-0.430	0.034	0.849
4	0.038	-0.577	0.220	1.289
5	-0.013	-0.471	0.352	1.573
6	-0.202	-0.210	0.429	1.701
7	-0.020	0.104	0.452	1.673
8	0.030	0.363	0.420	1.489
9	0.019	0.465	0.334	1.149
10	0.009	0.312	0.194	0.652
11	0.0	-0.205	0.0	0.0

Unit Cable Scaling Factors (Figure 5.14)

Inner Web		Outer Web	
1	-0.571	2	0.701

Table 5.2 - Unconstrained Cable Profile, Quadratic Terms Added

P_{inner}= 9.35 MN	T_{max} = 0.445 MNm
P_{outer}= 9.35 MN	I = 0.769 $(MNm)^2$

Node	Residual Moments (MNm)		Cable Eccentricities (m)	
	Bending	Torsion	Inner	Outer
1	-0.197	0.445	-0.500	-0.500
2	0.098	-0.091	-0.182	0.253
3	-0.012	-0.229	0.056	0.865
4	-0.068	-0.160	0.221	1.330
5	-0.129	0.032	0.321	1.643
6	-0.285	0.251	0.365	1.799
7	-0.044	0.397	0.359	1.790
8	0.061	0.286	0.312	1.611
9	0.072	0.051	0.232	1.257
10	0.369	-0.123	0.125	0.722
11	0.0	0.009	0.0	0.0

Unit Cable Scaling Factors (Figure 5.14)

Inner Web		Outer Web	
1	-0.547	2	1.295
3	-0.030	5	-0.478
4	-0.126	6	-0.405

Table 5.3 - Unconstrained Cable Profile, Quadratic and Cubic Terms Added

P_{inner} = 9.35 MN T_{max} = 0.026 MNm

P_{outer} = 9.35 MN I = 0.027 $(MNm)^2$

Node	Residual Moments (MNm)		Cable Eccentricities (m)	
	Bending	Torsion	Inner	Outer
1	0.009	0.004	-0.500	-0.500
2	-0.043	0.000	-0.172	0.231
3	-0.022	0.002	0.056	0.841
4	0.041	0.003	0.210	1.310
5	0.037	-0.003	0.296	1.623
6	-0.131	0.000	0.365	1.770
7	0.035	0.026	0.373	1.745
8	0.032	-0.023	0.370	1.548
9	-0.015	-0.014	0.310	1.184
10	-0.011	0.008	0.194	0.663
11	0.0	-0.002	0.0	0.0

Unit Cable Scaling Factors (Figure 5.14)

Inner Web		Outer Web	
1	-0.650	2	0.810
3	-0.183	5	-0.247
4	-0.169	6	0.173
7	0.255	10	0.221
8	0.128	11	0.001
9	0.000	12	-0.268

Table 5.4 - Unconstrained Cable Profile, Quadratic, Cubic and Quartic Terms Added

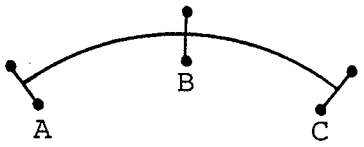

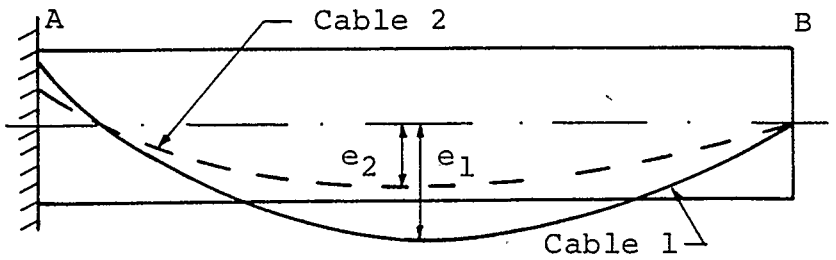

$$P_1 e_1 = P_2 e_2$$

Figure 5.15 Decreasing the Cable Eccentricity to Fit Within Beam

Transverse moments in the cross section are generated by the increase in the prestressing force in the outer web. However, given that the moment of inertia of most practical box sections is greater about its z' axis than about the y' axis, a section can sustain a significant transverse moment without large stresses occuring at the extreme fibres. In the following discussion the statically determinate transverse bending moments, due to different web prestressing forces, are considered. The determinate transverse moments give an indication of the changes in extreme fibre stresses due to different web prestressing forces. Indeterminate transverse moments are generated by reactions at the bearings, but they are not investigated here. In the example considered, Figure 5.11, $I_{z'}$ is given as 56.5 m^4. Referring to Table 5.5, the transverse bending moment $M_{z'}$, generated by decreasing the outer cable eccentricity is equal to 41.9 MNm, for the solution where quadratic terms only are added to the basic cable profile. The modulus of rupture for normal density concrete may be approximated by $f_r = 0.6 \sqrt{f'_c}$, so that for an assumed concrete strength of 40 MPa, f_r = 3.8 MPa. The extreme fibre stress due to a transverse moment of 41.9 MNm is (for y = 5.0 m):

$$f = \frac{41.9 \times 5.0}{56.5} = 3.7 \text{ MPa}$$

While less than the modulus of rupture; this value may or may not be considered excessive.

	P_{outer} (MN)	e_{max} (m)	$M_{z'}$ (MNm)
Quadratic			
(a)	9.35	1.701	0.0
(b)	15.90	1.000	41.92
Quadratic and Cubic			
(a)	9.35	1.799	0.0
(b)	16.82	1.000	47.81
Quadratic, Cubic and Quartic			
(a)	9.35	1.770	0.0
(b)	16.55	1.000	46.08

(a) = Unconstrained Profile

(b) = Cable Profile Factored to Fit within Bridge

Table 5.5 - Effect of Bringing Outer Cable Profile Within Bridge Depth

5.8.2 Constraint of the Cable Profile - As an alternative to manipulating the prestressing force and cable eccentricity as outlined above, constraints may be applied to the cable profile as discussed in Section 5.7. It is clear from Tables 5.2 to 5.4 that the eccentricity of the outer cable is always greater than that of the inner

cable. Thus by constraining the outer cable to have a maximum eccentricity, the inner cable will also be forced to lie inside the beam depth. In the present analysis the change in eccentricity of the outer cable is set to zero at midspan. Thus referring to Figure 5.14 the constraint equation is, when quadratic terms only are added:

$$1.0\ \eta_2 = 0.0 \tag{5.21}$$

For the case of quadratic and cubic terms added to the basic profiles the constraint equation is:

$$1.0\eta_2 + 0.5625\eta_5 + 0.5625\eta_6 = 0.0 \tag{5.22}$$

where 0.5625 is the magnitude of the unit cable profiles (5) and (6), Figure 5.14, at the midspan of the beam. Similarly for quadratic, cubic and quartic terms added the constraint equation becomes:

$$1.0\eta_2 + 0.5625\eta_5 + 0.5625\eta_6 + 1.0\eta_{11} = 0.0 \tag{5.23}$$

The quartic unit profiles (10) and (12), Figure 5.14, are not included since their magnitudes are zero at midspan.

The results of the constrained analysis are shown in Tables 5.6 to 5.8. It can be seen that the constrained

P_{inner}= 9.35 MN	T_{max} = 3.077 MNm
P_{outer}= 9.35 MN	I = 68.17 $(MNm)^2$

Node	Residual Moments (MNm)		Cable Eccentricities (m)	
	Bending	Torsion	Inner	Outer
1	-3.219	-1.968	-0.500	-0.500
2	-1.879	-2.376	-0.083	0.0
3	-0.739	-2.308	0.253	0.400
4	0.162	-1.869	0.507	0.700
5	0.772	-1.161	0.679	0.900
6	1.021	-0.281	0.770	1.000
7	1.411	0.669	0.779	1.000
8	1.445	1.581	0.707	0.900
9	1.191	2.355	0.553	0.700
10	0.710	2.889	0.317	0.400
11	0.000	3.077	0.000	0.000

Unit Cable Scaling Factors (Figure 5.14)

Inner Web		Outer Web	
1	-0.230	2	0.0

Table 5.6 - Constrained Cable Profile, Quadratic Terms Added

P_{inner}= 9.35 MN	T_{max} = 2.727 MNm
P_{outer}= 9.35 MN	I = 38.13 $(MNm)^2$

Node	Residual Moments (MNm)		Cable Eccentricities (m)	
	Bending	Torsion	Inner	Outer
1	-1.488	-0.314	-0.500	-0.500
2	-1.565	-1.458	-0.188	-0.013
3	0.111	-2.076	0.118	0.383
4	0.969	-2.089	0.398	0.685
5	1.151	-1.633	0.632	0.891
6	0.788	-0.818	0.801	1.000
7	0.573	0.250	0.887	1.008
8	0.230	1.889	0.869	0.915
9	0.047	2.727	0.728	0.717
10	0.143	1.993	0.445	0.413
11	0.000	-0.944	0.000	0.000

Unit Cable Scaling Factors (Figure 5.14)

Inner Web		Outer Web	
1	-0.762	2	-0.987
3	0.381	5	0.864
4	0.620	6	0.890

Table 5.7 - Constrained Cable Profile, Quadratic and Cubic Terms Added

P_{inner} = 9.35 MN T_{max} = -1.565 MNm

P_{outer} = 9.35 MN I = 10.36 $(MNm)^2$

Node	Residual Moments (MNm)		Cable Eccentricities (m)	
	Bending	Torsion	Inner	Outer
1	-0.420	-0.778	-0.500	-0.500
2	-0.440	-0.779	-0.169	-0.144
3	0.586	-0.854	0.123	0.299
4	0.518	-1.145	0.386	0.690
5	0.197	-1.544	0.649	0.892
6	-0.151	0.030	0.818	1.000
7	0.150	-1.565	0.980	0.823
8	0.707	0.334	0.989	0.594
9	0.293	0.144	0.883	0.260
10	-0.548	-0.359	0.577	0.002
11	0.000	-0.236	0.000	0.000

Unit Cable Scaling Factors (Figure 5.14)

Inner Web		Outer Web	
1	-0.919	2	-7.266
3	1.071	5	18.58
4	0.724	6	-6.499
7	-0.592	10	-15.57
8	-0.273	11	0.470
9	0.296	12	15.84

Table 5.8 - Constrained Cable Profile; Quadratic Cubic and Quartic Terms Added

analysis produces residual moments which are appreciably higher than those obtained in the unconstrained analysis. In addition the inner web cable profiles have a greater positive eccentricity than the corresponding unconstrained profiles. Thus the net effect of the geometric cable constraints is to produce a less optimal solution with respect to residual moments, but one in which no transverse moments are generated.

As can be seen in Figure 5.16 the reduction in torsional moments achieved by the constrained adjusted profiles is relatively small. It is obvious that equal prestressing forces of 9.35 MN in each web do not give the greatest reduction in torsional moments. It can be seen in Figure 5.17 that by increasing the prestressing force in the outer web of the beam, while maintaining a force of 9.35 MN in the inner web, a more significant decrease in torsional moments can be achieved. Referring to Figure 5.17, a force of 14.0 MN (approx.) in the outer web produces the maximum decrease in torsion. Thus by repeating the preceeding analysis, Steps (1) to (6), with the appropriate constraints applied to the cable profile, an approximate best combination of prestressing forces can be determined. If this combination of prestressing forces produces transverse moments which are too large, then a smaller difference in web prestressing forces can be

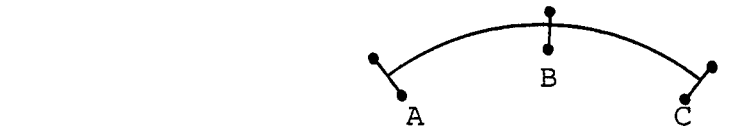

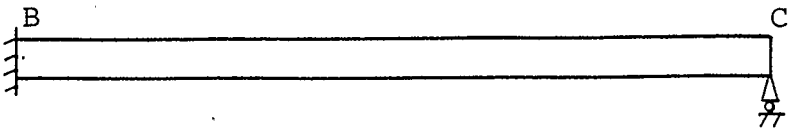

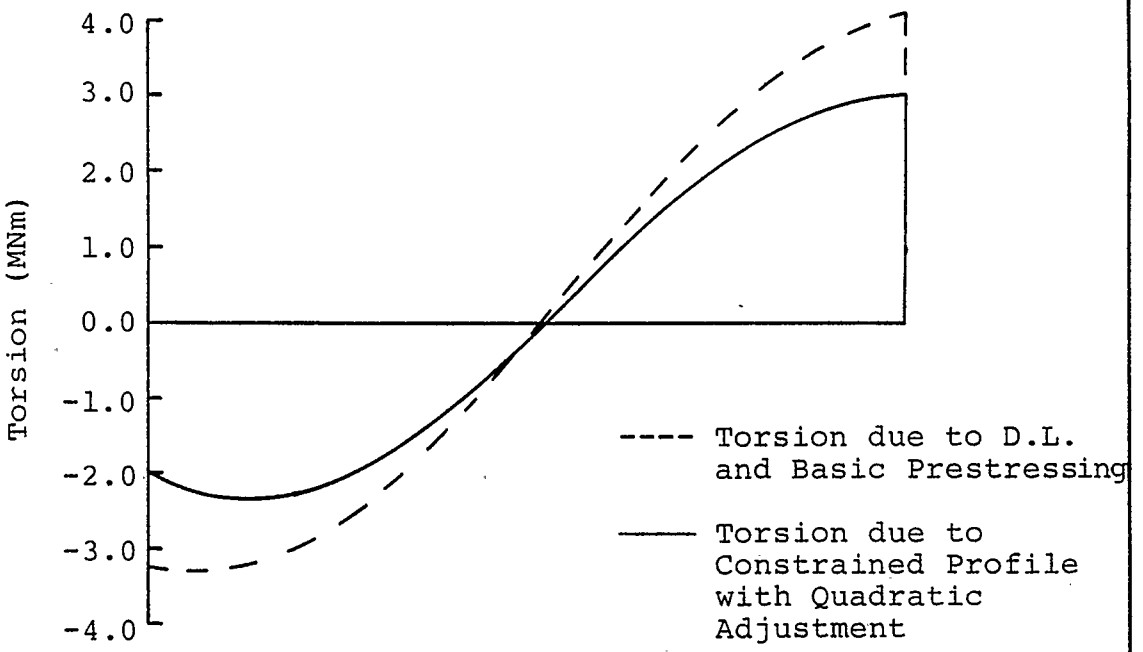

Figure 5.16 Torsional Moments, for Constrained Cable Profile, with Quadratic Terms Added

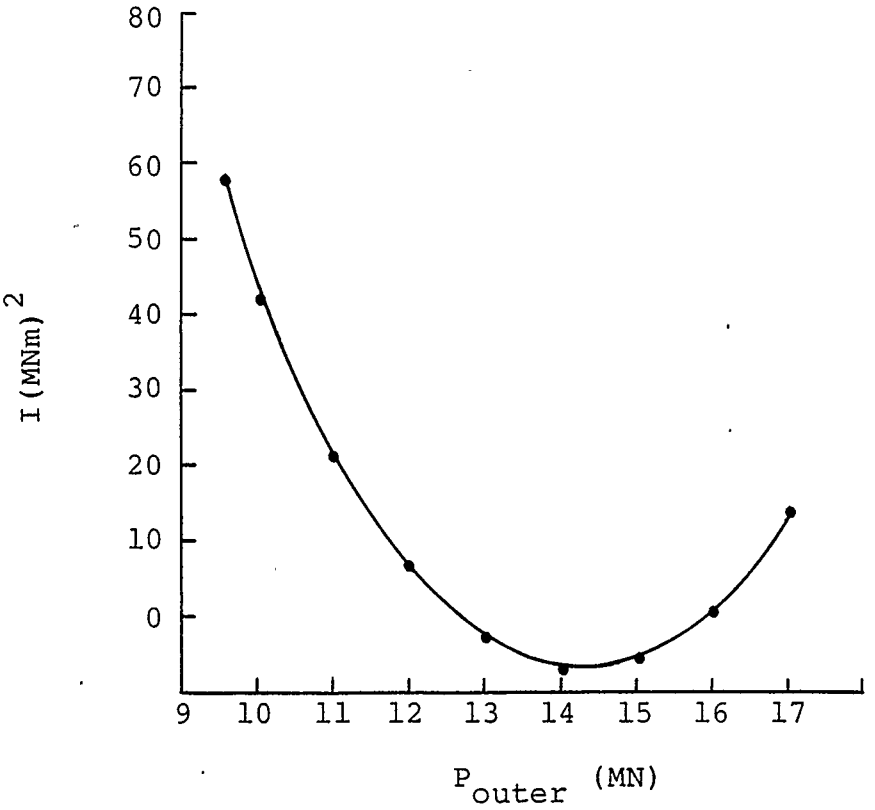

Figure 5.17 Variation of Sum of Squared Residual Moments I, with Outer Web Prestressing Force

selected. Thus the designer must establish a balance between the desired maximum reduction in torsional moments and the maximum permissible transverse moment.

5.9 Optimum Prestressing Forces

A more elegant formulation, than the process of repeating the analysis for different combinations of prestressing forces, is to incorporate an optimization subroutine into the procedure, to automatically compute the optimum web prestressing forces. In Section 5.6 it has been shown that I (= ΣR_i^2) is a measure of the closeness of any computed solution to a configuration of exactly balanced bending and torsional moments. In the present optimization procedure we seek a solution that minimizes the functional I. A subroutine, ZXMWD, from the IMSL library of fortran subroutines (24), is used to compute the optimum combination of prestressing forces, using a direct search technique (9,41). At each stage of the search process a specific set of prestressing forces is assumed. The vector, $\{\Delta M\}$, and the matrix, $[\Delta A_u]$, corresponding to these prestressing forces are formed (Step (6) of the analysis in Section 5.5). Equation 5.17 is then solved to give the appropriate cable profiles. The objective function, I, is computed and returned to the optimization subroutine, ZXMWD. The process is repeated until the

minimum value of I has been computed. The web prestressing forces corresponding to this value of I are the optimum values. The maximum and minimum prestressing forces allowable in each web are input as constraints to the problem. Thus the designer may constrain both the geometry of the cables, using Lagrange multipliers, and the permissible magnitudes of the prestressing forces in the bridge.

5.10 Optimum Prestressing Forces for the Bridge in Figure 5.11

The analysis carried out in Section 5.8 is now extended to include the computation of optimum prestressing forces. The analysis is again carried out for quadratic, quadratic plus cubic, and quadratic, cubic plus quartic unit profiles added to each web. The constraint equations 5.21 to 5.23 are again included to constrain the cable profiles to lie within the bridge depth. A number of prestressing force constraints are applied. For each set of added unit cable profiles, the minimum prestressing force in each web was successively set at 4.70 MN, 7.0 MN, 9.35 MN and 11.70 MN. In all cases the maximum prestressing force was set at a sufficiently high value, that it was not a governing constraint. The results of the analysis are given in Tables B.1 to B.12 in Appendix B, and

are summarized in Table 5.9. Specific reference will only be made to the quadratic unit profile analysis, but the other combinations are included for completeness.

Inspection of Table 5.9 reveals that the optimum solution minimizes the force in the inner web. The outer web forces vary by very little as the minimum permissible web force is changed. For a minimum allowable web force of 4.70 MN a large difference occurs between the optimum forces in each web, thus producing a high transverse moment of of 63.88 MNm. The extreme fibre stress corresponding to this moment is 5.6 MPa, which is substantially greater than the previously computed modulus of rupture (3.8 MPa). Thus while the total prestressing force required in this case is small, the solution is not feasible because of the high transverse moment.

A specified minimum prestressing force of 7.00 MN also generates prestressing forces in each web which result in a large transverse bending moment (47.45 MNm). This again produces an extreme fibre stress that is greater than the modulus of rupture. Therefore this solution is again deemed unsatisfactory.

For a minimum prestressing force of 9.35 MN a transverse moment is generated that produces an extreme fibre stress (2.8 MPa), that is less than the modulus of rupture. It can also be seen in this case that the

P_{min} (MN)	P_{inner} (MN)	P_{outer} (MN)	P_{total} (MN)	I $(MNm)^2$	T_{max} (MNm)	$M_{z'}$ (MNm)
Quadratic						
4.7	4.70	14.603	19.303	2.30	1.005	63.38
7.0	7.0	14.417	21.417	2.47	1.061	47.45
9.35	9.35	14.228	23.573	2.67	1.117	31.25
11.7	11.7	14.038	25.738	2.90	1.174	14.96
Quadratic and Cubic Terms						
4.7	4.7	15.271	19.971	0.74	0.435	67.65
7.0	7.0	15.089	22.089	0.76	0.438	51.77
9.35	9.35	14.902	24.247	0.79	0.442	35.56
11.7	11.7	14.715	26.415	0.82	0.445	19.30
Quadratic, Cubic and Quartic Terms						
4.7	4.7	15.077	19.777	0.028	0.025	66.41
7.0	7.0	14.899	21.899	0.034	0.028	50.55
9.35	9.35	14.719	24.064	0.042	0.032	34.39
11.7	11.7	14.537	26.237	0.051	0.035	18.16

Table 5.9 - Condensed Results for Two Span Bridge, Figure 5.11

computed optimum force in the outer web is in close agreement with the optimum estimated from Figure 5.17. This serves as a check that the results obtained from the optimization procedure are correct. Because the computed optimum force in the outer web varies little as the minimum allowable prestressing force is increased, the computed total amount of prestressing increases as P_{min} is increased, Table 5.9. For P_{min} = 9.35 MN the total computed prestressing force is 1.26 times the original force chosen for the straight beam of equivalent developed length. Given that the bending moments are almost exactly balanced and that the magnitude of the torsional moments are reduced very significantly, Table B.3, this force may not be excessive.

Relatively little difference in the computed adjusted moments occur for the four values of minimum allowable web prestressing force. Thus all four solutions are of approximately equal suitability as regards control of bending and torsional moments. However, the resulting transverse moments show a wider variation in magnitude, Figure 5.18. It is clear from Table 5.9 that if a larger total prestressing force is used then the magnitude of the transverse moments will be decreased. Thus a trade off must take place between how much total prestressing force is to be used and how great a transverse moment can be

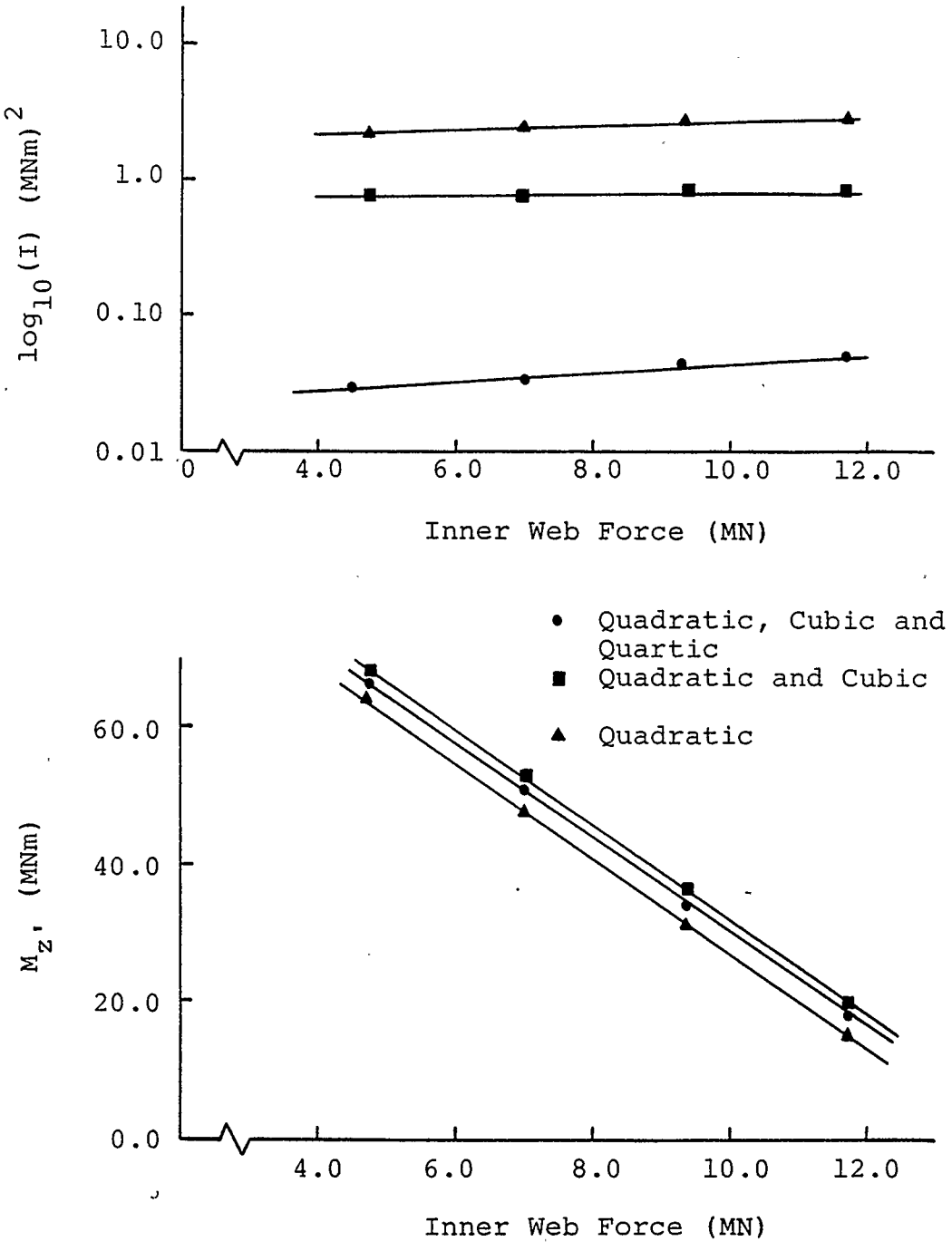

Figure 5.18 Variation of I and $M_{z'}$ with P_{inner}

sustained. If none of the above solutions is considered suitable with respect to total prestressing force and transverse moment, then a less optimal solution with respect to balancing of moments may be obtained. For example, in the case of P_{min} = 9.35 MN a more severe constraint may be applied to the maximum allowable prestressing force. If the value of P_{max} is set equal to 12.0 MN then the force in the outer web will adopt this value; the force in the inner web will remain at 9.35 MN. The resulting value of I will be greater than for an unconstrained P_{max}, however, the total prestressing force and transverse moment magnitude will be reduced. It is obvious, therefore, that to achieve desired cable profiles and prestressing forces an iterative procedure must be carried out to determine satisfactory values of residual torsional moments, total prestressing forces and transverse moments.

It can be seen in Table 5.9 that the closeness of the final solution to a condition of exactly balanced bending and torsional moments increases with an increase in the number of unit cable profiles added to each web. The resulting torsional moment diagrams, for P_{min} = 9.35 MN, are plotted in Figure 5.19 for the three combinations: quadratic, quadratic plus cubic, and quadratic, cubic plus quartic. The bending moments are in all cases very small.

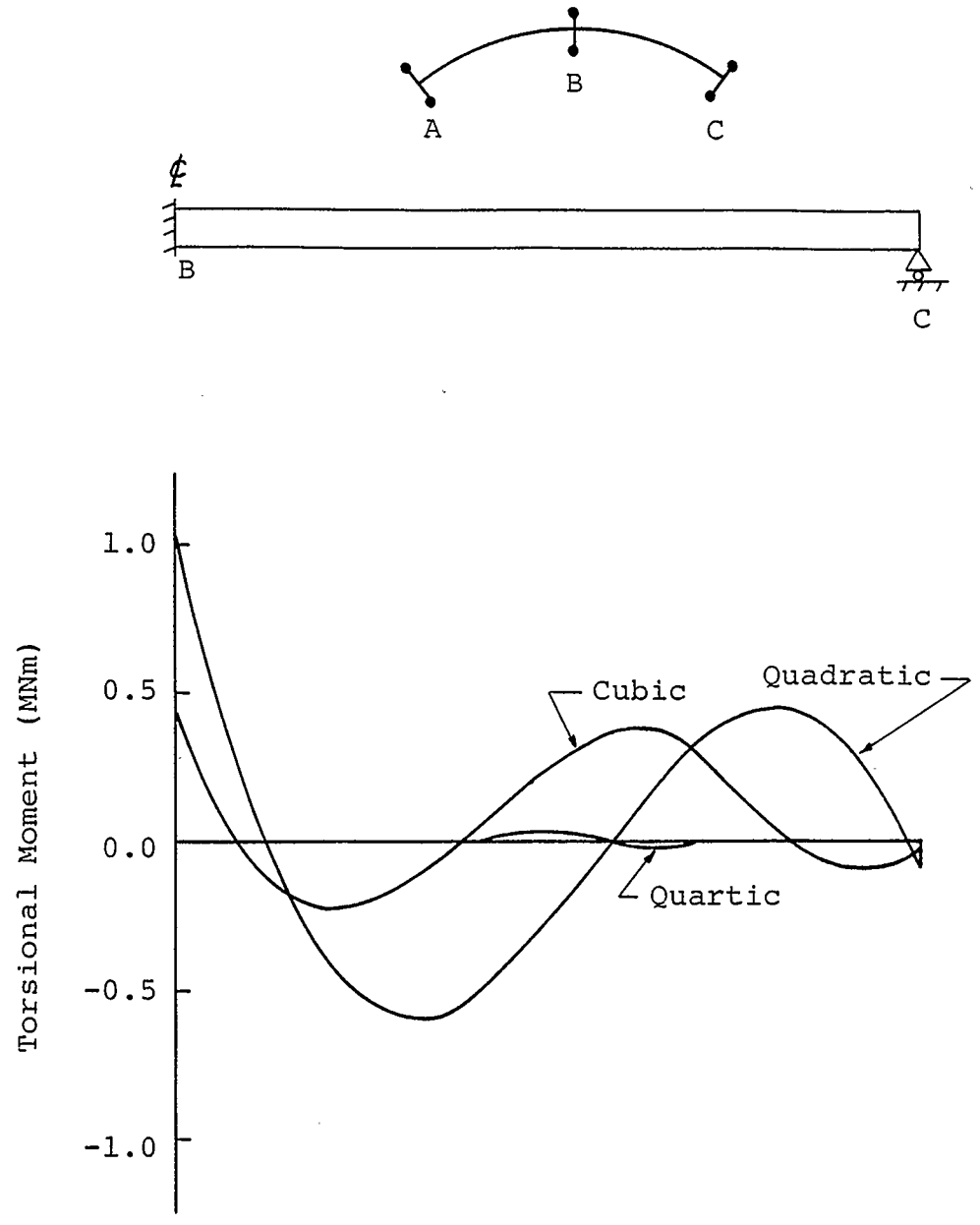

Figure 5.19 Residual Torsional Moments Obtained for the Bridge in Figure 5.11, when P_{min} is set at 9.35 MN

The magnitudes of the adjusted torsional moments may be compared with the unadjusted torsional moments in Figure 5.13. The difference in magnitude prevents all four torsion diagrams being shown on the same graph.

When quadratic, cubic and quartic terms are added to the basic cable profile very small residual moments occur. However, such complete balancing of the torsional moments is probably not warranted, and certainly the reduction achieved by using a cubic plus quadratic or even a quadratic analysis is satisfactory. The quadratic analysis is also desirable because it is the profile most commonly assumed by design engineers. The differences in computed cable profiles between the quadratic and the quadratic, cubic plus quartic analyses are shown in Figure 5.20. Though relatively small differences exist between the two sets of cable profiles, more significant differences in balancing capacity occur. Given the limitations on the degree of accuracy to which prestressing tendons may be placed on site, it may not be worthwhile to include the higher order terms in the analysis.

5.11 Three Span Example

The basic bridge geometry is shown in Figure 5.21. The two end spans are circular with centreline radii of 120m and 180m respectively, and span lengths of 50.26m and

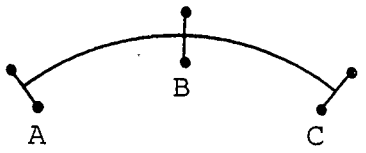

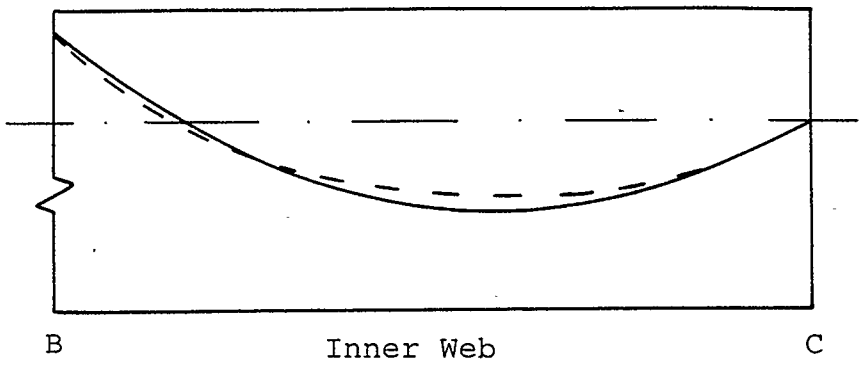

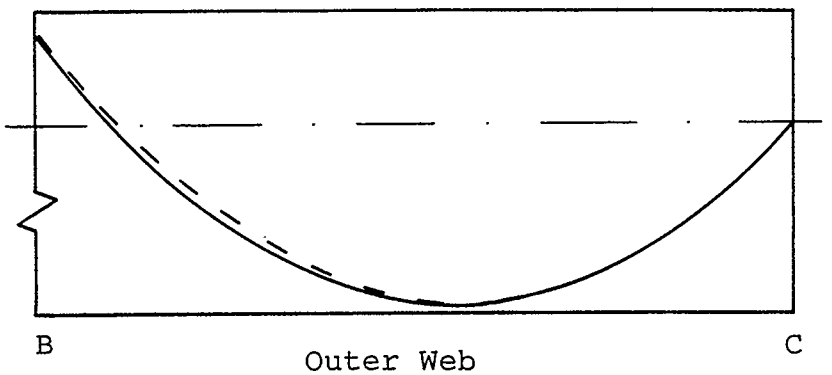

——— Quadratic

— — Quadratic, Cubic and Quartic

Figure 5.20 Comparison of Adjusted Profiles for Two Span Example with P_{min} = 9.35 MN

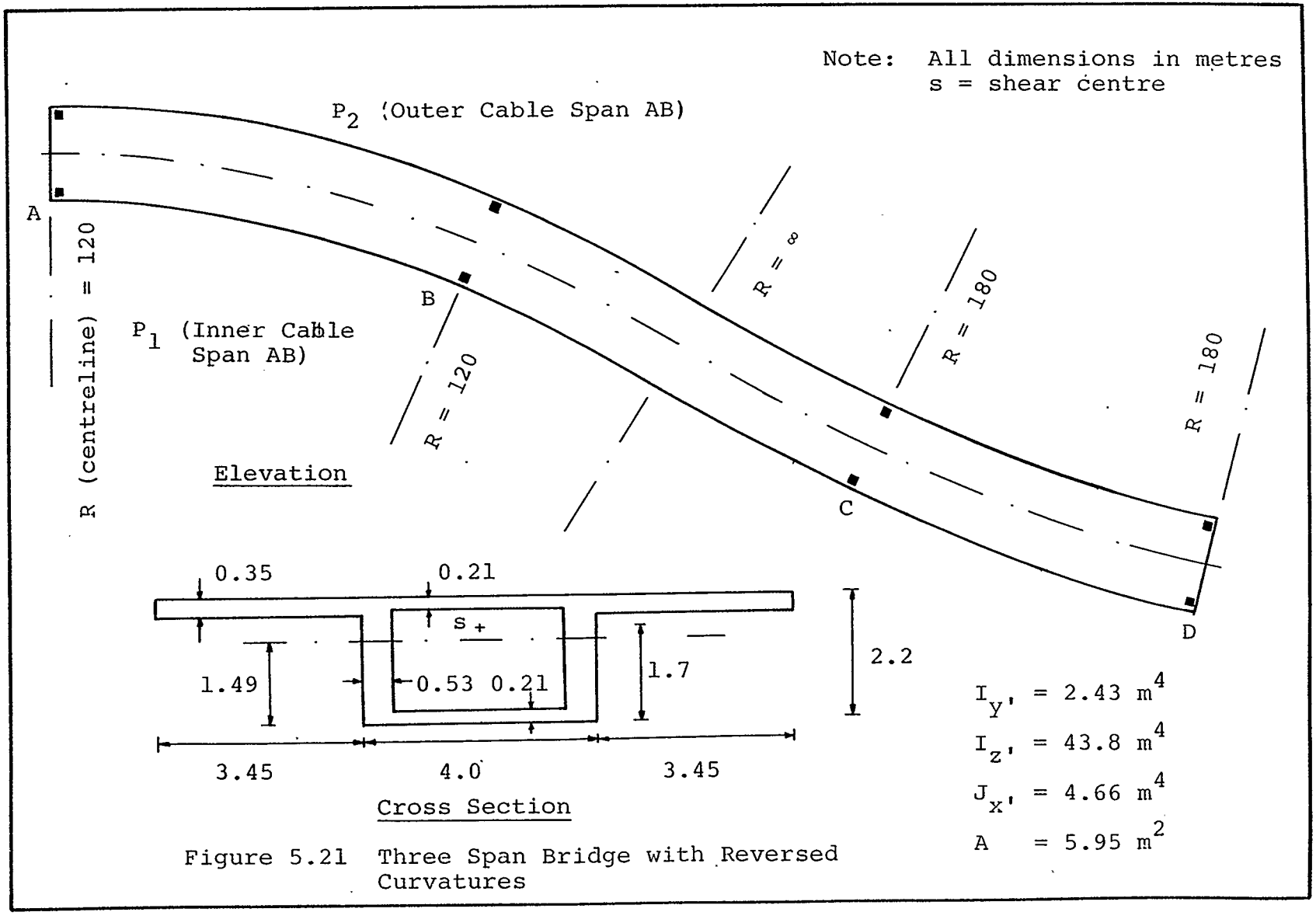

Figure 5.21 Three Span Bridge with Reversed Curvatures

40.75m respectively The centre span is composed of two cubic spirals, of total length 50m, connecting the reverse circular curves. A single box section with section properties as shown was assumed for the analysis. It was assumed that the prestressing was to balance the total dead load due to a self weight of 142.8 kN/m. The required prestressing force to balance bending moments in an equivalent straight beam was 26.53 MN, 13.625 MN in each web. The corresponding basic cable profiles are shown in Figure 5.22. The torsional moment diagram due to combined dead load and prestressing is plotted in Figure 5.23.

From the perspective of balancing torsional moments this example presents problems not encountered in the previous, symmetric example. Different radii of curvature occur in different spans, and different span lengths, are used. In addition, due to the reverse curvature, the inner web in Span AB, Figure 5.21, becomes the outer web in Span CD. As was seen in the previous two span example, a greater prestressing force is required in the outer web than in the inner, for torsional moment control. Thus there is a conflicting requirement between the two spans with respect to the web in which the greater prestressing force occurs. Because of the reverse curvatures, there is no "inner cable" or "outer cable"; for this reason cable 1

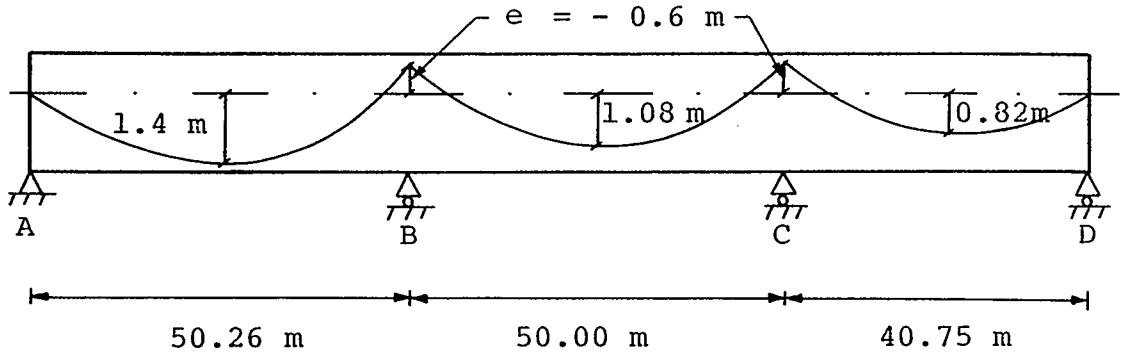

Figure 5.22 Basic Cable Profile for the Three Span Bridge in Figure 5.21

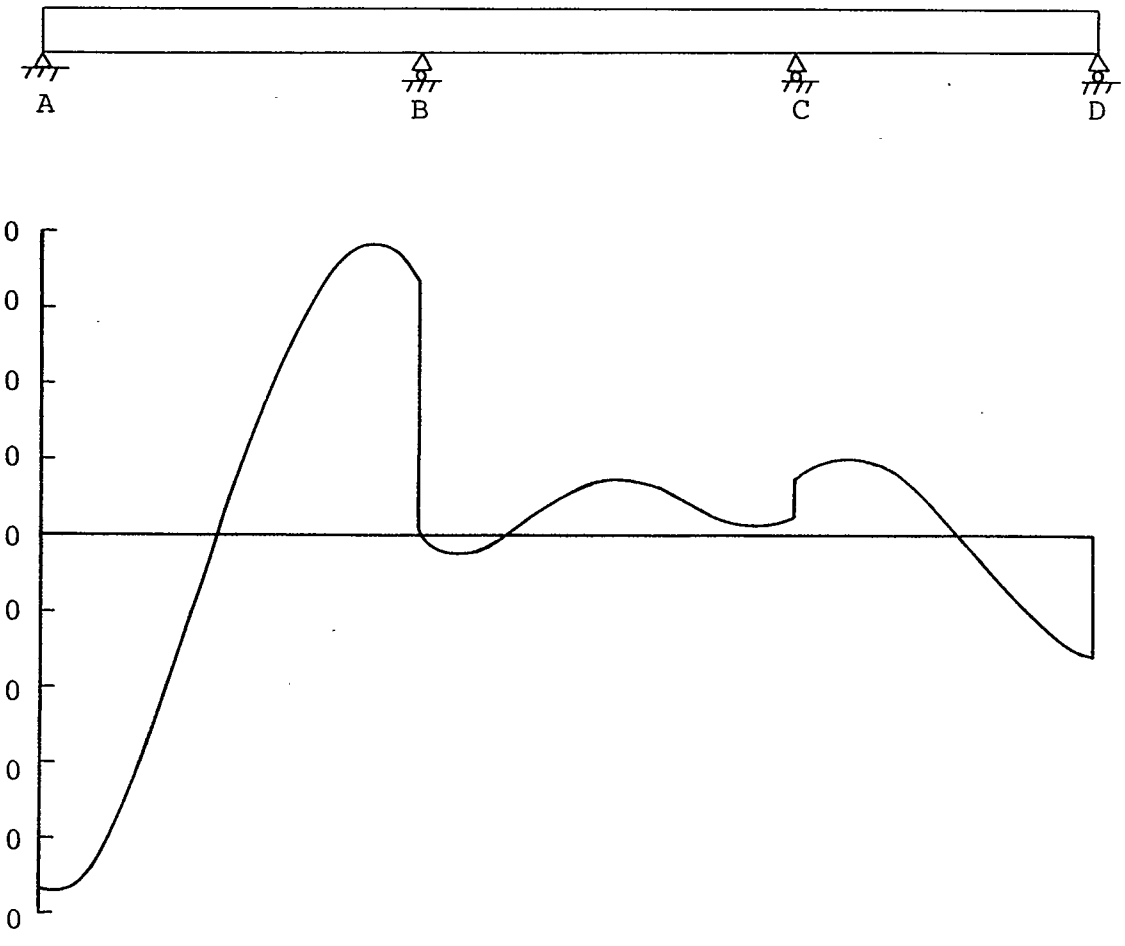

Figure 5.23 Torsion Diagram due to Dead Load and Basic Prestressing in Three Span Bridge, Figure 5.21

is defined to be in the inner web of Span AB and cable 2 in the outer web of Span AB.

The bridge was analysed using two six node Jirousek elements in each span, giving a total of six elements. The torsion control analysis was carried out with quadratic terms, only, added to the basic cable profile. Unit quadratic cables were added to each web in the three spans; thus a total of six was required. The unit profiles in Figure 5.24 are used in the analysis. With the present formulation it is possible to vary individually the cable sags in each of the three spans, but with the same force in each span.

From a number of preliminary runs it was determined that the maximum force constraint in the individual webs governed. As a result, the maximum prestressing force in each web was set successively at 17.5 MN, 20.0 MN, 22.5 MN, and 25.0 MN; and the optimum solution in each case sought. The cable profile constraint used in each case was:

$$1.0\eta_4 = 0.0 \qquad (5.24)$$

This implies that the profile of the cable in the outer web of Span AB is constrained to a maximum positive eccentricity of 1.4m. For all the solutions obtained, except the one in which a maximum cable force of 25.0 MN is prescribed, this constraint is sufficient to keep the

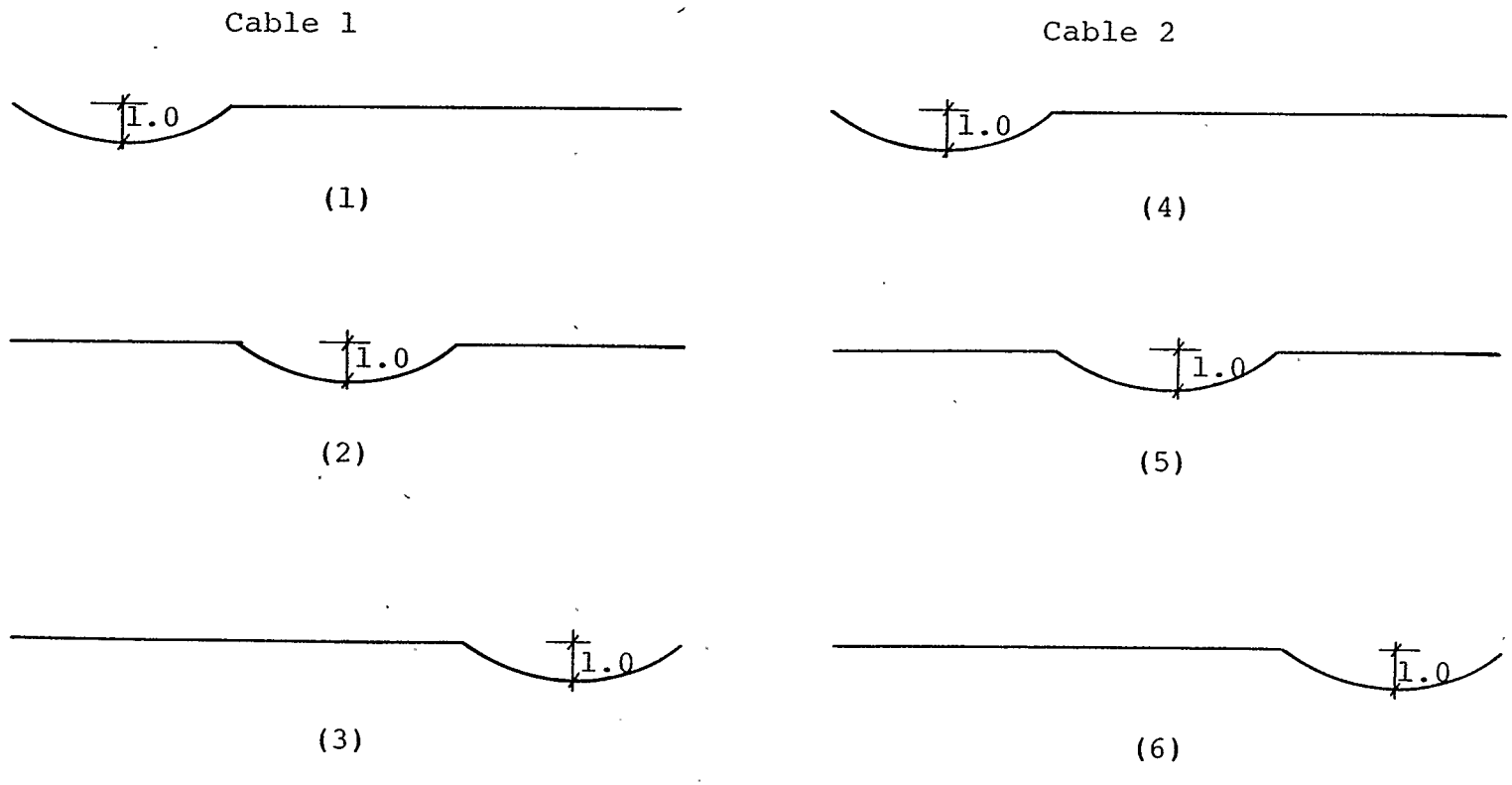

Figure 5.24 Unit Profiles Used in Three Span Bridge, Figure 5.21

resultant cable profiles within the bridge depth at all points.

5.11.1 Analysis of Results - The condensed results of the analysis for maximum web forces of 17.5 MN, 20.0 MN, 22.5 MN, and 25.0 MN are given by Solutions 1,2,3 and 4 respectively, in Table 5.10. It can be seen that for Solution 1 the optimum combination of forces is the maximum allowable, 17.5 MN in each web. The maximum torque of 4.70 MNm resulting from the basic cable profile, Figure 5.22, is reduced to 3.08 MNm - a reduction of 34%. This reduction is low, at least by comparison with the reduction achieved in the last example; however, no transverse moments are induced.

For a force of 20.0 MN in each web the maximum torsion is reduced by 59% to 1.95 MNm. In this case also, no transverse moments are induced but the prestressing force required is 1.47 times that required for an equivalent straight bridge. For Solution 3 the optimum force in the inner web of Span AB is less than the maximum allowable of 22.5 MN. The difference in cable force results in a transverse moment of 15.4 MNm. Using the section properties and dimensions given in Figure 5.21, the extreme concrete fibre stress is computed to be 1.9 MPa, which is

Soln.	P_{max} (MN)	P_1 (MN)	P_2 (MN)	P_{total} (MN)	I (MNm)	T_{max} (MNm)	$M_{z'}$ (MNm)
1	17.5	17.5	17.5	35.0	5.76E+2	3.08	0.0
2	20.0	20.0	20.0	40.0	2.67E+2	1.95	0.0
3	22.5	18.22	22.5	40.72	1.41E+2	1.11	15.4
4	25.0	8.23	24.76	32.99	1.12E+2	1.49	59.5
5	23.0	16.01	23.0	39.01	1.29E+2	1.20	25.2
6	23.5	13.81	23.5	37.31	1.21E+2	1.28	34.9
7	23.5	15.19	23.5	38.69	1.22E+2	1.39	29.9

Table 5.10 - Results for Three Span Bridge, Figure 5.21

only half the modulus of rupture (3.8 MPa) calculated in the previous example.

For a constraining maximum web force of 25.0 MN the resulting optimum cable forces are 8.23 MN and 24.76 MN. The total prestressing force is thus 32.99 MN, which is lower than for the other solutions. Because of the large difference in prestressing force between the two webs a very high transverse moment is generated. In addition, because of the very low force in cable 1, it no longer lies within the beam dimensions. Therefore this potential solution was not considered further.

Given that such a large reduction in prestressing force in cable 1 occurs between P_{max} = 22.5 MN and P_{max} = 25.0 MN, it was decided to obtain solutions for P_{max} = 23.0 MN and P_{max} = 23.5 MN, to investigate more closely the variation in optimum cable forces. For a maximum cable force of 23.0 MN, Solution 5, the total prestressing force is reduced, in comparison to Solution 3, Table 5.10, to 39.01 MN. The maximum torsional moment is slightly greater and the transverse moment of 25.2 MNm still gives an extreme fibre stress (3.1 MPa) less than the modulus of rupture. For Solution 6 the total prestressing force is further reduced but the transverse moment rises to 34.9 MN, producing an extreme fibre stress of 4.3 MPa. In addition, cable 1 sags beneath the beam depth in Span BC, Figure

5.25. Thus an extra constraint has to be applied to the profile, namely,

$$1.0\eta_2 = 0.0 \qquad (5.25)$$

The resulting profile, Solution 7, lies entirely within the beam dimensions and while producing a slightly larger maximum torsional moment it also reduces the imbalance between the web prestressing forces. The resulting transverse moment of 29.9 MNm generates an extreme fibre stress of 3.7 MPa which is less than the modulus of rupture of the concrete.

It is difficult to make categoric conclusions as to which of the above combinations of prestressing forces is the best. A reduction to a maximum torsional moment of 3.08 MNm, as achieved in Solution 1, may not be adequate. Similarly, the difference in web prestressing forces which was obtained in Solution 4 is too large and so this is not satisfactory. For Solution 6 the cable profile lies outside the girder dimensions so it too must be eliminated. However Solutions 2,3,5 and 7 might all be satisfactory. The residual torsional moment diagrams for these solutions are plotted in Figure 5.26. It will require a check by the designer of other governing design parameters to decide on which solution ought to be adopted.

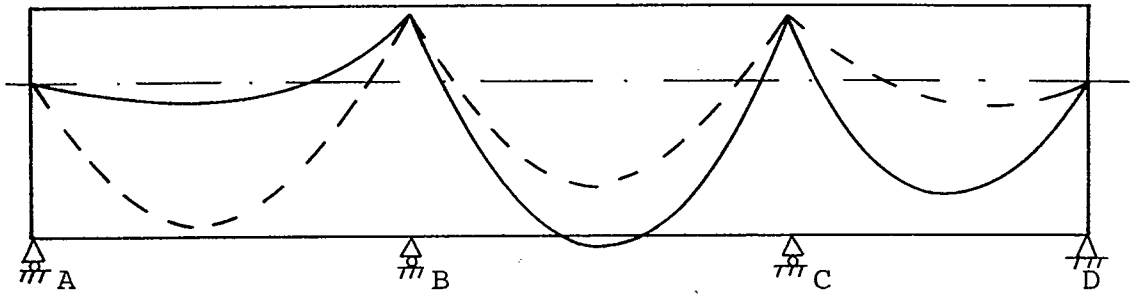

Solution 6

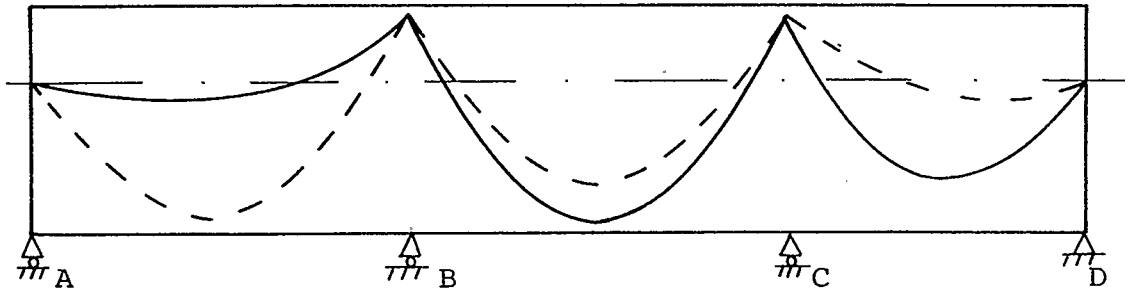

Solution 7

——— Web 1 (Inner Web in Span AB)

---- Web 2 (Outer Web in Span AB)

Figure 5.25 Adjusted Cable Profiles for Solutions 6 and 7, Table 5.10

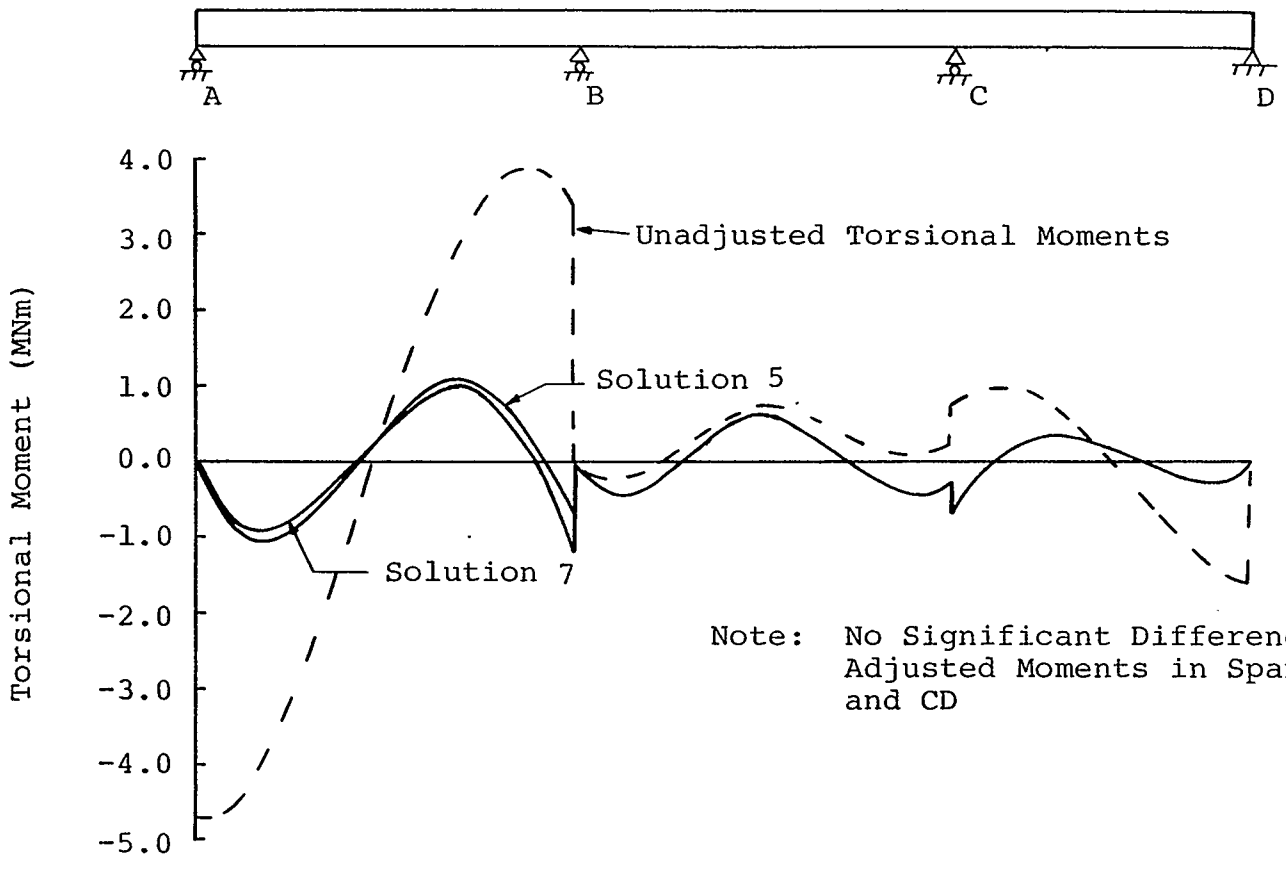

Figure 5.26 Residual Torsional Moments in Three Span Bridge, Figure 5.21, for Solutions 2, 3, 5 and 7 (see also overleaf)

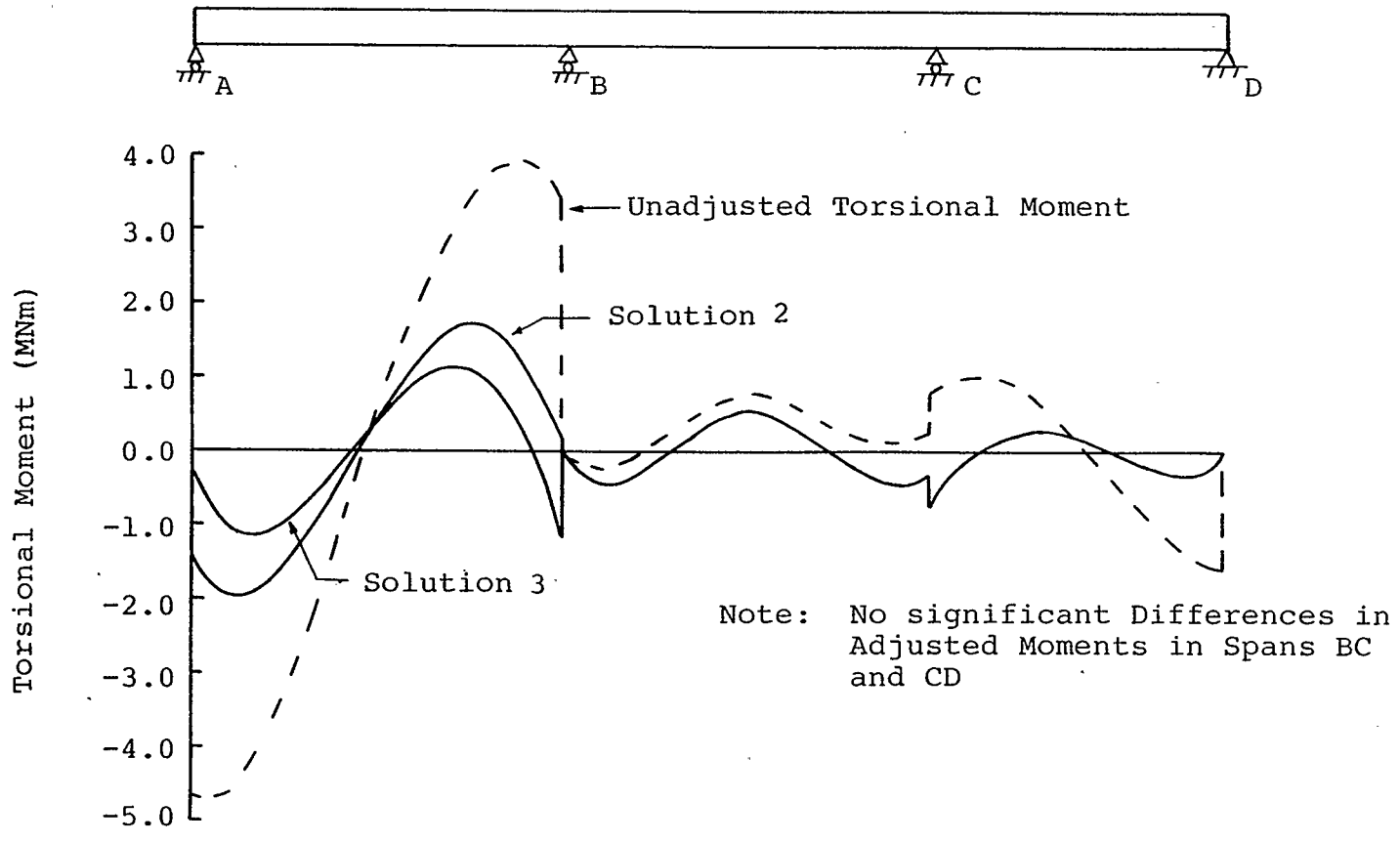

Figure 5.26 (Continued)

5.12 Concluding Remarks

An analytic technique for the control of torsional moments in curved box girder bridges has been developed in this chapter. The method enables a designer to chose a cable profile and prestressing forces that minimize torsion, subject to appropriate constraints with respect to the prestressing and the cable geometry. The technique has been applied to two box girder bridge examples, and in both cases substantial reductions in the magnitude of torsional moments have been achieved. Both examples also illustrate that a range of potential solutions to each situation exists.

CHAPTER SIX

CONCLUSIONS AND RECOMMENDATIONS

6.1 Summary and General Conclusions

The work outlined in this thesis may be divided into two distinct parts. Firstly, the development of the Jirousek beam element, an element suitable for the analysis of curved prestressed bridges, is presented. Secondly, a technique is developed for controlling torsional moments in curved box girder bridges by the use of appropriate cable profiles and prestressing forces.

The Jirousek element gives correct results under distributed loading and under concentrated loads applied to external nodes. However, when subjected to concentrated forces at internal degrees of freedom, inexact results are obtained. The source of the errors is the element's behaviour in approximating the true deflected shape by a continuous function. In reality, when concentrated loads are applied at internal nodes the deflection field is discontinuous at the point of application of the load. Thus, in structures where large concentrated forces are applied it is preferable to have the point of application of the load coincident with the end nodes of the Jirousek element. In the present analysis of curved bridges only

applied dead loads and prestressing loads were considered, and in addition, cable anchorages were constrained to coincide with external element nodes. As a result, the element performed very well under the applied loading, and as seen in Section 5.2, gave results in very close agreement with the exact values.

The automatic computation of prestressing loads was of major benefit in the present work. The method developed for controlling torsion requires that the bending and torsional moments due to a number of prestressing cable profiles be computed. This would have been a very tedious task by hand, particularly for cubic and quartic profiles. However, with automatic computation of prestressing forces the induced torsional moments are computed very easily and efficiently, with each cable profile being analysed as a separate load case.

The method for control of torsional moments, outlined in this thesis, has been presented for box sections, in which the cable profiles are constrained to lie in a particular plane corresponding to the section webs. However, the method may also be applied to solid cross sections by the use of unit cables in both the y' and z' directions of the cross section.

A basic premise of the analysis is that superposition of individual unit cable profiles is possible. This has

been shown to be valid provided the radial forces produced by a prestressing tendon are linearly proportional to the eccentricity. All bridges in practice have a sufficiently small depth to span ratio to comply with this requirement.

The technique differs from previous methods of controlling torsional moments in that it enables the designer to constrain the cable profiles and to prescribe the amount of prestressing to be used in the bridge. By specifying appropriate cable profile and prestressing force constraints the designer may eliminate as little, or as much torsional moment as he deems necessary. In this respect the method is more general than those previously proposed (11,14). The method is also more general in that it may be applied to curved bridges of non circular geometry, or to bridges with both vertical and horizontal components of curvature.

Two examples have been included to demonstrate the use of the method. The analysis of the two span symmetric bridge demonstrates the relative amounts of torsion that can be eliminated using quadratic, cubic and quartic analysis. In this particular example the quartic analysis gives an almost totally balanced configuration of bending and torsional moments. However, the greater reduction in torsional moments may not warrant the extra computational effort, particularly for bridges with a large number of

spans. Furthermore, in practice, it is not necessary to reduce torsional moments to zero; rather, it is sufficient to reduce the torsional moment such that no (or only a small amount of) additional reinforcement is required in the bridge. In addition, for simplicity of construction and detailing, designers may prefer to use parabolic cable profiles.

The three span example shows that a quadratic analysis can achieve a significant reduction in the magnitude of torsional moments along a bridge. It also demonstrates that a number of different combinations of prestressing forces and cable profiles may give a satisfactory solution.

6.2 Recommendations for Future Research

The method presented in Chapter Five can be conveniently applied to the control of torsional moments in curved bridges. Its practical usefulness could be further improved, however, by the addition of some simple refinements.

Firstly, as the method is presently formulated, the cable profile is geometrically constrained using the Lagrange multiplier technique. With this technique, only equality constraints may be applied - thus the adjusted cable is prescribed to have a specified eccentricity at some section. Using inequality constraints, the cable

profile could be constrained to lie within set limits, as is applied in the constraining of the prestressing forces.

A second refinement of the analysis would be to include additional constraints on the final solution. These could be applied with respect to such quantities as a maximum allowable transverse moment and a satisfactory value of ultimate strength. These additional constraints would have the effect of further automating the procedure, something that is in keeping with modern design trends.

REFERENCES

(1) ACI Manual of Concrete Practice, Part 4, American Concrete Institute, Detroit, 1984.

(2) ACI 343R-77, Reaffirmed 1981, "Analysis and Design of Reinforced Concrete Bridge Structures", American Concrete Institute, Detroit, 1977.

(3) Albuquerque, F.C.S., "A Beam Element for use with the Semiloof Shell Element", M.Sc. Thesis, University College of Swansea, 1973.

(4) Bassi, K.G. et al., "Continuous Post-Tensioned Torsionally Stiff Concrete Bridges", First International Symposium on Concrete Bridge Design, ACI Publication SP-23, American Concrete Institute, Detroit, 1967, pp. 563-577.

(5) Bathe, K.J., and Wilson, E.L., "Numerical Methods in Finite Element Analysis", Prentice Hall, Englewood Cliffs, New Jersey, 1976.

(6) Bazant, Z.P., and El Nimeiri, M., "Stiffness Method for Curved Box Girders at Initial Stress", Journal of the Structural Division, ASCE, Vol. 100, No. ST10, 1974, pp. 2071-2090.

(7) Bell, L.C., and Heins, C.P., "Analysis of Curved Girder Bridges", Journal of the Structural Division, ASCE, Vol. 96, No. ST8, 1970, pp. 1657-1673.

(8) Bouberguig, A., "MAPS - Macro Element Analysis of Prestressed and Stiffened Shells", Ecole Polytechnique Federale de Lausanne, Lausanne, Switzerland, 1982. (In French)

(9) Box, M.J., "A comparison of several current optimization methods, and the use of transformations in constrained problems", Computer Journal, Vol. 9, 1966, pp. 67-77.

(10) Buragohain, D.N., et al., "A Matching Superparametric Beam Element for Shell Beam Systems", Computers and Structures, Vol. 9, No. 2, 1978, pp. 175-182.

(11) Campbell, T.I., and Chitnuyanondh, L., "Horizontally Curved Continuous Post-Tensioned Concrete Beams",

Prestressed Concrete Institute Journal, Vol. 20, No. 2, 1975, pp. 58-71.

(12) Cook, R.D., "Concepts and Applications of Finite Element Analysis", John Wiley and Sons, Toronto, 2nd ed., 1981.

(13) CSA Standard A23.3-1984, "Code for the Design of Concrete Structures for Buildings", Canadian Standards Association, 1984.

(14) Egger, H., "Torsion and Prestressing in Curved Beams", Wilhelm Ernst and Son, Berlin, 1968. (In German)

(15) El-Amin, F.M., and Brotton, D.M., "Horizontally Curved Beam Finite Element Including Warping", Int. J. Num. Meth. Engng., Vol. 10, No. 6, 1976, pp. 1397-1404.

(16) Engel, S., "Structural Analysis of Circular Curved Beams", Journal of the Structural Division, ASCE, Vol. 93, No. ST1, 1967, pp. 221-234.

(17) Ferguson, G.H., and Clark, R.D., "A Variable Thickness Curved Beam and Shell Stiffening Element with Shear Deformations", Int. J. Num. Meth. Engng., Vol. 14, No. 4, 1979, pp. 581-592.

(18) Ghali, A., and Dilger, W.H., Class Notes for ENCI 635, "Design and Behaviour of Prestressed Concrete Bridges and Other Prestressed Structures", The Department of Civil Engineering, University of Calgary.

(19) Ghali, A., and Maher, P.G., "Manual and Computer Program SFRAME: Space Frames with Curved or Straight Elements", Forthcoming report to The Department of Civil Engineering, University of Calgary.

(20) Ghali, A., and Neville, A.M., "Structural Analysis - A Unified Classical and Matrix Approach", Chapman and Hall, London, 2nd ed., 1978.

(21) Graybill, F.A., "Introduction to Matrices with Applications in Statistics", Wadsworth Publishing Company, Belmont, California, 1969.

(22) Heins, C.P., "Bending and Torsional Design in Structural Members", D.C. Heath and Company, Lexington, Massachusetts, 1975.

(23) Heins, C.P., and Spates, K.R., "Behaviour of a Single Horizontally Curved Girder", Journal of the Structural Division, ASCE, Vol. 96, No. ST7, 1970, pp. 1511-1524

(24) IMSL Library, Fortran Subroutines for Mathematics and Statistics, Users Manual, Vol. 4, November 1984, Houston, Texas.

(25) Jirousek, J., "A Family of Variable Section Curved Beam and Thick Shell Stiffening Elements", Int. J. Num. Meth. Engng., Vol. 17, No. 2, 1981, pp. 171-186.

(26) Jirousek, J., et al., "A Macro Element Formulation of Prestressed Curved Box Girder Bridges", Computers and Structures, Vol. 10, No. 3, 1979, pp. 467-482.

(27) Kreyszig, E., "Advanced Engineering Mathematics", John Wiley and Sons, New York, 3rd ed., 1972.

(28) Leonhardt, F., "Prestressed Concrete, Design and Construction", Wilhelm Ernst and Son, Berlin, 2nd ed. (English), 1964.

(29) Lin, T.Y., "Load Balancing Method for Design and Analysis of Prestressed Concrete Structures", Proc. ACI, Vol. 60 , No. 6, 1963, pp. 719-741.

(30) McManus, P.F., et al., "Horizontally Curved Girders - State of the Art", Journal of the Structural Division, ASCE, Vol. 90, No. ST5, 1969, pp. 855-870.

(31) Naaman, A.E., "Prestressed Concrete - Analysis and Design", McGraw Hill, New York, 1982.

(32) Oden, J.T., and Ripperger, E.A., "Mechanics of Elastic Structures", McGraw Hill, New York, 2nd ed., 1981.

(33) Ontario Highway Bridge Design Code, Ministry of Transportation and Communications, Ontario, 1983.

(34) Purcell, E.J., "Calculus with Analytic Geometry", Meredith Publishing Company, New York, 1965.

(35) Reddy, M.N., and Tuma, J.J., "Analysis of Laterally Loaded Continuous Curved Beams", Journal of the Structural Division, ASCE, Vol. 93, No. ST1, 1967, pp. 495-513.

(36) Rozvany, G.I.N., Discussion to "Load Balancing Method for Design and Analysis of Prestressed Concrete Structures", Proc. ACI, Vol. 60, No. 12, 1963, pp. 1862-1870.

(37) Salse, E.A.B., "Analysis and Design of Prestressed Circular Bow Girders for Bridge Structures", Second International Symposium on Concrete Bridge Design, ACI Publication SP-26, American Concrete Institute, Detroit, 1969, pp. 714-740.

(38) Scordelis, A.C., et al., "Computer Programs for Prestressed Concrete Box Girder Bridges", Report No. UCB/SESM - 85/02, Department of Civil Engineering, University of California, Berkeley, California, March 1985.

(39) Scordelis, A.C., and Larsen, P.K., " Structural Response of Curved R.C. Box Girder Bridge", Journal of the Structural Division, ASCE, Vol. 103, No. ST8, 1977, pp. 1507-1524.

(40) Shames, I.H., and Dym, C.L., "Energy and Finite Element Methods in Structural Mechanics", McGraw - Hill, New York, 1985.

(41) Siddall, J.N., "Optimal Engineering Design", Marcel Dekker Inc., New York, 1982.

(42) Surana, K.S., "Isoparametric Elements for Cross Sectional Properties and Stress Analysis of Beams", Int. J. Num. Meth. Engng., Vol. 14, No. 4, 1979, pp. 475-497.

(43) Tadros, G., et al., "Construction Stages and Design Considerations for a Curved Box Girder Bridge", Canadian Journal of Civil Engineering, Vol. 9, No. 3, 1982, pp. 483-488.

(44) Thomas, G.B., "Calculus and Analytic Geometry", Addison-Wesley, Reading, Massachusetts, 4th ed., 1968.

(45) Thornton, W.A., and Master, B.G., "Direct Stiffness Formulation for Horizontally Curved Beams", Journal of the Structural Division, ASCE, Vol. 103, No. ST1, 1977, pp. 284-289.

(46) Van Zyl, S.F., and Scordelis, A.C., "Analysis of Curved Prestressed Segmental Bridges", Journal of the

Structural Division, ASCE, Vol. 105, No. ST11, 1979, pp. 2399-2417.

(47) Velutini, B., "Analysis of Continuous Circular Curved Beams", Proc. ACI, Vol. 22, No. 3, 1950, pp. 217-228.

(48) Vlasov, V.Z., "Thin Walled Elastic Beams", National Science Foundation, Washington D.C., 1961.

(49) Vreden, W., (J. Scott translation), "Curved Continuous Beams for Highway Bridges", Frederick Ungar Publishing Co., New York, 1969.

(50) Witecki, A.A., "Simplified Method for the Analysis of Torsional Moment as an Effect of a Horizontally Curved Multispan Continuous Bridge", First International Symposium on Concrete Bridge Design, ACI Publication SP-23, American Concrete Institute, Detroit, 1967, pp. 193-204.

APPENDIX A

LOCATION OF SHEAR CENTRE IN BOX SECTIONS

Most box sections in practical use, though symmetrical about a vertical axis, are unsymmetrical with respect to the y' axis, Figure A.1. Thus the shear centre no longer coincides with the centroid of the section, but lies on the z' axis at some distance above the centroid. This implies that the horizontal radial forces, caused by prestressing in a curved beam, have a proportionally higher eccentricity with respect to the centre of twist (or shear centre) of the cross section.

The location of the shear centre may be computed, for thin walled open sections, by computing the shear flow through the section due to an applied shearing force in the appropriate direction. Moments are then taken about a suitable point to determine the distance of the shear centre from the centroid. For the case of closed sections, however, the shear flow around the section cannot be directly computed. However given that, for a cross section subject to bending about one of its principal axes, no twist occurs, we may write the following equation for any closed section (32):

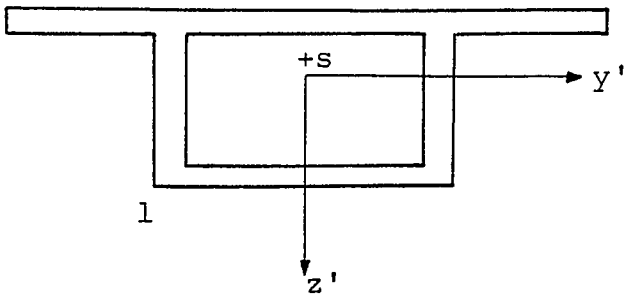

Figure A.1 Unsymmetric Box Section

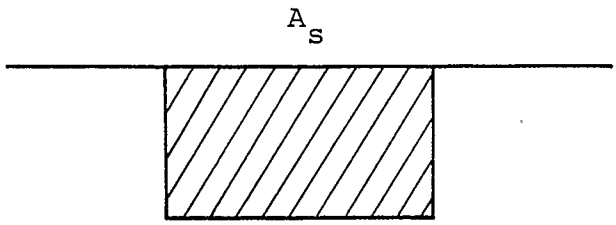

Figure A.2 Definition of Term A_s as in Equation A.1

$$\omega = \frac{1}{2A_s G} \oint q \frac{ds}{t} \qquad (A.1)$$

where q = shear flow

ω = angle of twist

A_s = area enclosed by centreline of box section (see Figure A.2)

G = shear modulus

t = thickness

The shear flow at some point, say point 1 of Figure A.1, may initially be assumed to be zero. The resulting shear flow at any section may then be computed using the equation

$$q_o = \frac{VQ}{I} \qquad (A.2)$$

where q_o = the shear flow at the required section

V = the applied shearing force

Q = the first moment of area of the segment considered about the appropriate centroidal axis

I = the moment of Inertia

However, when substituted into Equation A.1 the shear flows, thus computed do not give zero twist. The assumed shear flows differ by a constant term, q_r, from the correct

distribution, required to give zero twist. Thus the correct shear flow is given by:

$$q = q_o + q_r \tag{A.3}$$

Substituting into Equation A.1 gives :

$$\omega = \frac{1}{2 A_s G} \oint (q_o + q_r) \frac{ds}{t} \tag{A.4}$$

Since q_r is constant around the box it may be taken outside the integral and thus:

$$q_r = - \frac{\oint \frac{q_o ds}{t}}{\oint \frac{ds}{t}} \tag{A.5}$$

The correcting term, q_r, may then be added to the assumed shear flow to give the actual shear flow distribution around the box, Figure A.3. Since the shear flow in the overhangs is determinate, the redundant shear flow only acts in the closed box portion of the cross section.

Once the shear flow diagram has been obtained, the shear centre may be located by taking moments of forces about a suitable point. The shearing force along each section of the box is given by the integral of the shear flow.

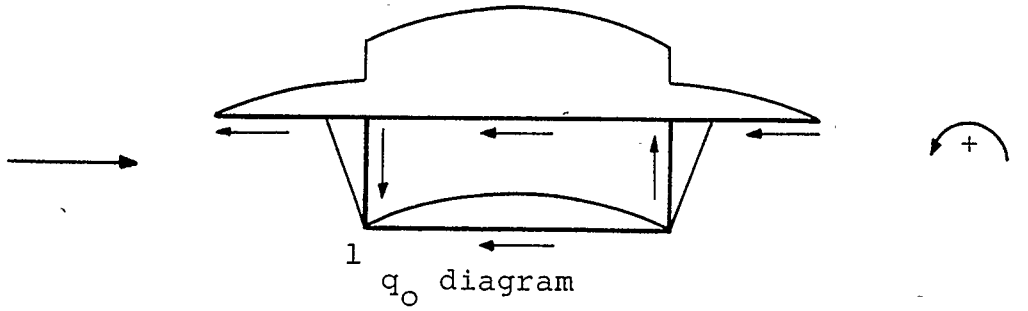

q_o diagram

Shear flow assumed to be zero at point 1

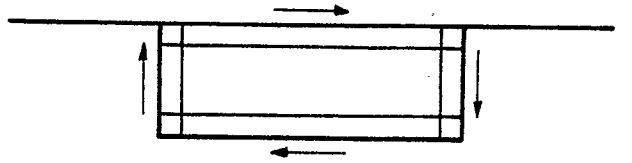

q_r diagram

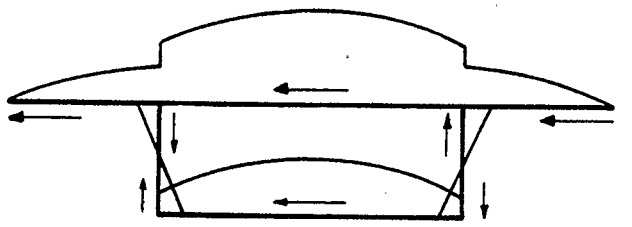

Combined Shear Flow Diagram

Figure A.3 Shear Flow Diagrams

APPENDIX B

OPTIMIZED RESULTS FOR THE TWO SPAN BRIDGE, FIGURE 5.11

P_{min} =	4.70 MN	T_{max} =	1.005 MNm
P_{inner} =	4.70 MN	I =	2.30 (MNm)
P_{outer} =	14.60 MN	$M_{z'}$ =	63.38 MNm

Node	Residual Moments (MNm)		Cable Eccentricities (m)	
	Bending	Torsion	Inner	Outer
1	-0.025	1.005	-0.50	-0.50
2	-0.017	0.065	0.034	0.0
3	0.018	-0.424	0.460	0.40
4	0.038	-0.566	0.779	0.70
5	-0.011	-0.461	0.990	0.90
6	-0.197	-0.202	1.093	1.0
7	-0.016	0.101	1.090	1.0
8	0.034	0.355	0.979	0.90
9	0.021	0.458	0.760	0.70
10	0.010	0.310	0.434	0.40
11	0.0	-0.194	0.0	0.0

Unit Cable Scaling Factors (Figure 5.14)

Inner Web		Outer Web	
1	0.094	2	0.0

Table B.1 - Quadratic Terms Added To Basic Profile

P_{min} = 4.70 MN

P_{min} =	7.00 MN	T_{max} =	1.061 MNm
P_{inner} =	7.00 MN	I =	2.47 $(MNm)^2$
P_{outer} =	14.42 MN	$M_{z'}$ =	47.45 MNm

Node	Residual Moments (MNm)		Cable Eccentricities (m)	
	Bending	Torsion	Inner	Outer
1	-0.028	1.061	-0.50	-0.50
2	-0.015	0.088	-0.015	0.0
3	0.025	-0.425	0.195	0.40
4	0.045	-0.583	0.431	0.70
5	-0.012	-0.486	0.593	0.90
6	-0.221	-0.229	0.680	1.0
7	-0.018	0.081	0.693	1.0
8	0.040	0.345	0.631	0.90
9	0.027	0.463	0.495	0.70
10	0.014	0.336	0.285	0.40
11	0.0	-0.145	0.0	0.0

Unit Cable Scaling Factors (Figure 5.14)

Inner Web		Outer Web	
1	-0.332	2	0.0

Table B.2 - Quadratic Terms Added to Basic Profile, P_{min} = 7.0 MN

P_{min} =	9.35 MN	T_{max} =	1.117 MNm
P_{inner} =	9.35 MN	I =	2.67 $(MNm)^2$
P_{outer} =	14.23 MN	$M_{z'}$ =	31.25 MNm

Node	Residual Moments (MNm)		Cable Eccentricities (m)	
	Bending	Torsion	Inner	Outer
1	-0.031	1.117	-0.50	-0.50
2	-0.013	0.111	-0.191	0.0
3	0.032	-0.426	0.060	0.40
4	0.052	-0.600	0.253	0.70
5	-0.013	-0.512	0.340	0.90
6	-0.245	-0.257	0.468	1.0
7	0.020	0.059	0.490	1.0
8	0.045	0.335	0.453	0.90
9	0.033	0.469	0.360	0.70
10	0.018	0.362	0.209	0.40
11	0.0	-0.095	0.0	0.0

Unit Cable Scaling Factors (Figure 5.14)

Inner Web		Outer Web	
1	-0.532	2	0.0

Table B.3 - Quadratic Terms Added to Basic Profile, P_{min} = 9.35 MN

P_{min} = 11.70 MN		T_{max} =	1.174 MNm
P_{inner} = 11.70 MN		I =	2.90 $(MNm)^2$
P_{outer} = 14.04 MN		$M_{z'}$ =	14.96 MNm

Node	Residual Moments (MNm)		Cable Eccentricities (m)	
	Bending	Torsion	Inner	Outer
1	-0.034	1.174	-0.50	-0.50
2	-0.011	0.135	-0.237	0.0
3	0.039	-0.427	-0.022	0.40
4	0.060	-0.617	0.146	0.70
5	-0.014	-0.538	0.267	0.90
6	-0.270	-0.285	0.341	1.0
7	-0.023	0.038	0.367	1.0
8	0.051	0.324	0.346	0.90
9	0.039	0.474	0.278	0.70
10	0.022	0.388	0.163	0.40
11	0.0	-0.044	0.0	0.0

Unit Cable Scaling Factors (Figure 5.14)

Inner Web		Outer Web	
1	-0.659	2	0.0

Table B.4 - Quadratic Terms Added To Basic Profile, P_{min} = 11.70 MN

P_{min} =	4.70 MN	T_{max} =	0.435 MNm
P_{inner} =	4.70 MN	I =	0.74 $(MNm)^2$
P_{outer} =	15.27 MN	$M_{z'}$ =	67.65 MNm

Node	Residual Moments (MNm)		Cable Eccentricities (m)	
	Bending	Torsion	Inner	Outer
1	-0.193	0.435	-0.50	-0.50
2	0.094	-0.090	0.084	-0.021
3	-0.011	-0.225	0.508	0.372
4	-0.062	-0.157	0.789	0.675
5	-0.124	0.031	0.941	0.886
6	-0.286	0.248	0.980	1.000
7	-0.042	0.386	0.920	1.014
8	0.063	0.278	0.776	0.925
9	0.072	0.051	0.563	0.728
10	0.036	-0.119	0.301	0.421
11	0.0	0.008	0.0	0.0

Unit Cable Scaling Factors (Figure 5.14)

Inner Web		Outer Web	
1	0.148	2	0.297
3	-0.056	5	-0.286
4	-0.243	6	-0.242

Table B.5 - Quadratic and Cubic Terms Added to Basic Profile, P_{min} = 4.70 MN

P_{min} =	7.00 MN	T_{max} =	0.438 MNm
P_{inner} =	7.00 MN	I =	0.76 $(MNm)^2$
P_{outer} =	15.09 MN	$M_{z'}$ =	51.77 MNm

Node	Residual Moments (MNm)		Cable Eccentricities (m)	
	Bending	Torsion	Inner	Outer
1	-0.198	0.438	-0.50	-0.50
2	0.094	-0.091	-0.078	-0.023
3	-0.005	-0.226	0.231	0.369
4	-0.055	-0.159	0.441	0.673
5	-0.125	0.030	0.562	0.885
6	-0.309	0.248	0.603	1.0
7	-0.040	0.389	0.576	1.015
8	0.069	0.281	0.492	0.927
9	0.079	0.052	0.360	0.731
10	0.040	-0.119	0.193	0.423
11	0.0	0.007	0.0	0.0

Unit Cable Scaling Factors (Figure 5.14)

Inner Web		Outer Web	
1	-0.288	2	0.306
3	-0.031	5	-0.295
4	-0.163	6	-0.248

Table B.6 - Quadratic and Cubic Terms Added to Basic Profile, P_{min} = 7.0 MN

P_{min} =	9.35 MN	T_{max} =	0.442 MNm
P_{inner} =	9.35 MN	I =	0.79 $(MNm)^2$
P_{outer} =	14.90 MN	$M_{z'}$ =	35.56 MNm

Node	Residual Moments (MNm)		Cable Eccentricities (m)	
	Bending	Torsion	Inner	Outer
1	-0.204	0.442	-0.50	-0.50
2	0.093	-0.091	-0.162	-0.025
3	0.001	-0.228	0.089	0.370
4	-0.048	-0.160	0.263	0.671
5	-0.126	0.029	0.337	0.883
6	-0.333	0.248	0.410	1.0
7	-0.046	0.391	0.400	1.016
8	0.075	0.284	0.346	0.929
9	0.086	0.052	0.255	0.733
10	0.045	-0.118	0.137	0.425
11	0.0	0.005	0.0	0.0

Unit Cable Scaling Factors (Figure 5.14)

Inner Web		Outer Web	
1	-0.511	2	0.315
3	-0.019	5	-0.306
4	-0.122	6	-0.255

Table B.7 - Quadratic and Cubic Terms Added to Basic Profile, P_{min} = 9.35 MN

P_{min} =	11.7 MN	T_{max} =	0.445 MNm
P_{inner} =	11.7 MN	I =	0.82 $(MNm)^2$
P_{outer} =	14.72 MN	$M_{z'}$ =	19.30 MNm

Node	Residual Moments (MNm)		Cable Eccentricities (m)	
	Bending	Torsion	Inner	Outer
1	-0.210	0.445	-0.50	-0.50
2	0.093	-0.092	-0.212	-0.027
3	0.007	-0.229	0.004	0.364
4	-0.041	-0.161	0.156	0.669
5	-0.127	0.029	0.250	0.882
6	-0.358	0.248	0.294	1.0
7	-0.048	0.394	0.294	1.017
8	0.082	0.287	0.258	0.931
9	0.093	0.053	0.192	0.736
10	0.050	-0.118	0.104	0.427
11	0.0	0.004	0.0	0.0

Unit Cable Scaling Factors (Figure 5.14)

Inner Web		Outer Web	
1	-0.645	2	0.325
3	-0.011	5	-0.316
4	-0.097	6	-0.261

Table B.8 - Quadratic and Cubic Terms Added to Basic Profile, P_{min} = 11.7 MN

P_{min} =	4.7 MN	T_{max} =	0.025 MNm
P_{inner} =	4.7 MN	I =	0.028 $(MNm)^2$
P_{outer} =	15.08 MN	$M_{z'}$ =	66.41 MNm

Node	Residual Moments (MNm)		Cable Eccentricities (m)	
	Bending	Torsion	Inner	Outer
1	0.008	0.004	-0.50	-0.50
2	-0.044	-0.002	0.102	-0.028
3	-0.022	0.001	0.506	0.369
4	0.043	0.002	0.765	0.678
5	0.038	-0.003	0.887	0.890
6	-0.133	0.001	0.977	1.0
7	0.036	0.025	0.942	1.0
8	0.034	-0.025	0.886	0.901
9	0.015	-0.001	0.717	0.695
10	-0.011	0.008	0.434	0.392
11	0.0	-0.001	0.0	0.0

Unit Cable Scaling Factors (Figure 5.14)

Inner Web		Outer Web	
1	-0.055	2	0.026
3	-0.369	5	-0.152
4	-0.034	6	0.105
7	0.512	10	0.135
8	0.259	11	0.000
9	0.001	12	-0.164

Table B.9 - Quadratic, Cubic and Quartic Terms Added to Basic Profile, P_{min} = 4.7 MN

P_{min} =	7.0 MN	T_{max} =	0.028 MNm
P_{inner} =	7.0 MN	I =	0.034 $(MNm)^2$
P_{outer} =	14.90 MN	$M_{z'}$ =	50.55 MNm

Node	Residual Moments (MNm)		Cable Eccentricities (m)	
	Bending	Torsion	Inner	Outer
1	0.010	0.004	-0.50	-0.50
2	-0.049	-0.003	-0.065	-0.029
3	-0.025	0.001	0.231	0.367
4	0.048	0.002	0.425	0.676
5	0.042	-0.004	0.523	0.889
6	-0.149	0.001	0.601	1.0
7	0.039	0.028	0.589	1.004
8	0.038	-0.027	0.567	0.903
9	-0.016	-0.002	0.464	0.698
10	-0.013	0.009	0.284	0.394
11	0.0	-0.001	0.0	0.0

Unit Cable Scaling Factors (Figure 5.14)

Inner Web		Outer Web	
1	-0.427	2	0.034
3	-0.278	5	-0.166
4	-0.260	6	0.104
7	0.385	10	0.142
8	0.200	11	0.001
9	-0.007	12	-0.170

Table B.10 - Quadratic, Cubic and Quartic Terms Added to Basic Profile, P_{min} = 7.0 MN

P_{min} =	9.35 MN	T_{max} =	0.032 MNm
P_{inner} =	9.35 MN	I =	0.042 $(MNm)^2$
P_{outer} =	14.72 MN	$M_{z'}$ =	34.39 MNm

Node	Residual Moments (MNm)		Cable Eccentricities (m)	
	Bending	Torsion	Inner	Outer
1	0.011	0.005	-0.50	-0.50
2	-0.055	-0.003	-0.151	-0.030
3	-0.027	0.002	0.090	0.365
4	0.053	0.002	0.251	0.675
5	0.047	-0.005	0.336	0.888
6	-0.164	0.0	0.408	1.0
7	0.043	0.032	0.408	1.005
8	0.042	-0.031	0.403	0.905
9	-0.017	-0.002	0.334	0.700
10	0.015	0.010	0.207	0.396
11	0.0	-0.002	0.0	0.0

Unit Cable Scaling Factors (Figure 5.14)

Inner Web		Outer Web	
1	-0.619	2	0.044
3	-0.231	5	-0.183
4	-0.022	6	0.104
7	0.320	10	0.151
8	0.169	11	0.001
9	0.007	12	-0.178

Table B.11 - Quadratic, Cubic and Quartic Terms Added to Basic Profile, P_{min} = 9.35 MN

P_{min} =	11.7 MN	T_{max} =	0.035 MNm
P_{inner} =	11.7 MN	I =	0.051 $(MNm)^2$
P_{outer} =	14.54 MN	$M_{z'}$ =	18.16 MNm

Node	Residual Moments (MNm)		Cable Eccentricities (m)	
	Bending	Torsion	Inner	Outer
1	0.012	0.005	-0.50	-0.50
2	-0.061	-0.003	-0.203	-0.032
3	-0.030	0.002	0.005	0.363
4	0.058	0.003	0.147	0.673
5	0.051	-0.006	0.224	0.887
6	-0.180	0.001	0.292	1.0
7	0.047	0.035	0.299	1.006
8	0.046	-0.034	0.304	0.907
9	-0.019	-0.002	0.256	0.072
10	-0.017	0.011	0.161	0.397
11	0.0	-0.001	0.0	0.0

Unit Cable Scaling Factors (Figure 5.14)

Inner Web		Outer Web	
1	-0.733	2	0.053
3	-0.203	5	-0.199
4	-0.019	6	0.103
7	0.281	10	0.159
8	0.151	11	0.002
9	0.001	12	-0.185

Table B.12 - Quadratic, Cubic and Quartic Terms Added to Basic Profile, P_{min} = 11.7 MN